Saturation of fishbone modes by self-generated zonal flows and constants of motions EP distributions in tokamak plasmas

G. Brochard[1,2], C. Liu[3], X. Wei[2], W. Heidbrink[2], Z. Lin[2], N. Gorelenkov[3], C. Chrystal[4], X. Du[4], J. Bao[5], A. R. Polevoi[1], M. Schneider[1], S. H. Kim[1], S.D. Pinches[1], P. Liu[2], J.H. Nicolau[2], H. Lütjens[6] and ISEP team

[1] ITER organization
[2] University of California Irvine
[3] Princeton Plasma Physics Laboratory
[4] General Atomics
[5] Chinese Academy of Science
[6] École Polytechnique - CPHT

Outline

I) Interplay fishbone/zonal flows in gyrokinetic simulations

A) Experimental fishbone validation on a DIII-D discharge

B) Predicted fishbone dynamics in ITER PFPO-2 scenario

II) Computation of CoMs EP distribution in IMAS

A) Versatile method for coordinate transformation

B) Application for NBI and alpha distributions in a JET-DT pulse

Importance of gyrokinetic simulations of fishbone modes for EP transport

- ➢ **Zonal flows (ZFs)** can impact significantly **thermal and EP transport** by **mitigating microturbulence** [1] and **AEs** [2] saturation amplitudes
- ➢ **Drift-waves modes** and **EP-driven AEs** can trigger **ZFs** respectively through **modulational instability** [3] and **EPs-induced polarisation [4]**
- ➢ **Fishbones** known to **trigger ITBs** in **ASDEX** [5], **MAST** [6], **HL-2A** [7], **EAST** [8] plasmas, and were observed **to destabilise strong zonal sheared flows** in **kinetic-MHD** simulations [9,10]
- ➢ A **gyrokinetic** formalism for **self-consistent ZFs evolution** is **crucial** to capture their **collisionless damping** [11], requiring **kinetic treatment** of **thermal ions**
- ➢ **GTC** is applied to study **self-consistently fishbone-induced EP transport** in **DIII-D** and **ITER**, as a **stepping stone** towards **upcoming cross-scale gyrokinetic simulations**

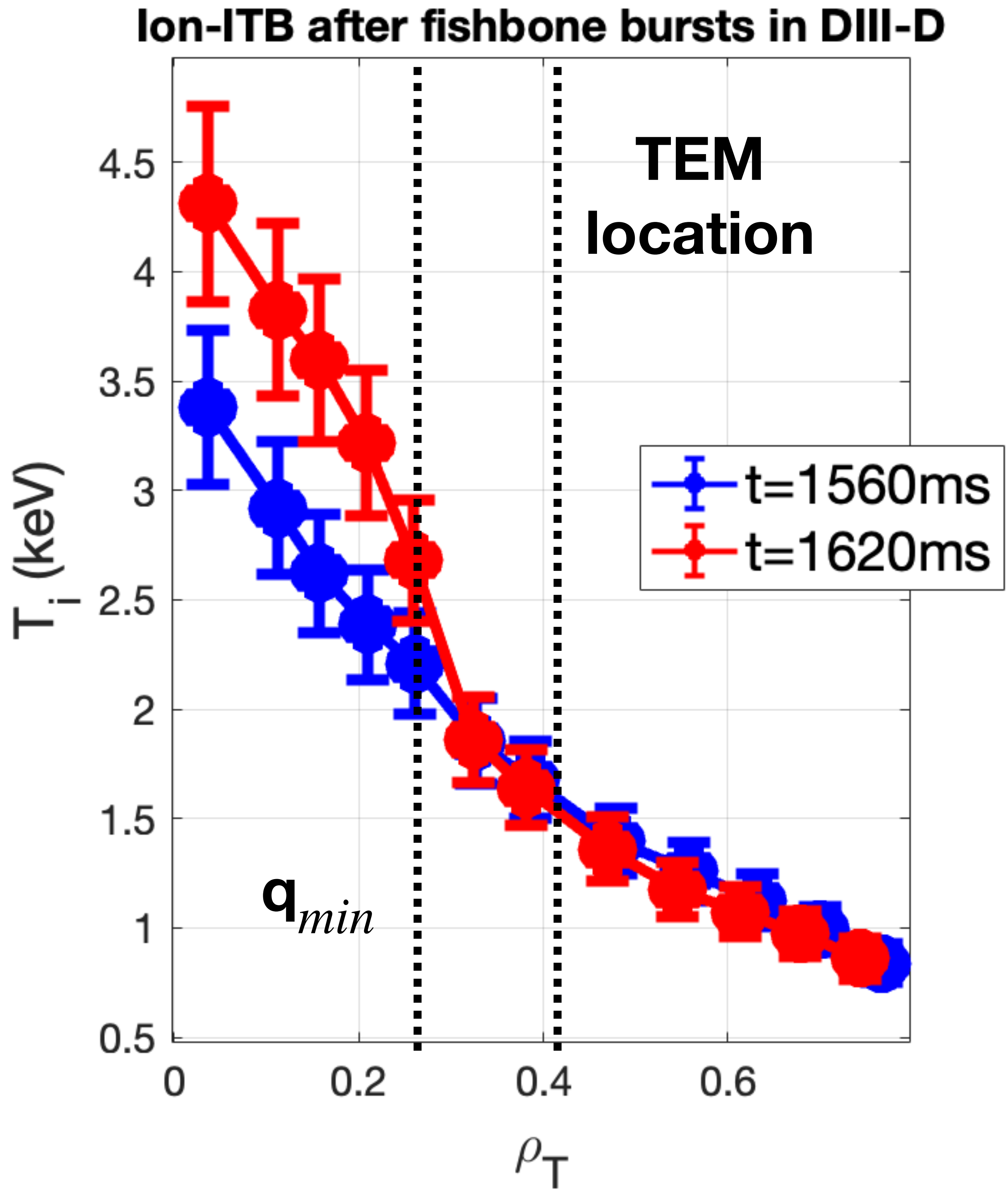

[1] Z. Lin et al. 1998, *Science*
[2] Y. Todo et al. 2012, *Nucl. Fusion*
[3] L. Chen et al. 2000, *Phys. Plasmas*
[4] Z. Qiu et al. 2016, *Phys. Plasmas*
[5] S. Günter et al. 2001, *Nucl. Fusion*
[6] A.R. Field et al. 2011, *Nucl. Fusion*
[7] W. Chen et al. 2016, *Nucl. Fusion*
[8] X. Gao et al. 2018, *Phys. Lett. A*
[9] G. Brochard et al. 2020b, *Nucl. Fusion*
[10] G. Wanling et al. 2023, *Nucl. Fusion*
[11] M.N. Rosenbluth et al. 1998, *PRL*

GTC capable of simulating macroscopic modes [1]

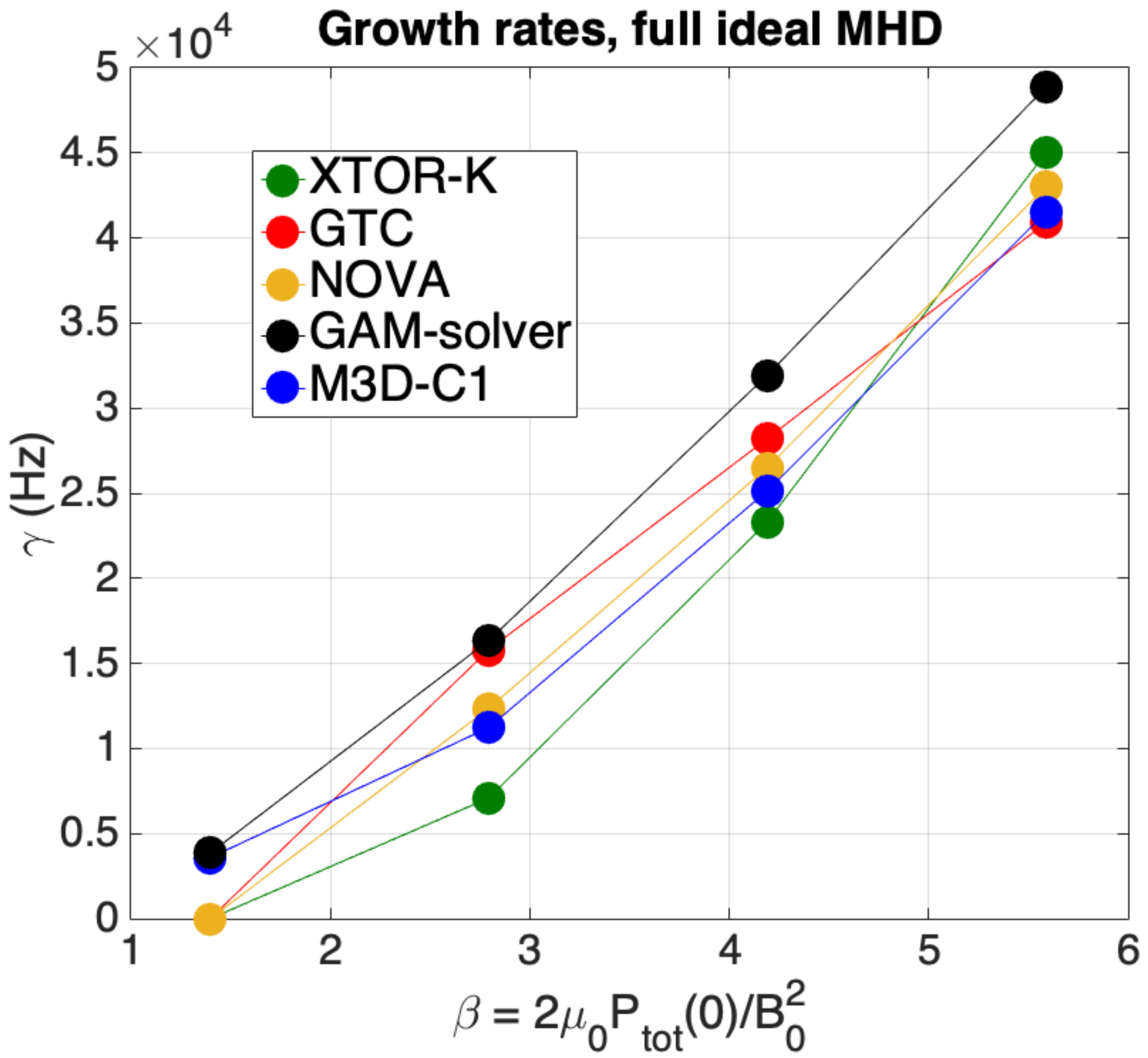

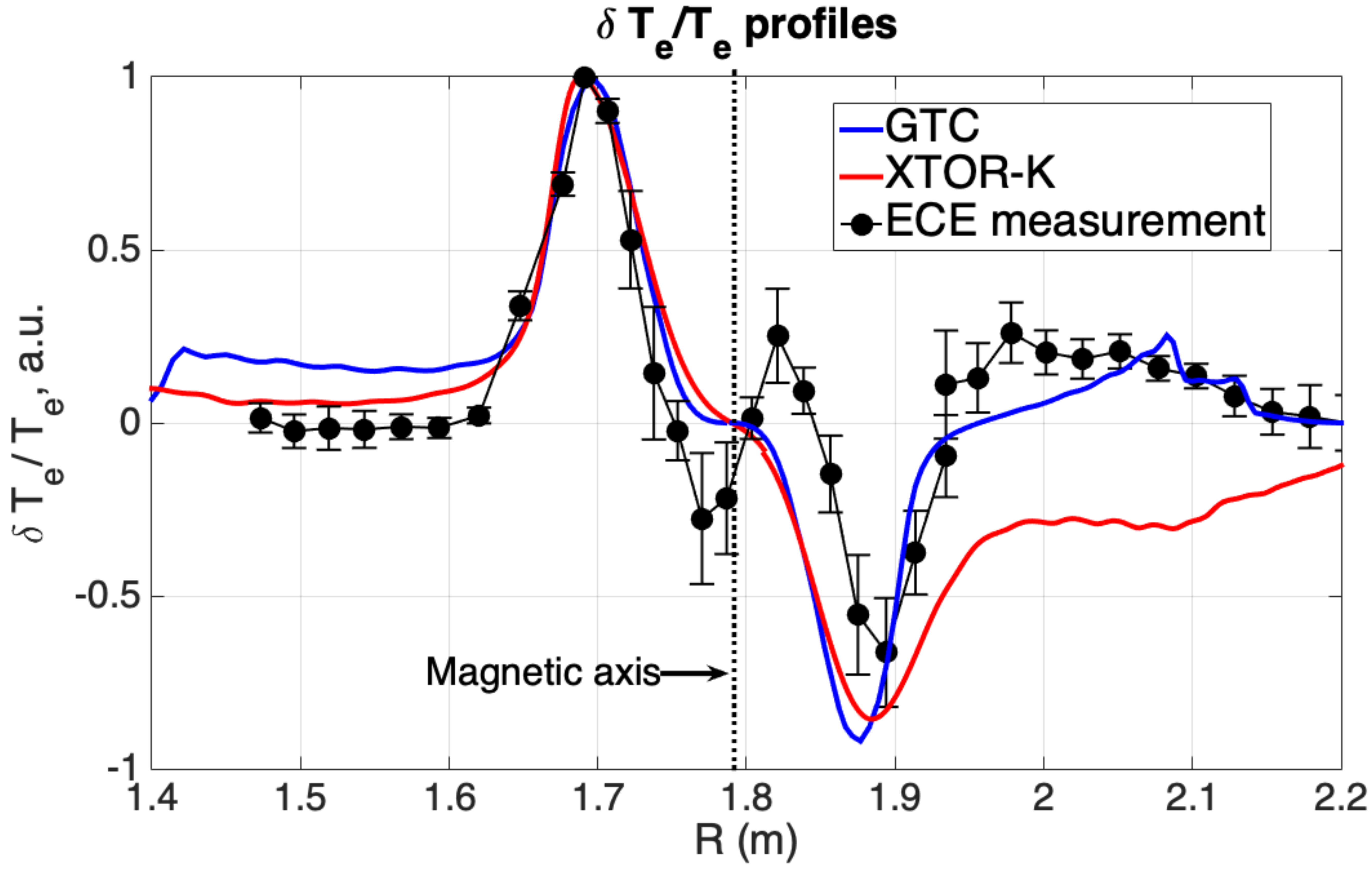

- **GTC** has been **verified** and **linearly validated** for **internal kink instability** in **DIII-D** plasmas

- **Successful benchmark** for **kink growth rate** in **ideal MHD** limit between **GTC** and **kinetic-MHD** codes

- **Linear validation** obtained between **ECE and** δT_e **profiles** in **GTC** and **XTOR-K** simulations

[1] G. Brochard et al. 2022, *Nucl. Fusion*

ITER baseline pre-fusion #101006

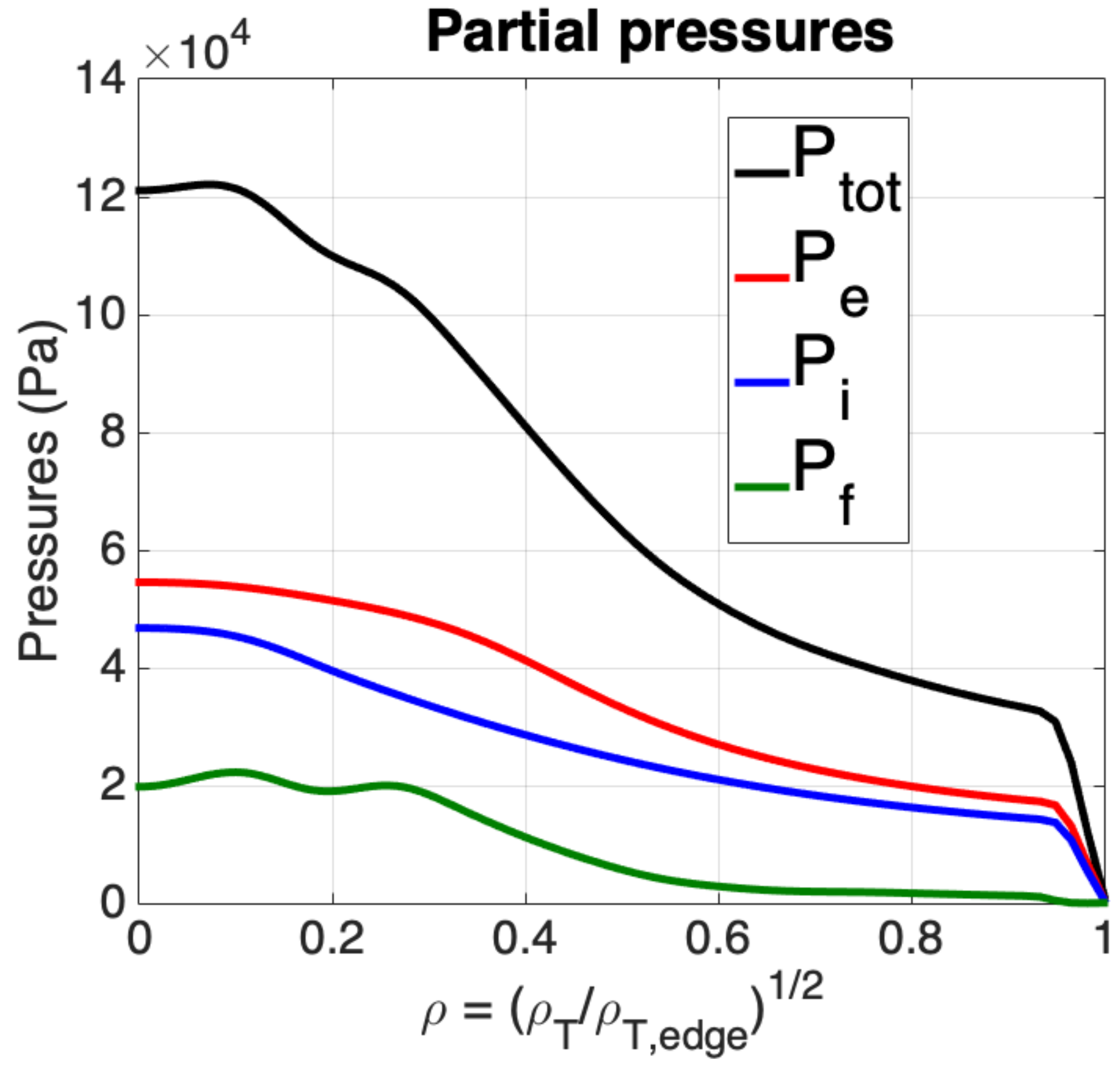

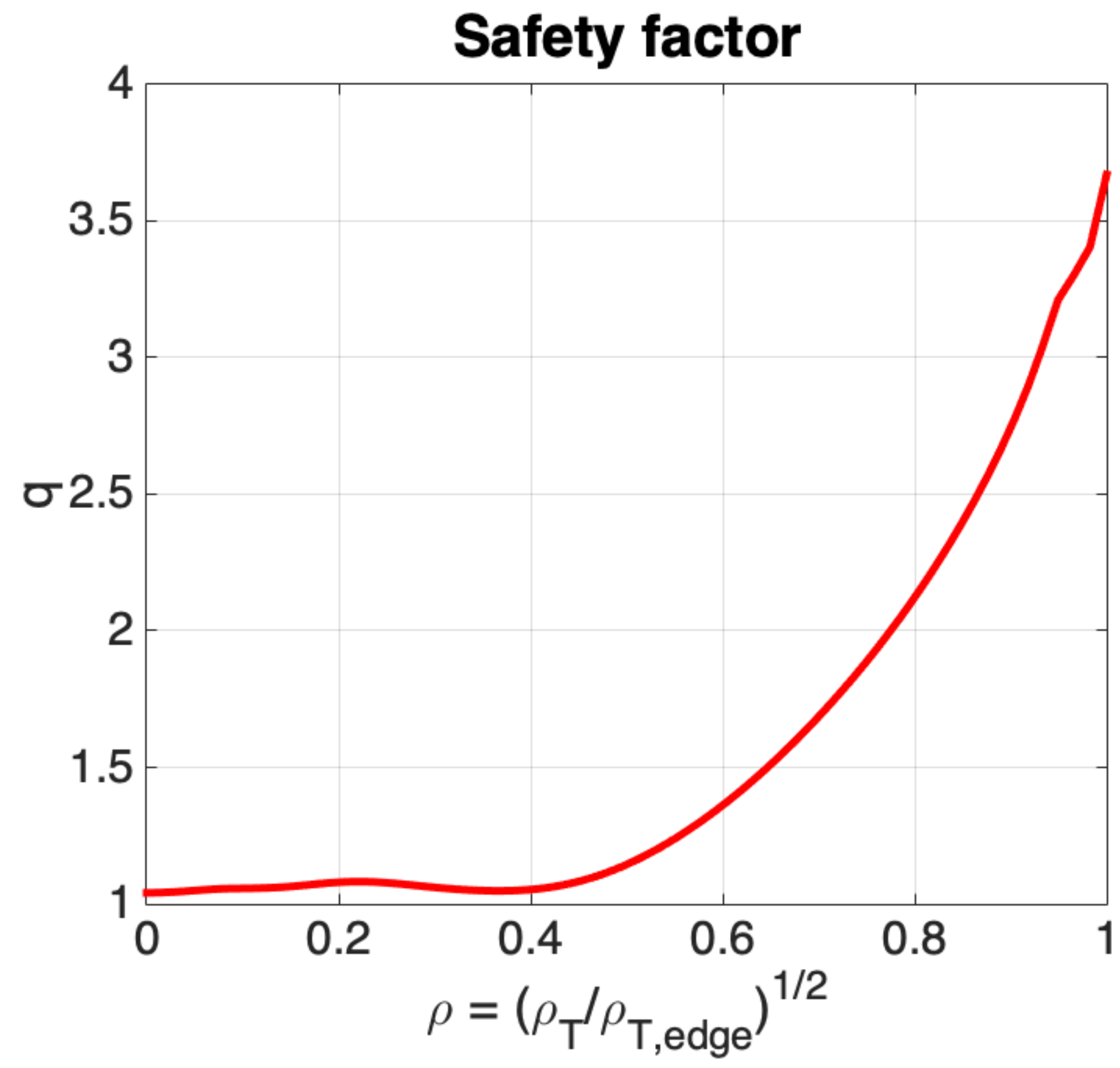

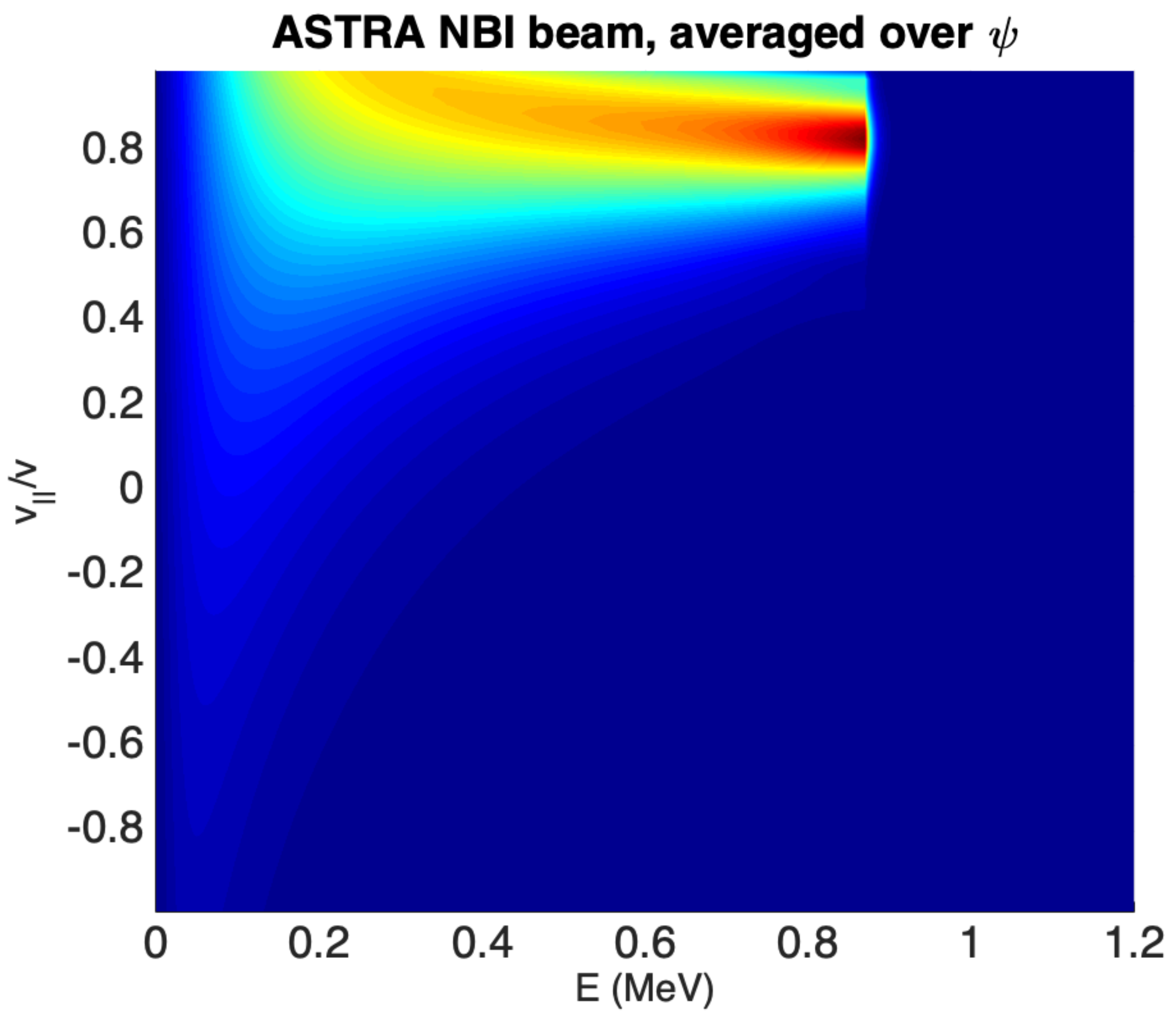

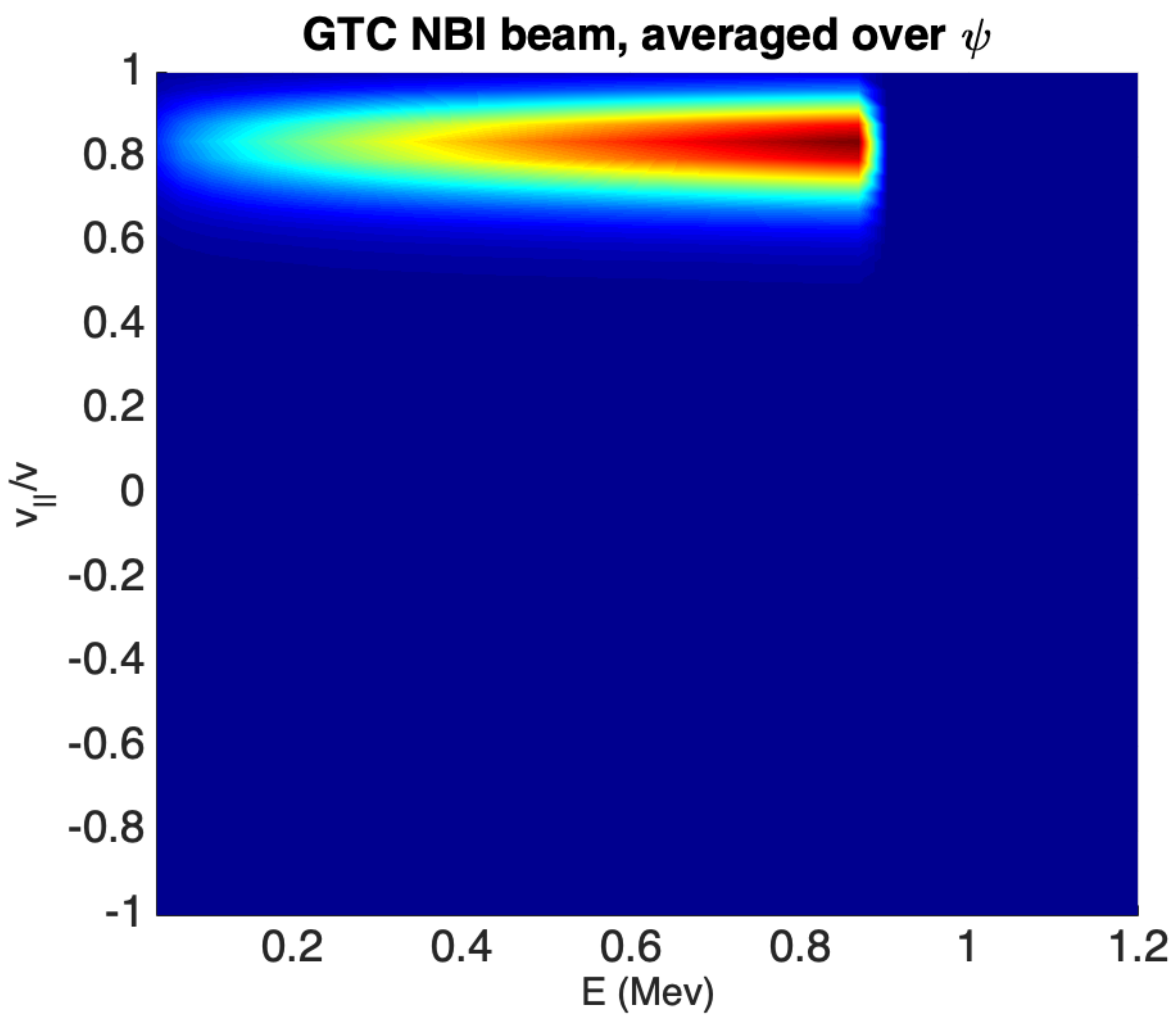

- ➢ Analysing **ITER scenarios** as part of **ITPA-EP 15** joint activity and **ISEP US DOE theory milestones 2022**
- ➢ **15 codes** from **Europe, US** and **Asia** used to **study EP transport** for **all scales**
- ➢ A **baseline pre-fusion** plasma is chosen by IO[1] for **macroscopic** simulations
- ➢ Scenario found **ideal MHD stable** [1], but **kinetic effects** need to be included
  - ➢ **NBI** modelized in **GTC** with a co-passing **anisotropic slowing-down** pdf

[1] A. R. Polevoi et al. 2020 *Nucl. Fusion* **60** 096024

DIII-D discharge #178631 as ITER matching shot

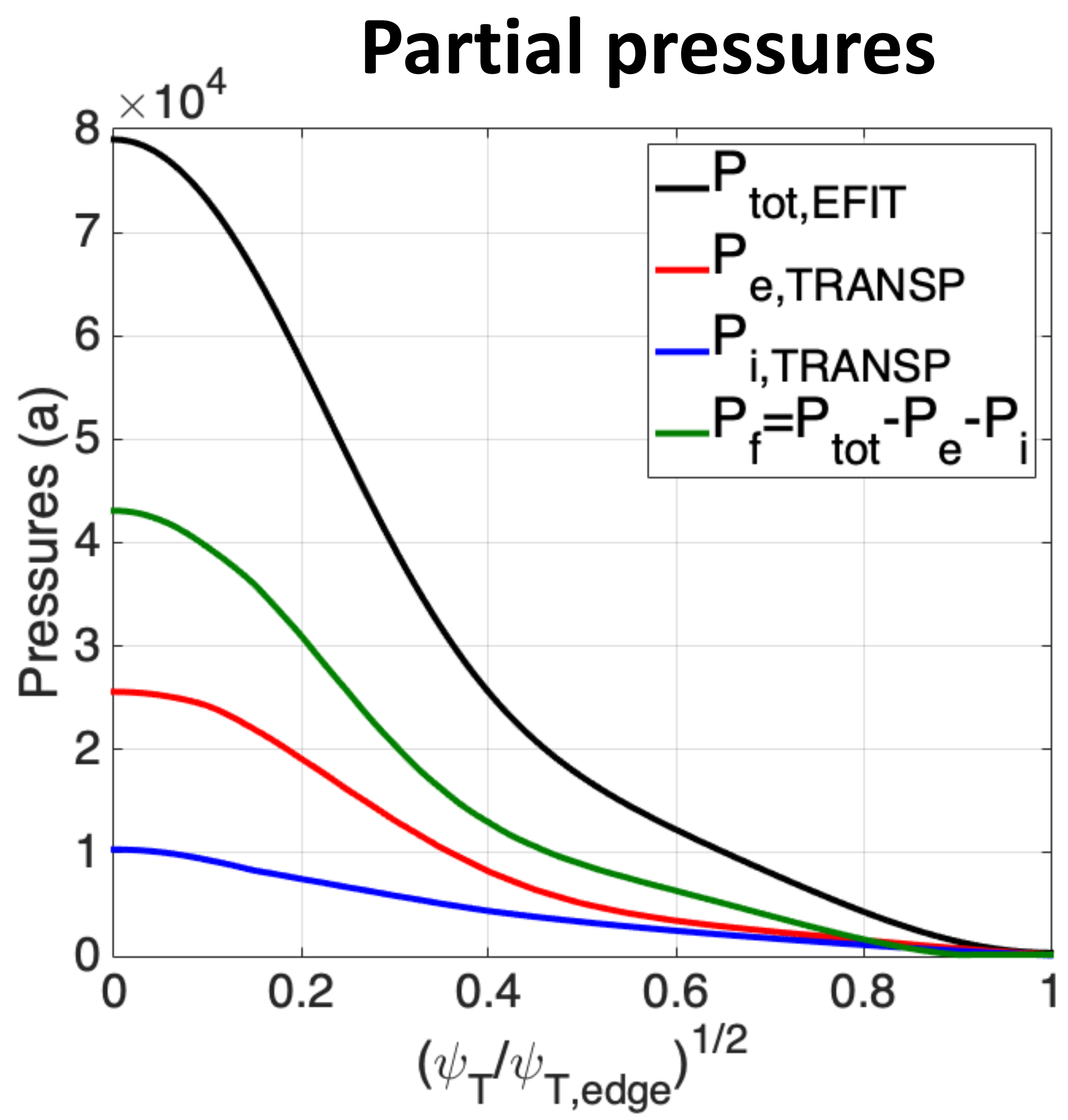

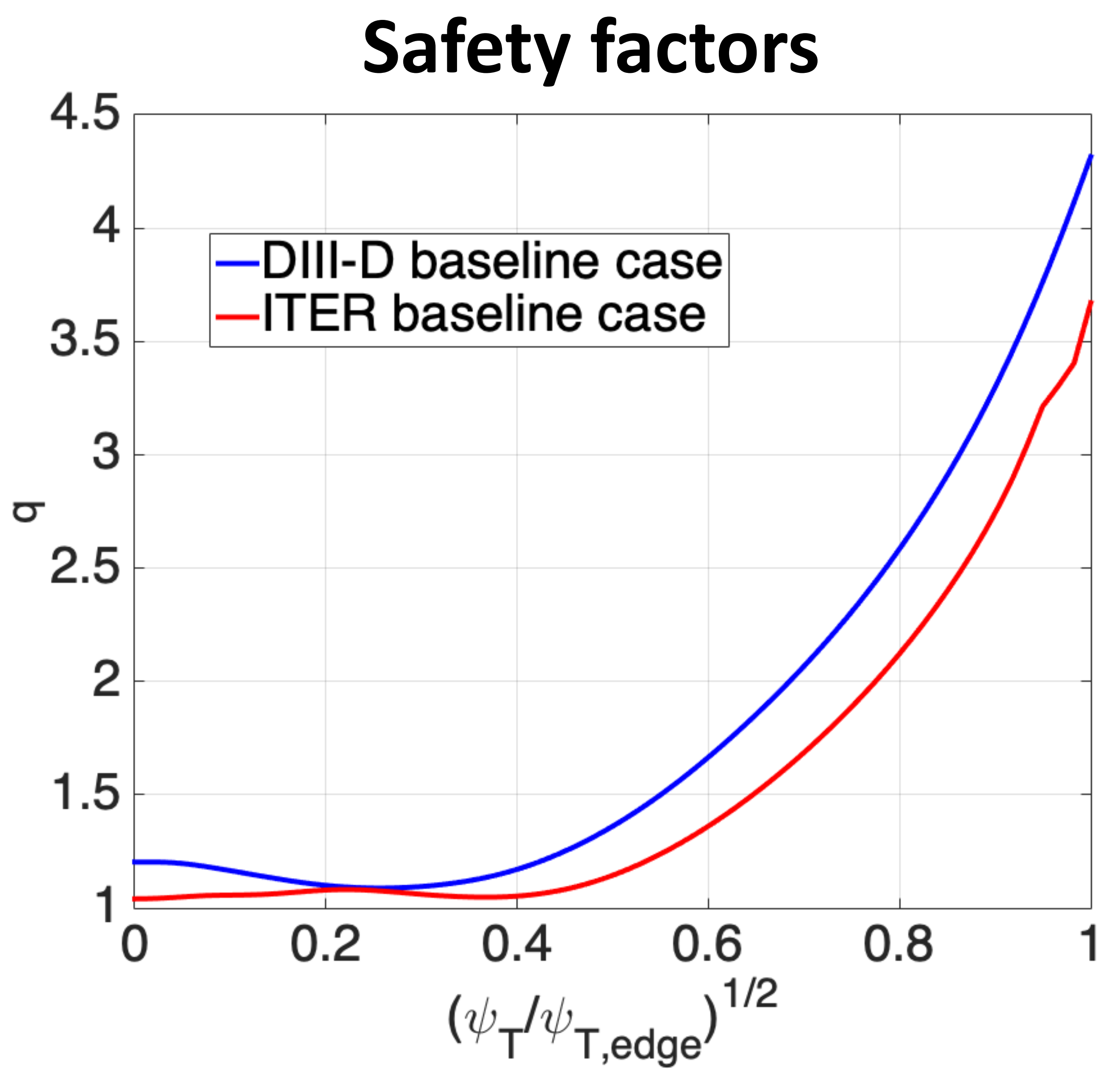

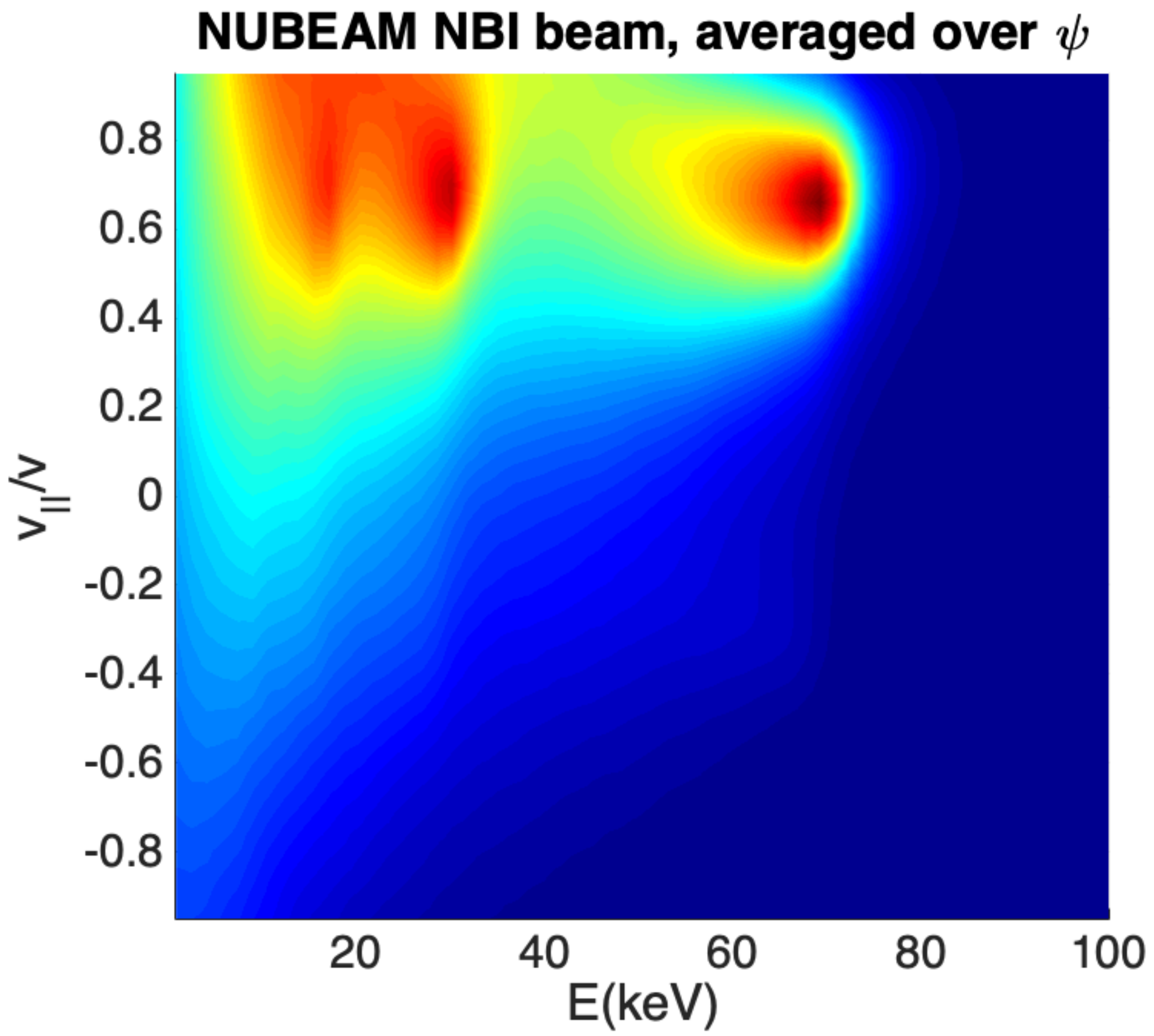

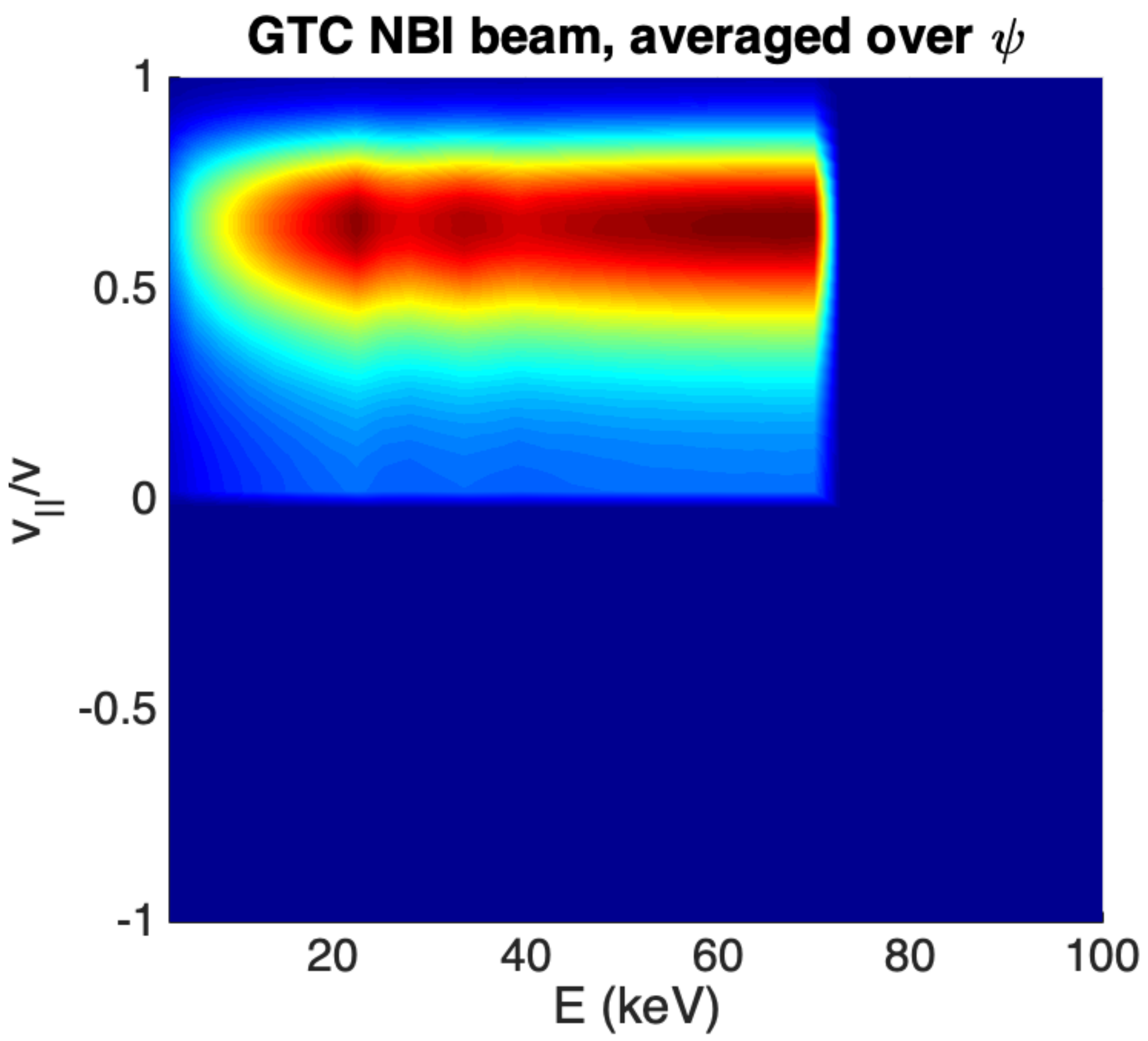

- A **DIII-D discharge** chosen for **experimental validation** with **ITER prefusion baseline scenario (similar q, profile shapes and** β_N**)**
- **N=1 fishbone modes experimentally observed,** with frequencies of order **20kHz**
- **NBI** also modelized with a **anisotropic slowing-down** pdf

Fishbone unstable for DIII-D discharge

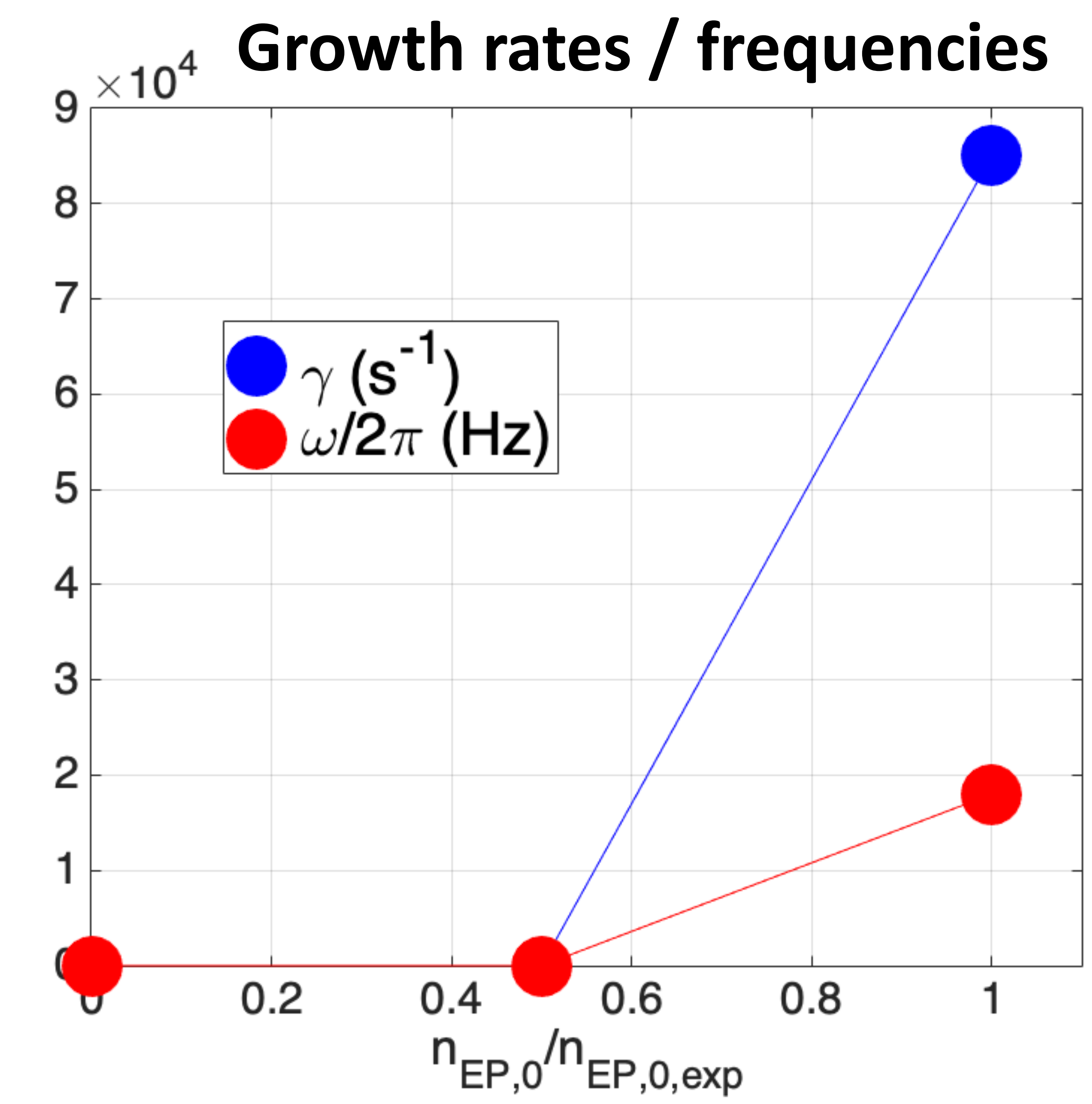

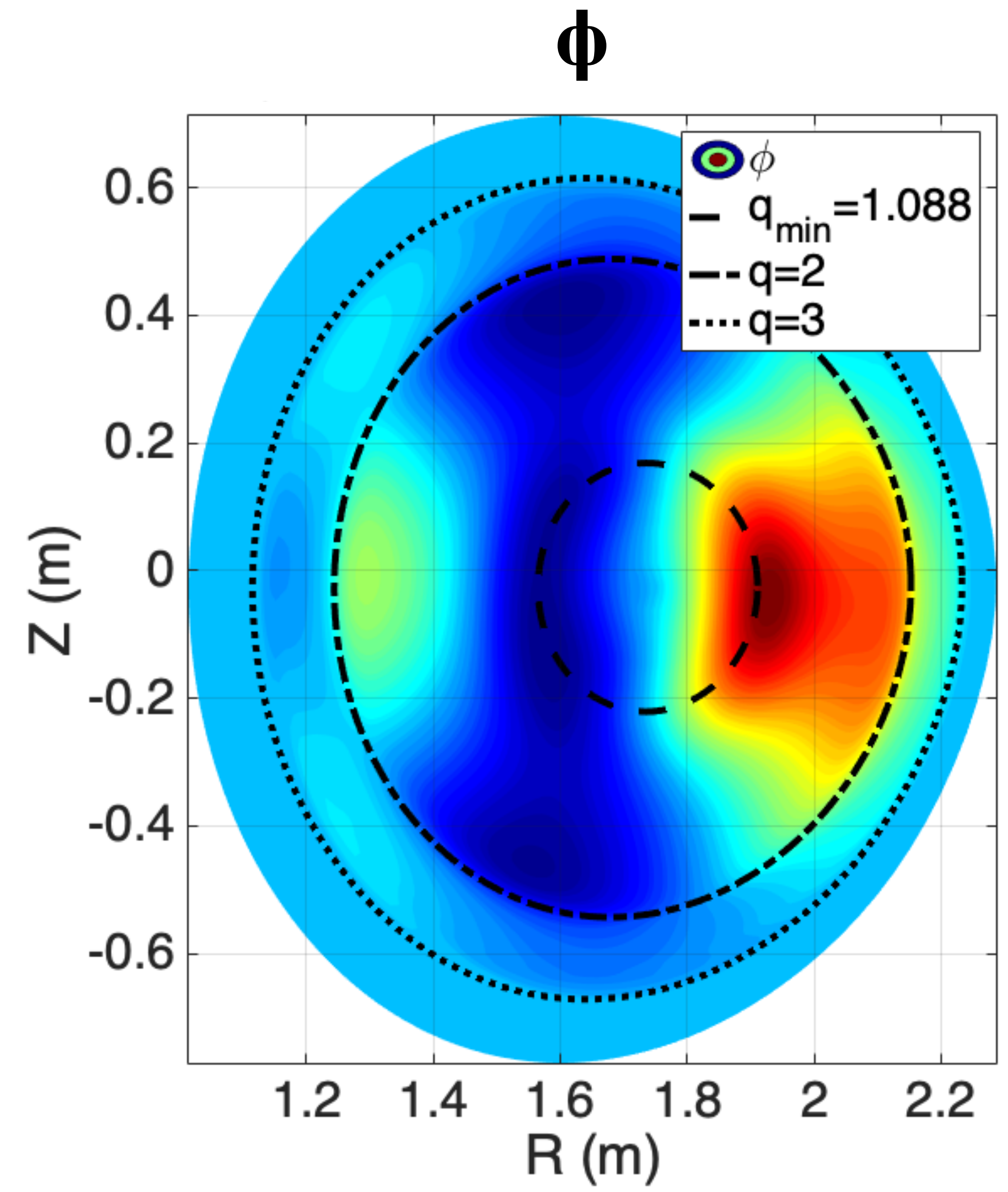

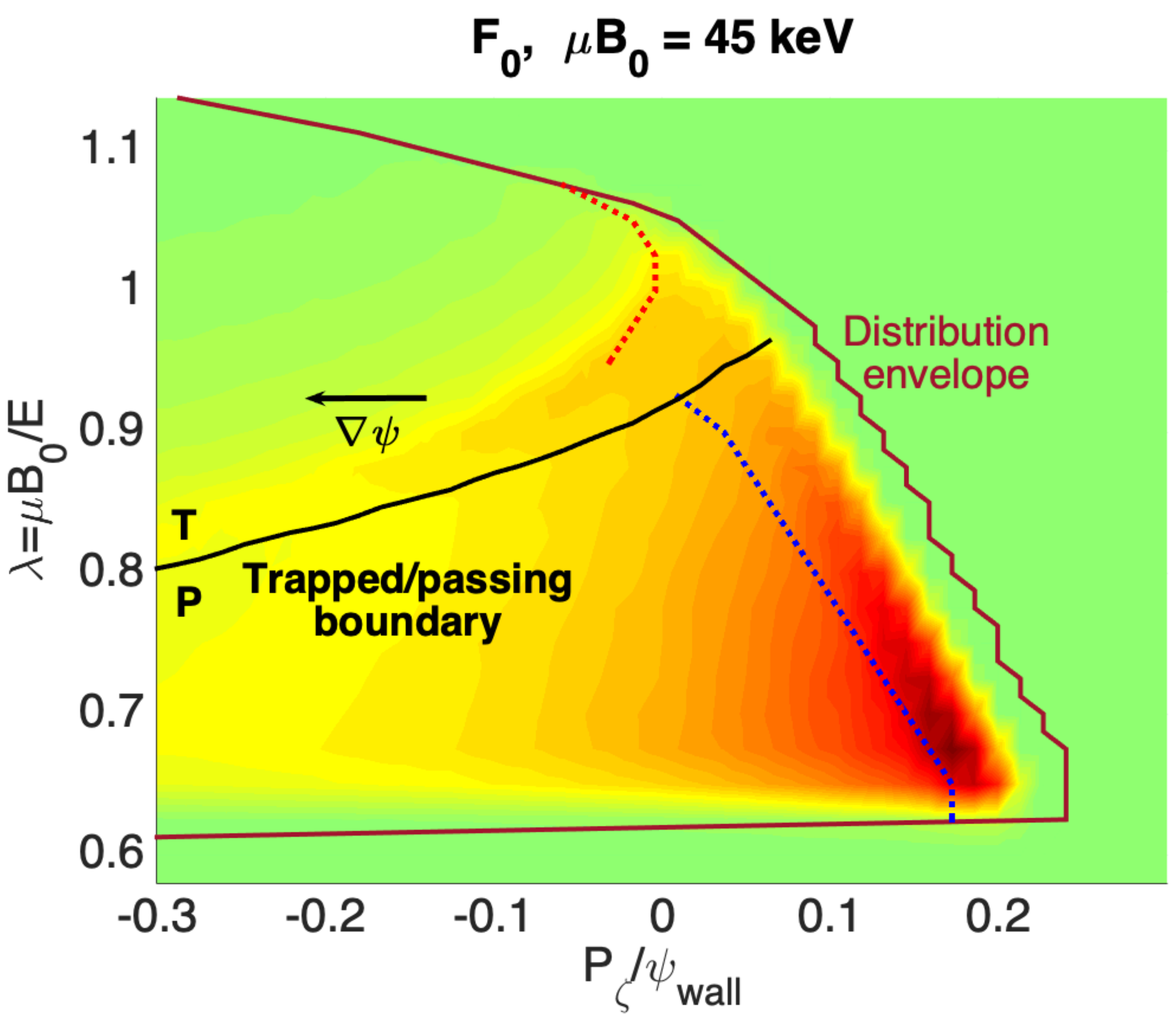

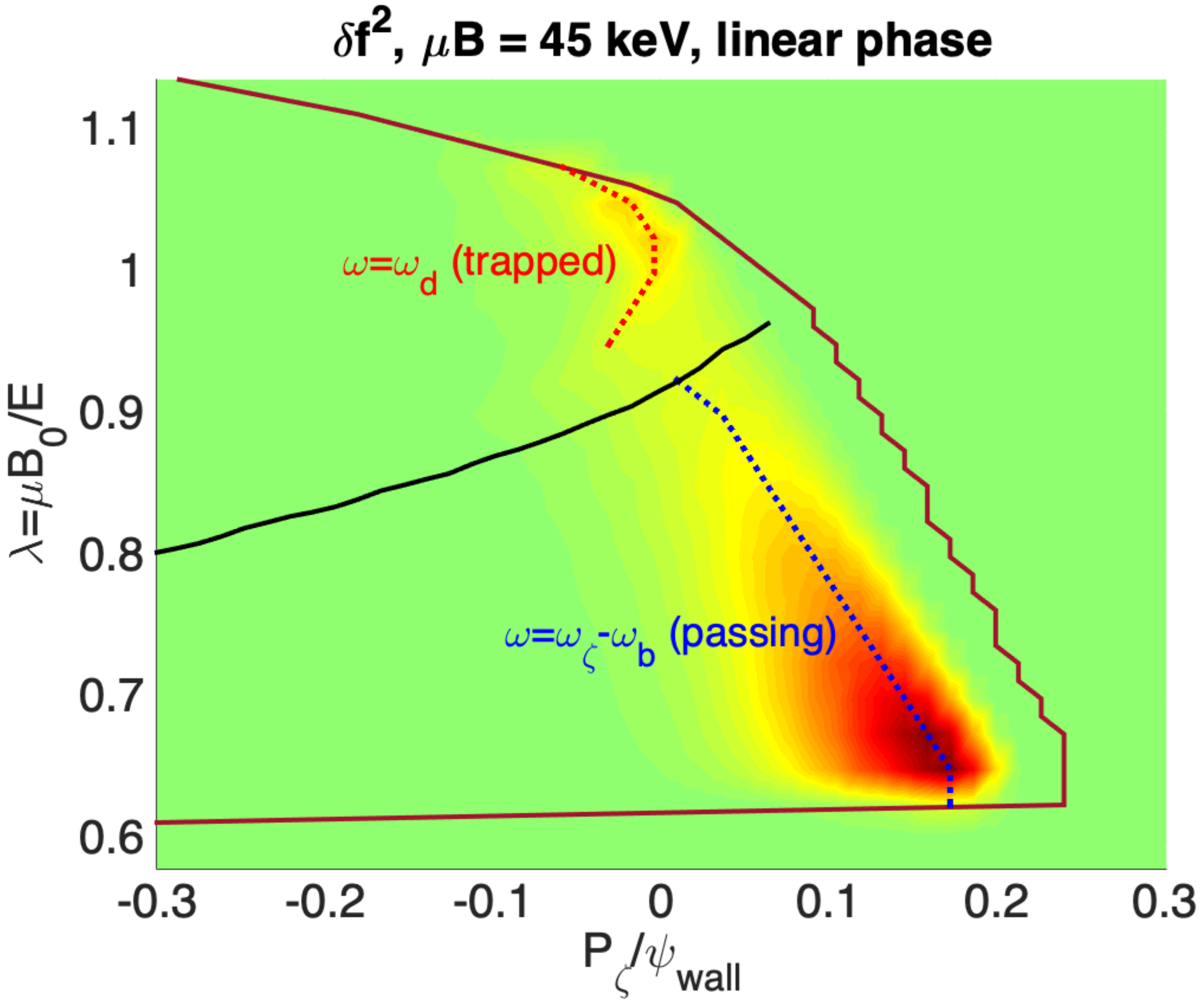

- **Low n modes** stable with **maxwellian EP distributions**
- Using **realistic beam**, a **n=1 fishbone mode destabilised** past a **EP beta,** close to **marginal stability**
- **m=2 side-band** is **significant** and **extends mode structure** close to **plasma edge**
- Both **trapped** and **passing particles** contribute to **resonant interaction**
- **Resonant contribution** from **passing particles** is **dominant**

Zonal flows lower fishbone saturation amplitude

DIII-D NATIONAL FUSION FACILITY

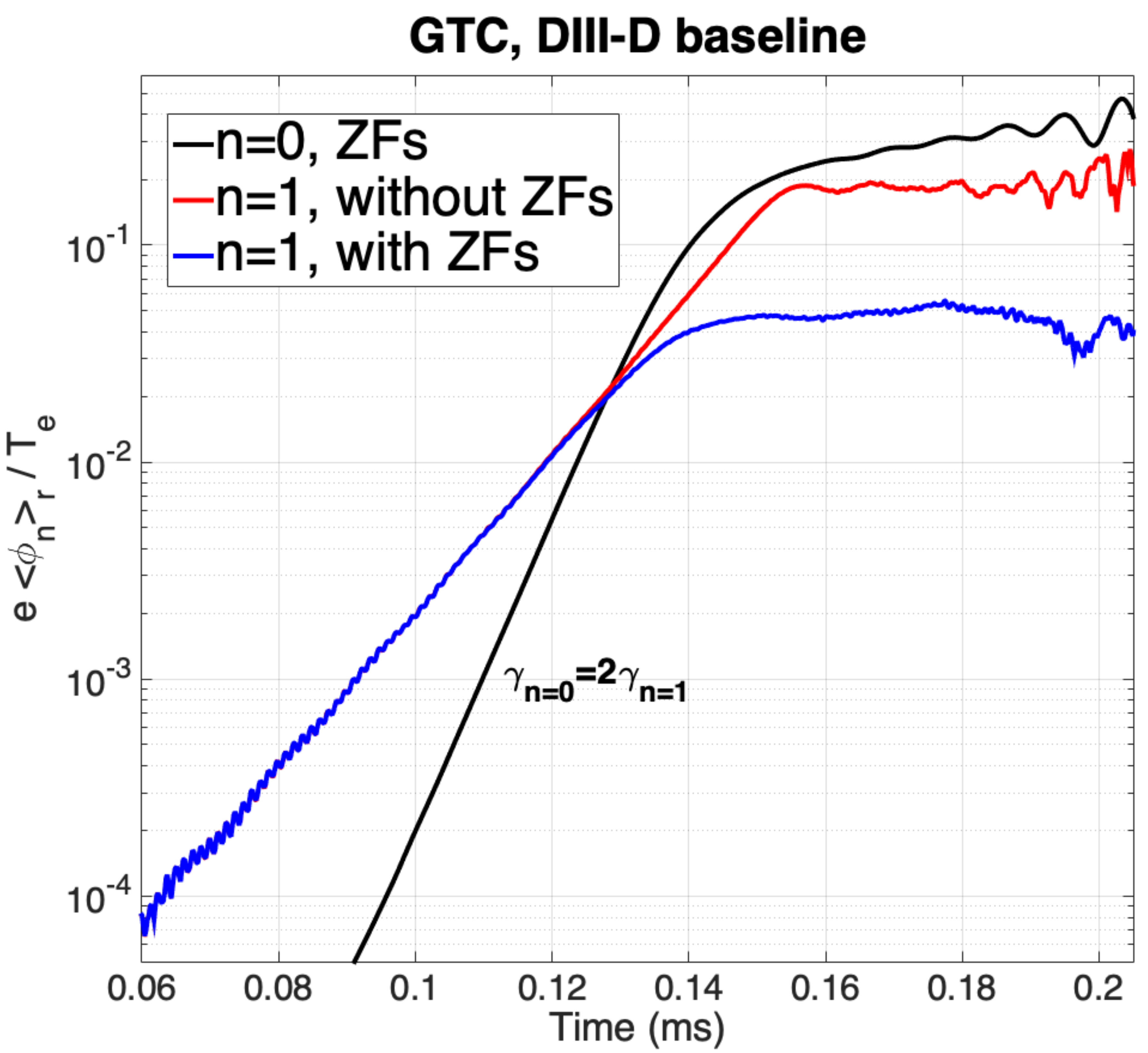

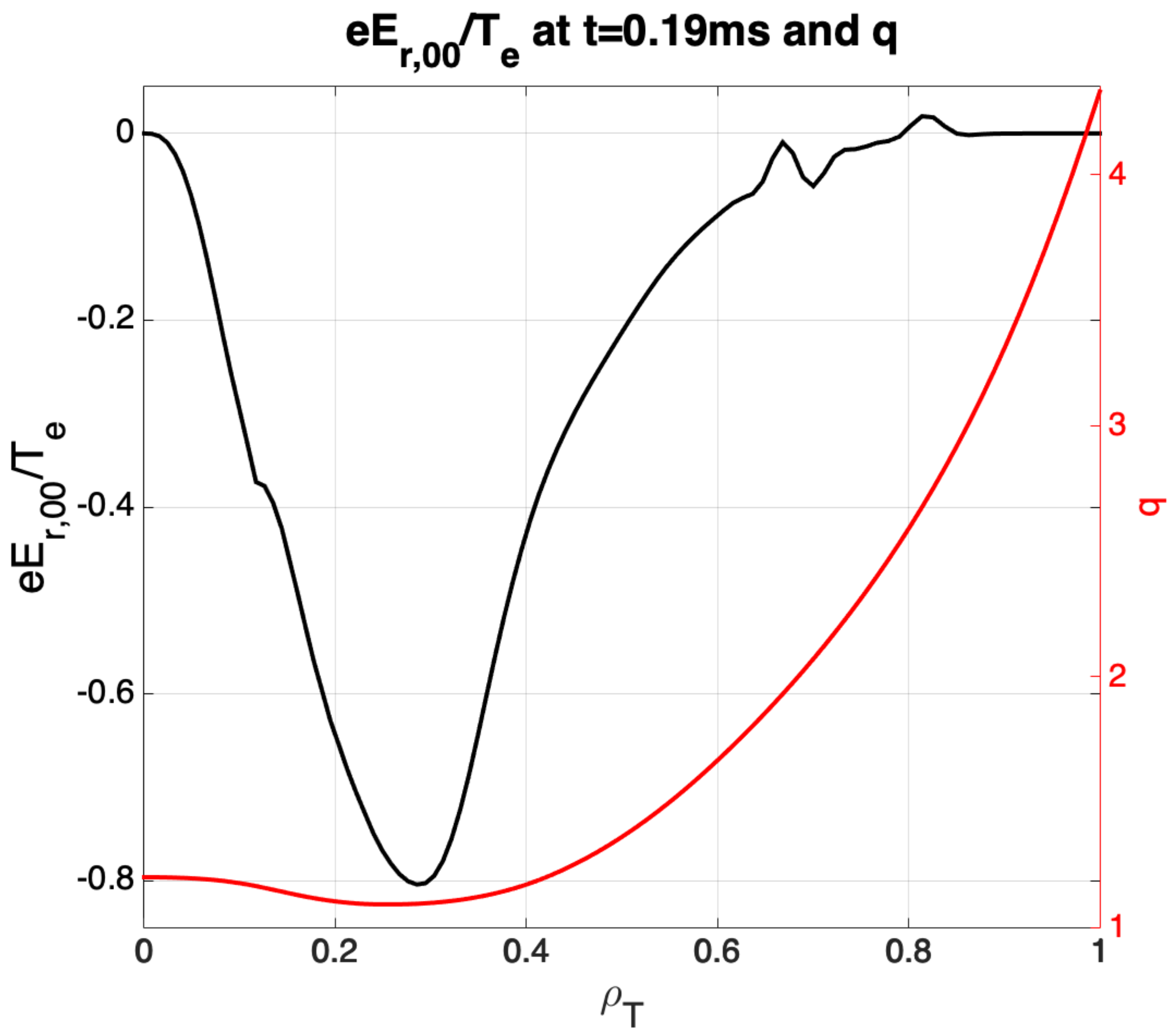

➢ **Nonlinear** GTC simulations performed keeping **only n=1 mode, with and without zonal flows**

➢ **ZFs inclusion** significantly **lowers saturation amplitude,** from $|\delta B/B_0|\sim 8\times10^{-3}$ to 2×10^{-3} **at** q_{min}, highlighting that **wave-particle trapping** is **not** always the **main saturation mechanism** for **fishbones**

➢ **ZFs** have a **growth rate twice of n=1 mode**, typical of force-driven ZFs generation [1]

[1] Z. Qiu et al. 2016, *Phys. Plasmas*

Nonlinear validation against ECE measurements

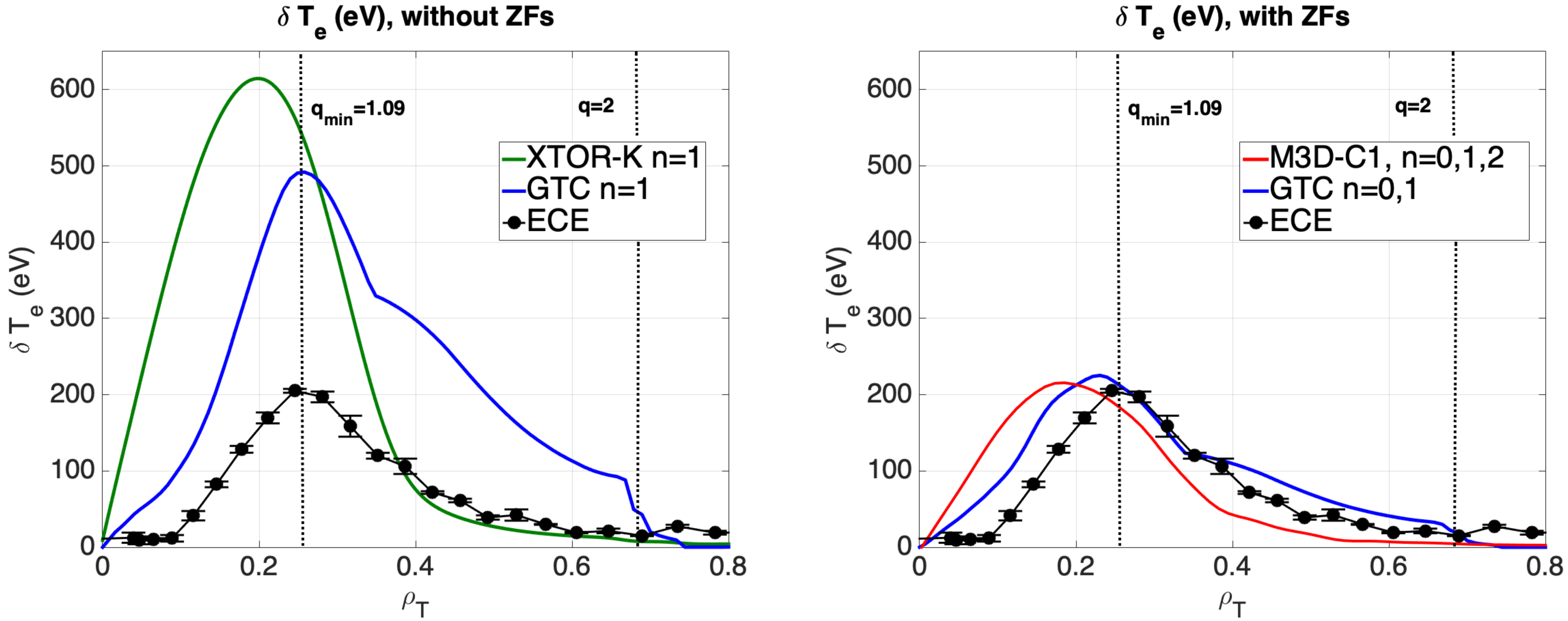

- **Zonal flows inclusion** allow GTC and M3D-C1 to obtain **saturation amplitudes comparable with ECE** [1]
- The significant **m=2 side-band** allows GTC to obtain **a quantitative agreement** with the **ECE**
- Validation **to be completed** with **cross-scales** GTC simulation for more **realistic zonal flows levels**

[1] G. Brochard et al. 2022, to be submitted to *Phys. Rev. Lett.*

Outward EP transport and neutron drop

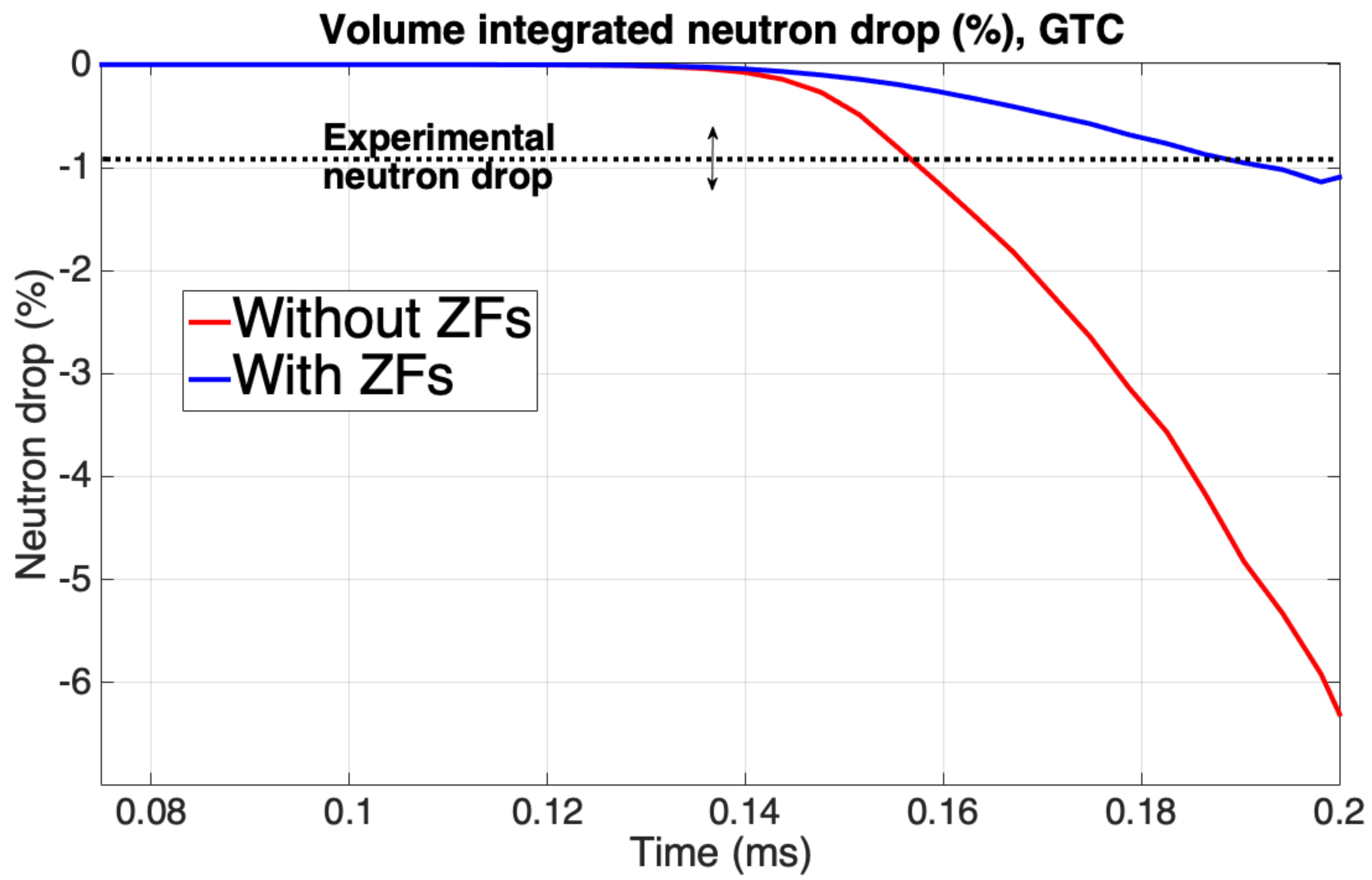

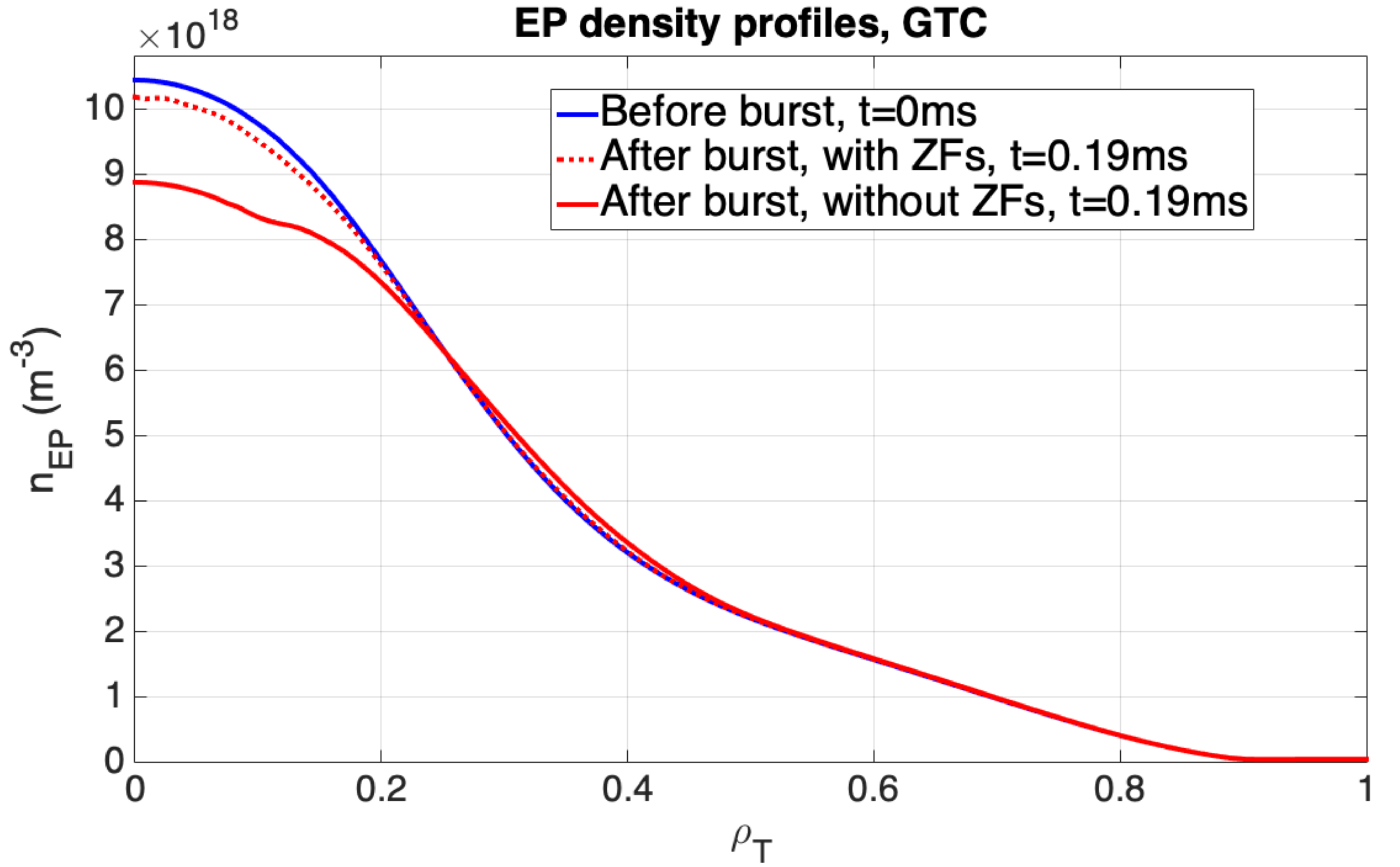

- **Zonal flows** also **lowers** the simulated **neutron drop,** providing a **quantitative** agreement with the **experimental one,** further **validating GTC** for fishbone simulations

- The EP density profile is **flattened** due to **resonant transport** (**$|\delta n_{EP}/n_{EP}| \sim 15\%$ inside q_{min} without zonal flows)**

- **Zonal flows** inclusion lead to **weaker EP transport** (**$|\delta n_{EP}/n_{EP}| \sim 3\%$ inside q_{min}**)

Zonal flows generate additional drift for EPs

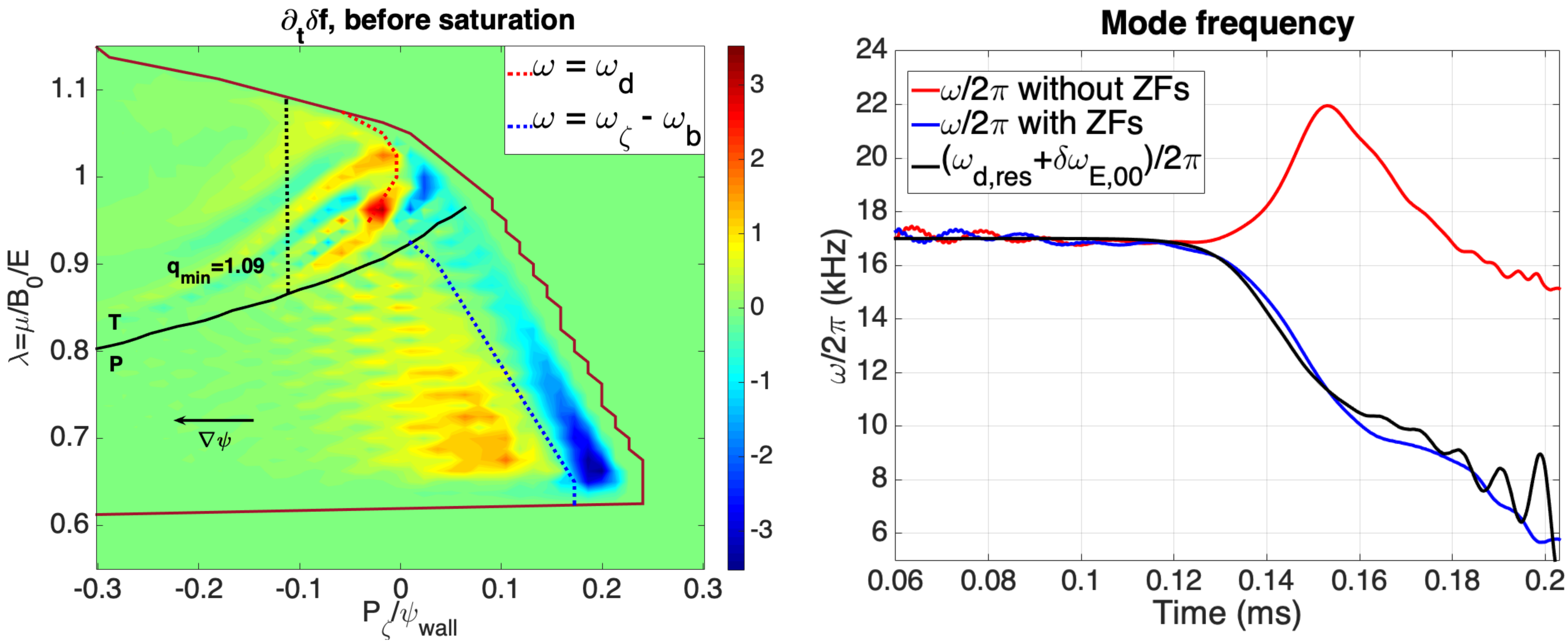

➢ **Hole and clump** structures **appear** around both **trapped** and **passing resonances**

➢ Fishbone **frequencies chirp down** at **saturation with** and **without ZFs**

➢ ZFs provide an additional **drift frequency** $\delta\omega_{E,00} = -\partial_\psi\phi_{00}$**, locking linearly resonant EPs**

Zonal flows prevent more EPs to become resonant

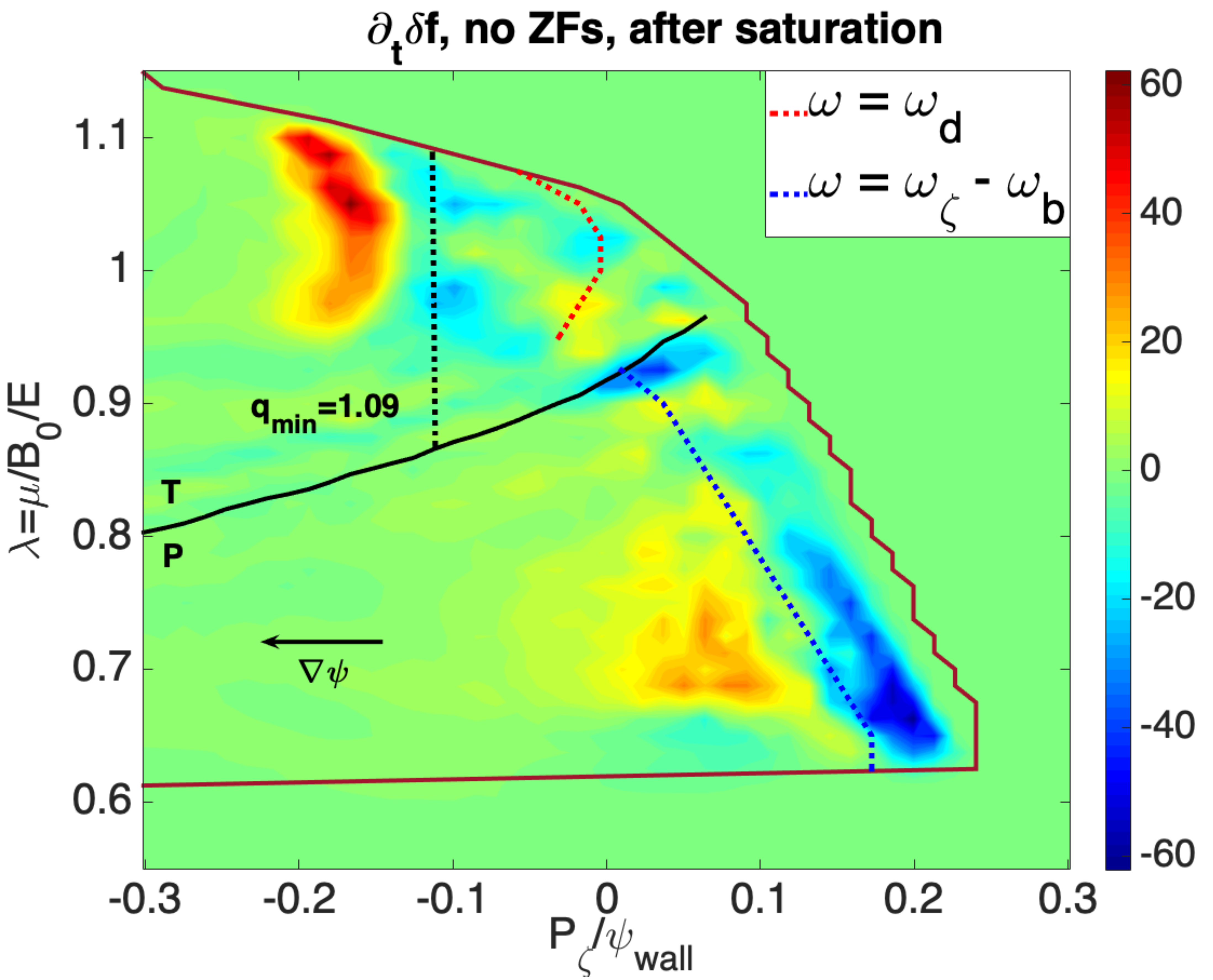

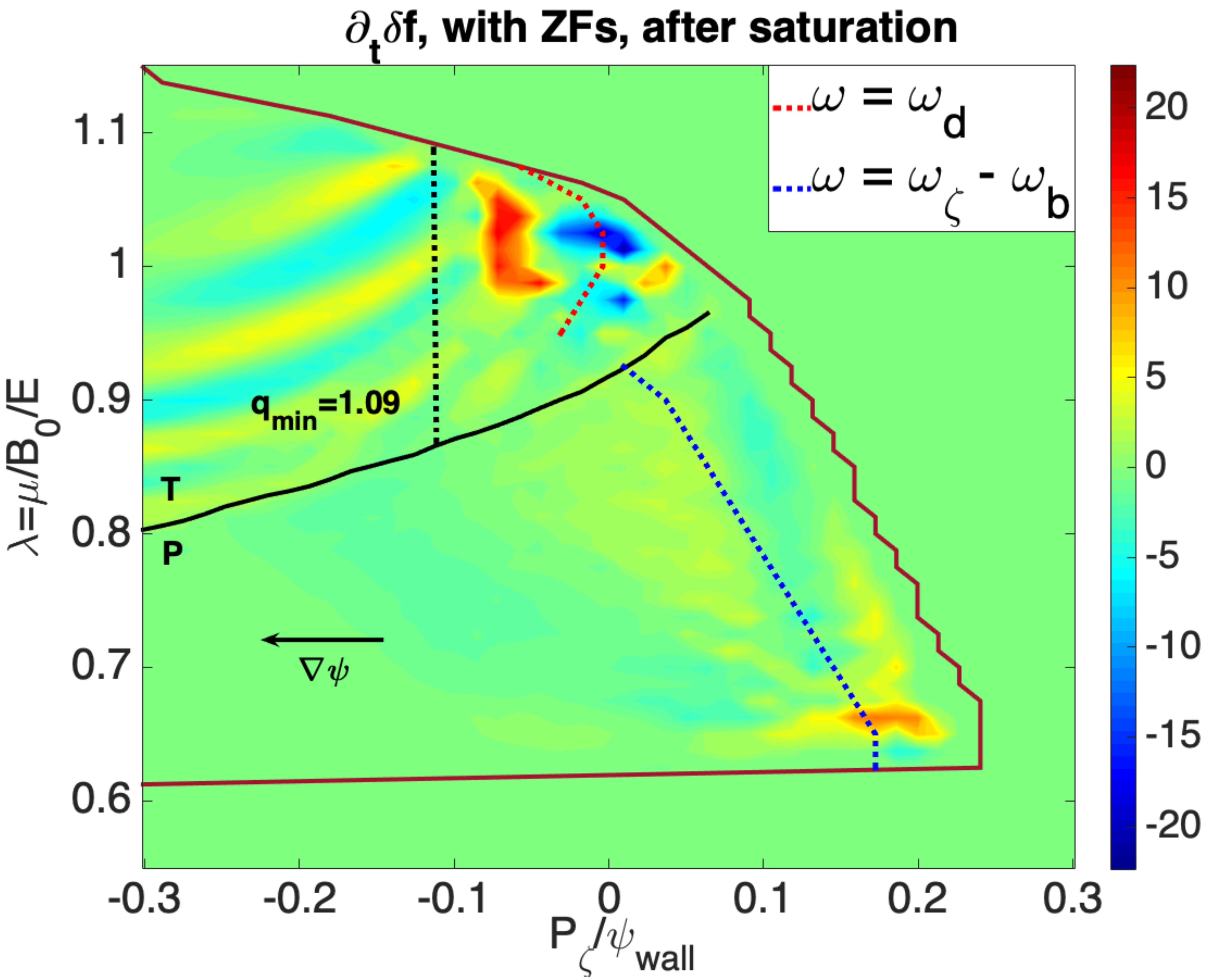

- **Precessional hole** and **clump** stays indeed **static** with **zonal flows**, reducing
- **Resonant passing EPs** are **detuned by ZFs**, potentially due to ZFs effects on **transit frequency**
- **ZFs prevent** phase space **structures** from **affecting new EPs, explaining fishbone mitigation** by **ZFs**

Fishbone-induced ZFs can lead to ion-ITB

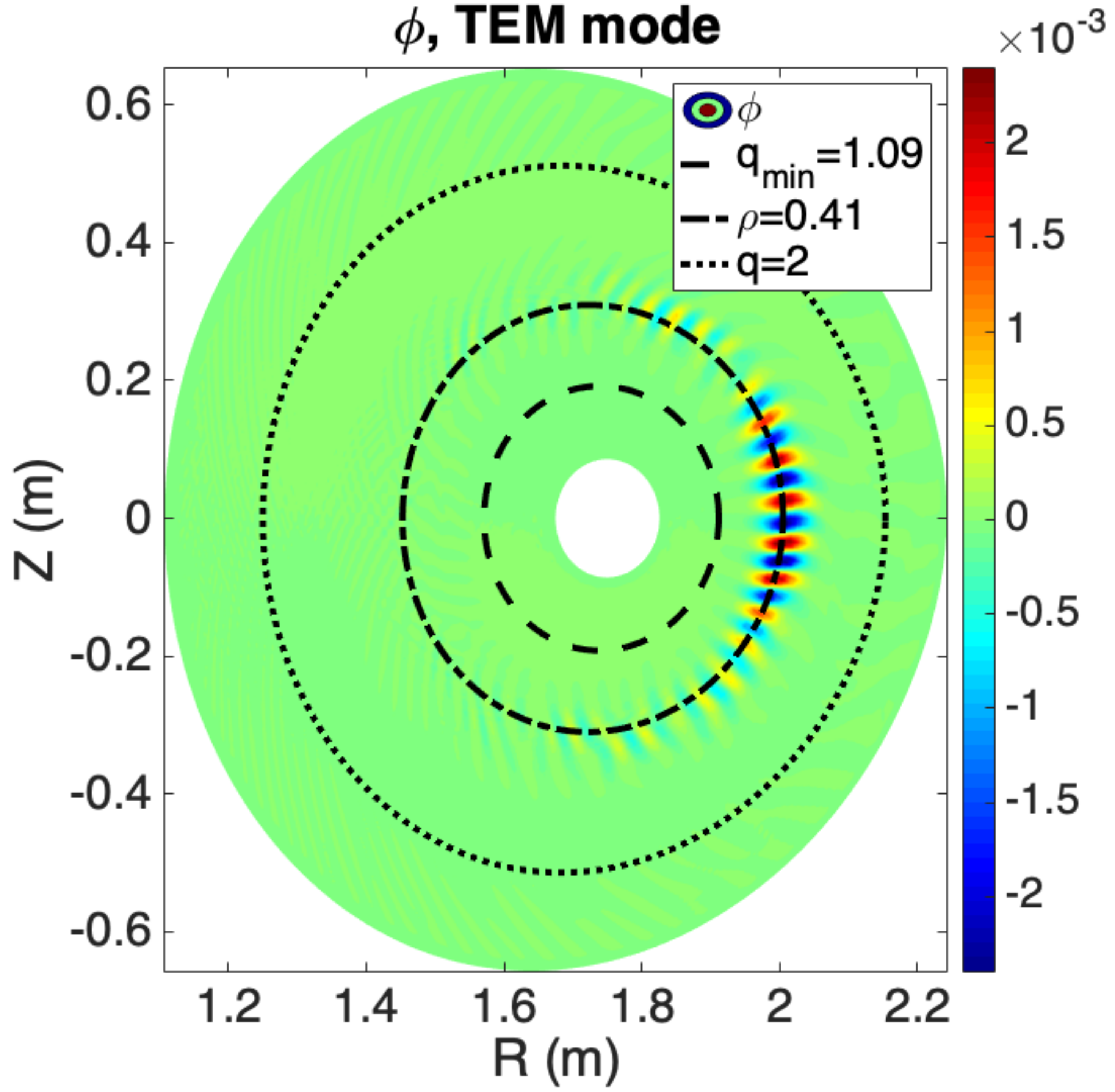

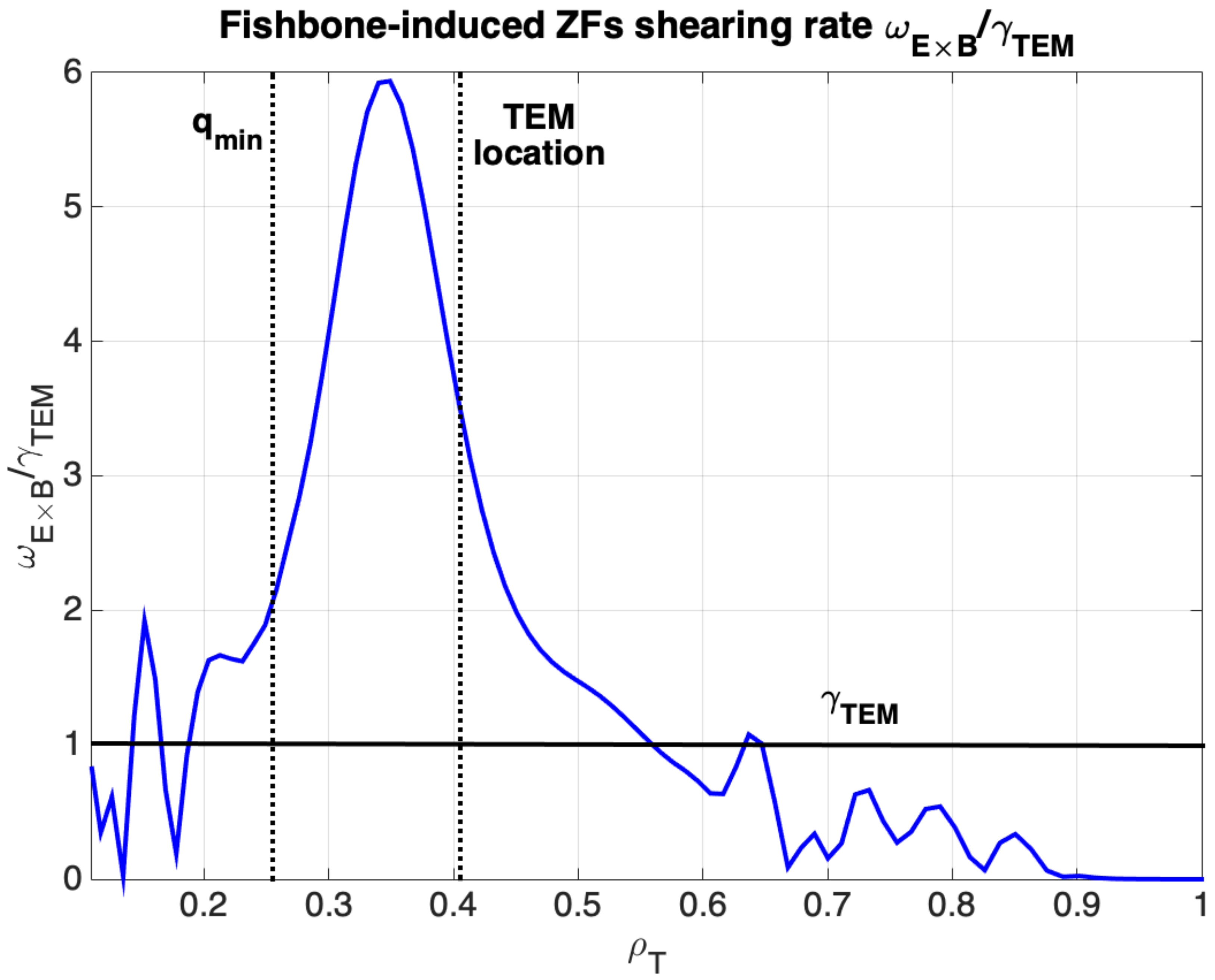

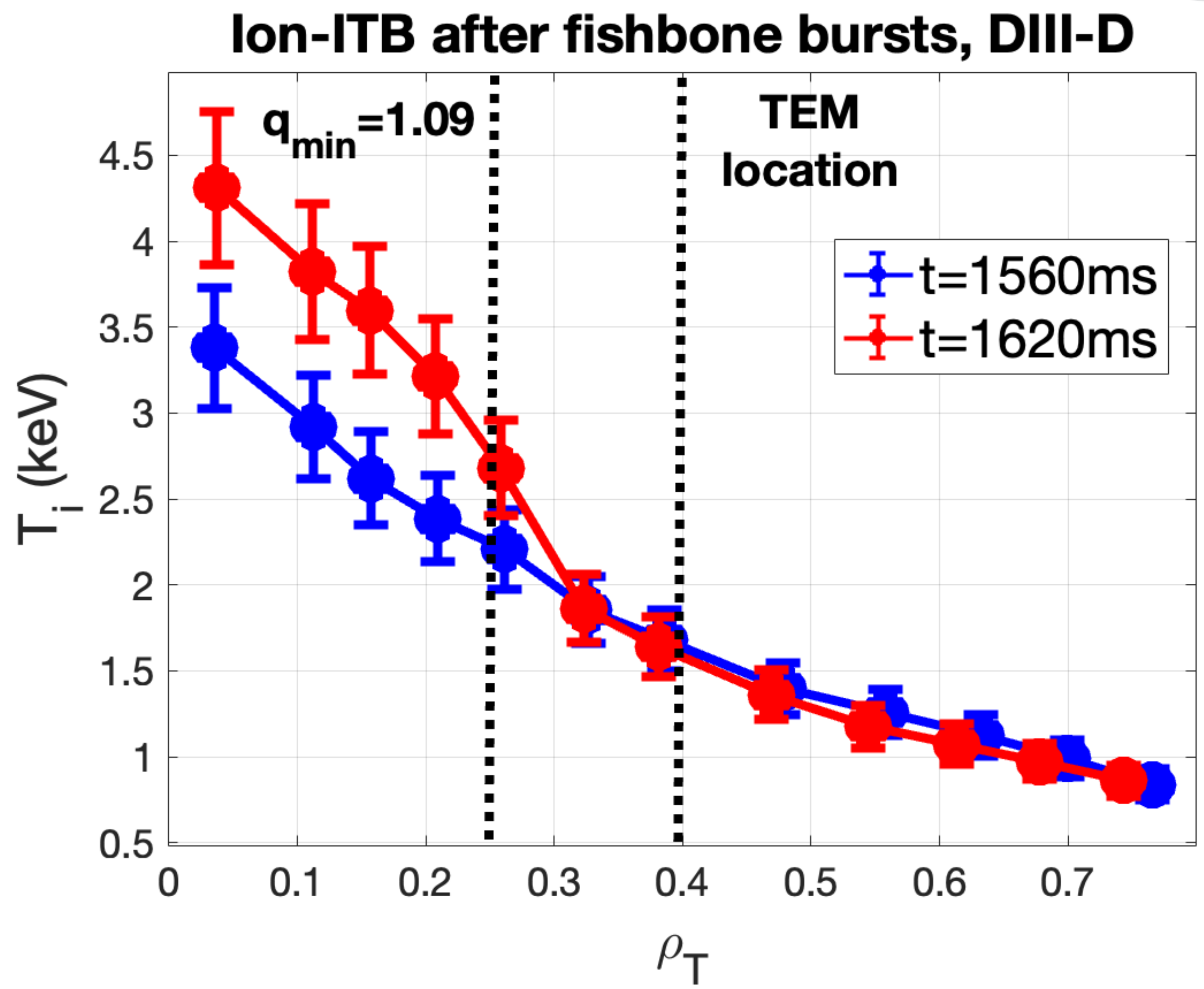

- GTC **electrostatic** simulations find an **unstable TEM mode** at $\rho = 0.41$ with $\gamma_{TEM} = 1.38 \times 10^5 s^{-1}$
- **Fishbone-induced $\omega_{E\times B}$** much **larger** at saturation than γ_{TEM}, which can lead to **turbulence suppression**
- **Ion-ITB** observed in **DIII-D** after **fishbone bursts** occuring at $t \in [1580,1620]$ ms, as in ASDEX [1], MAST [2], HL-2A [3], EAST [4]
- **Cross-scales** GTC simulations with $n \in [0,50]$ **required** to confirm **fishbone-induced ITB**

[1] S. Günter et al. *Nucl. Fusion,* 2001
[2] A. R. Field et al., *Nucl. Fusion* 2011
[3] W. Chen et al. *Nucl. Fusion,* 2016
[4] X. Gao et al. *Physics Letters A* 2018

Outline

I) Interplay fishbone/zonal flows in gyrokinetic simulations

A) Experimental fishbone validation on a DIII-D discharge

B) Predicted fishbone dynamics in ITER PFPO-2 scenario

II) Computation of CoMs EP distribution in IMAS

A) Versatile method for coordinate transformation

B) Application for NBI and alpha distributions in a JET-DT pulse

Fishbone unstable with realistic beam in ITER

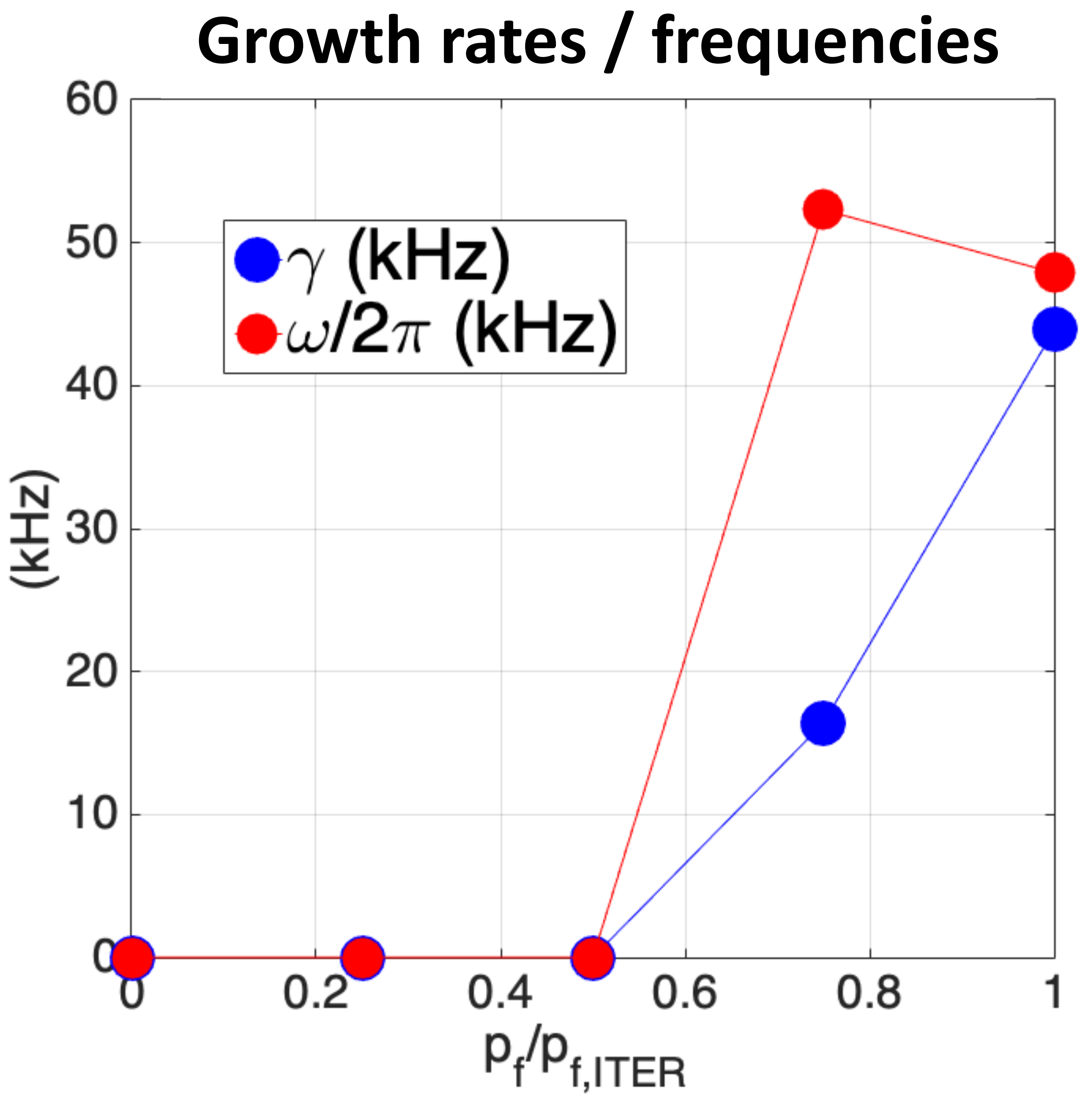

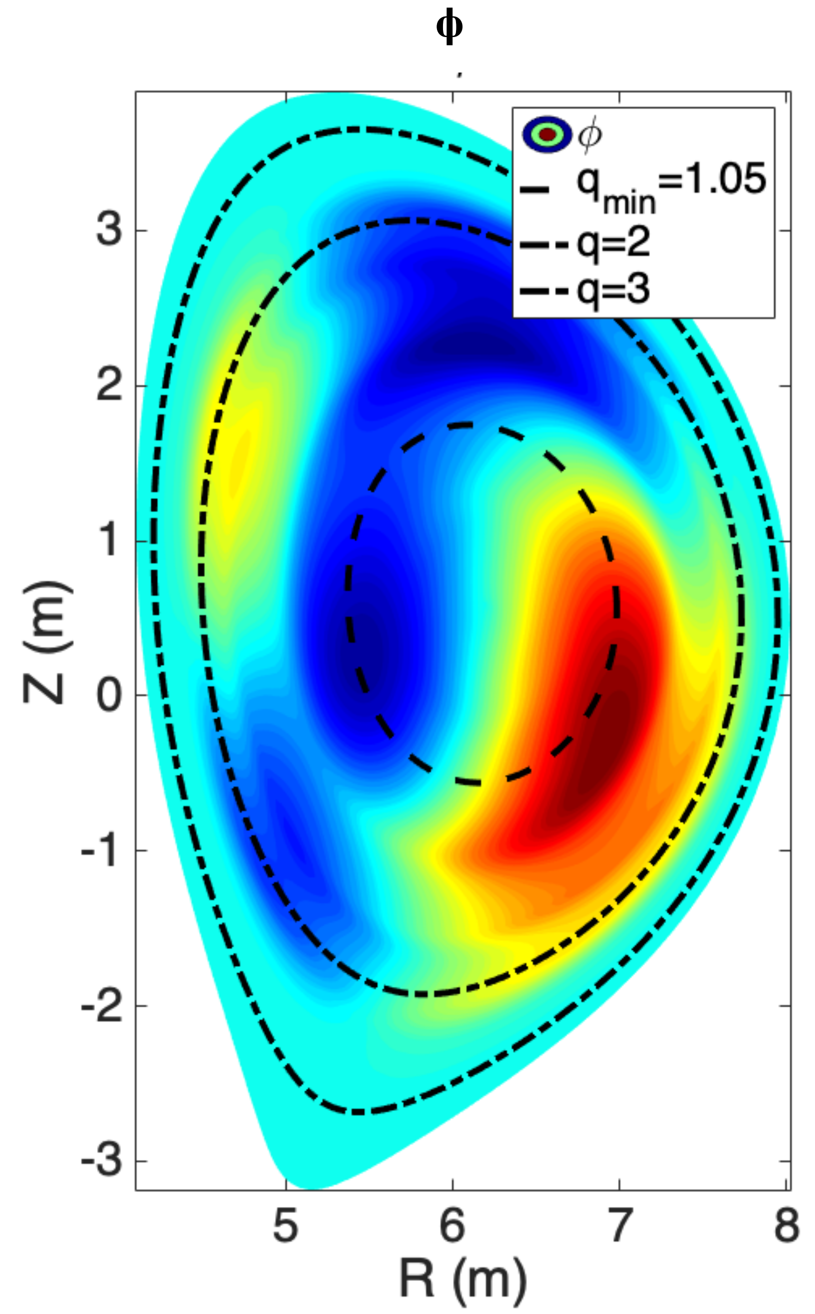

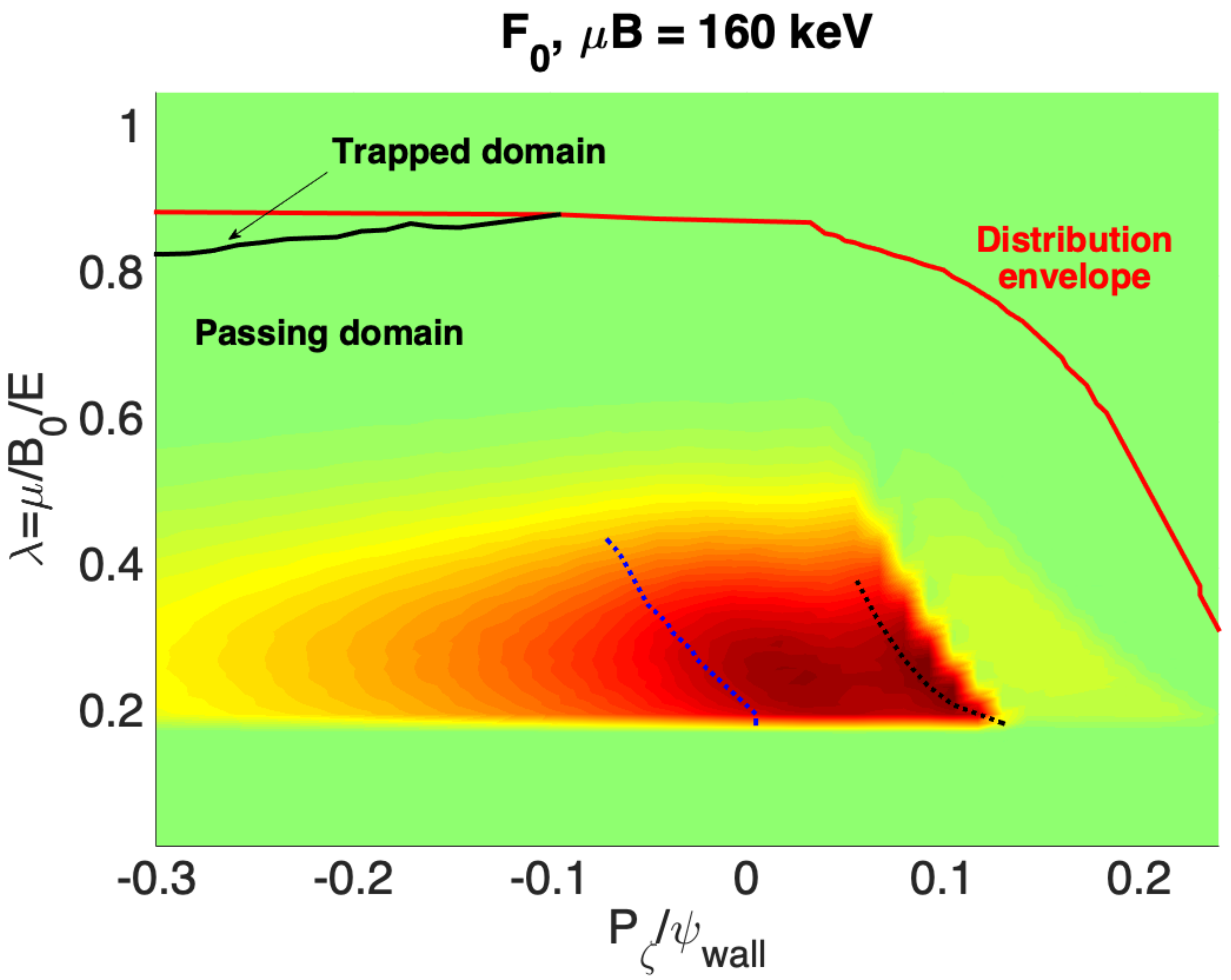

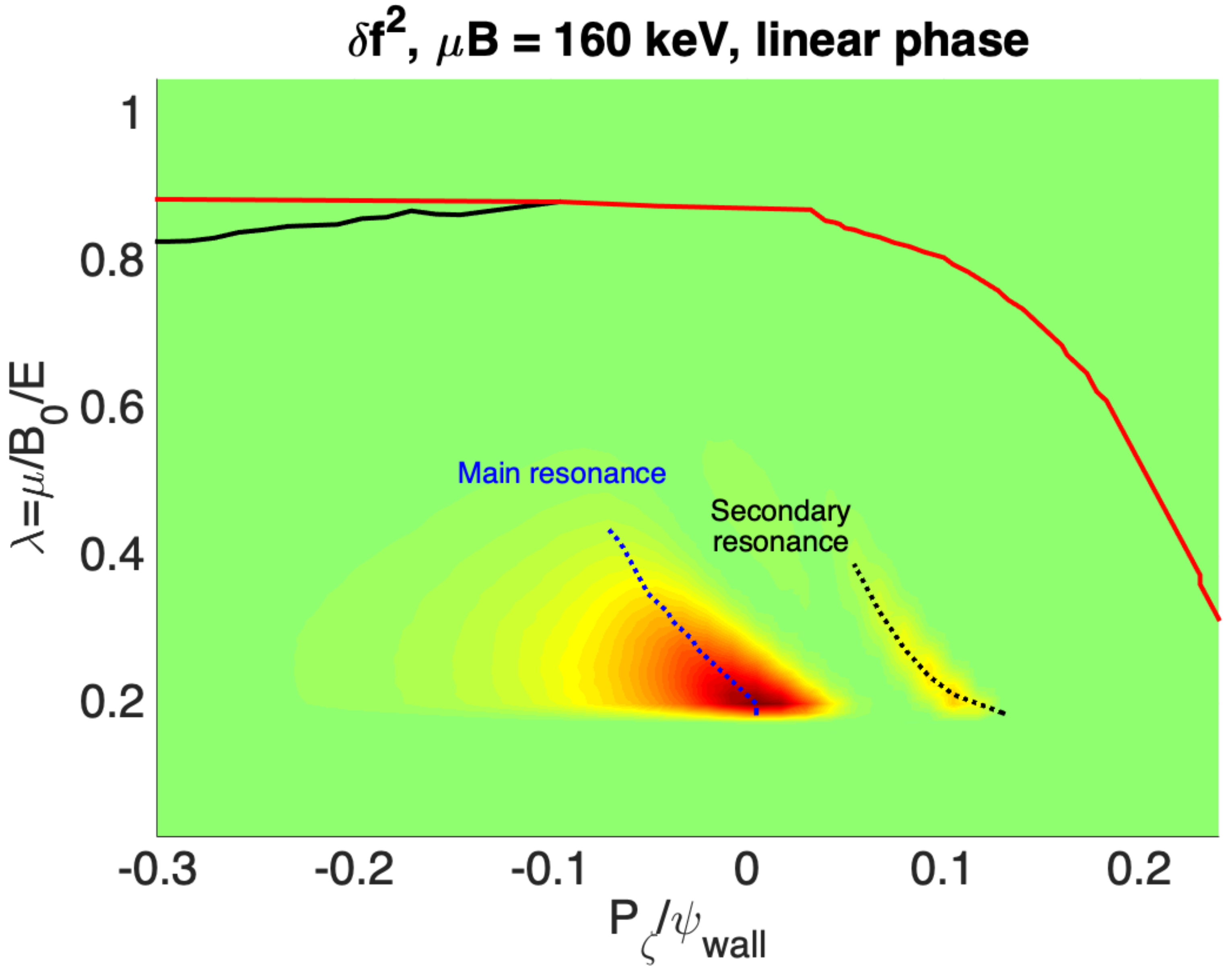

- Low n modes also **stable** with **maxwellian fast ion** kinetic effects
- With **anisotropic slowing-down pdf** for **fast ions**, a dominant n=m=1 fishbone mode is **destabilized**
- Similarly to the **DIII-D discharge,** the **mode has** a **significant m=2 side-band**
- **Fishbone** mode **driven** by **passing particles** through **two drift-transit resonances [1]**

[1] R. Betti et al. PRL 1993

Zonal flows also impact the ITER scenario

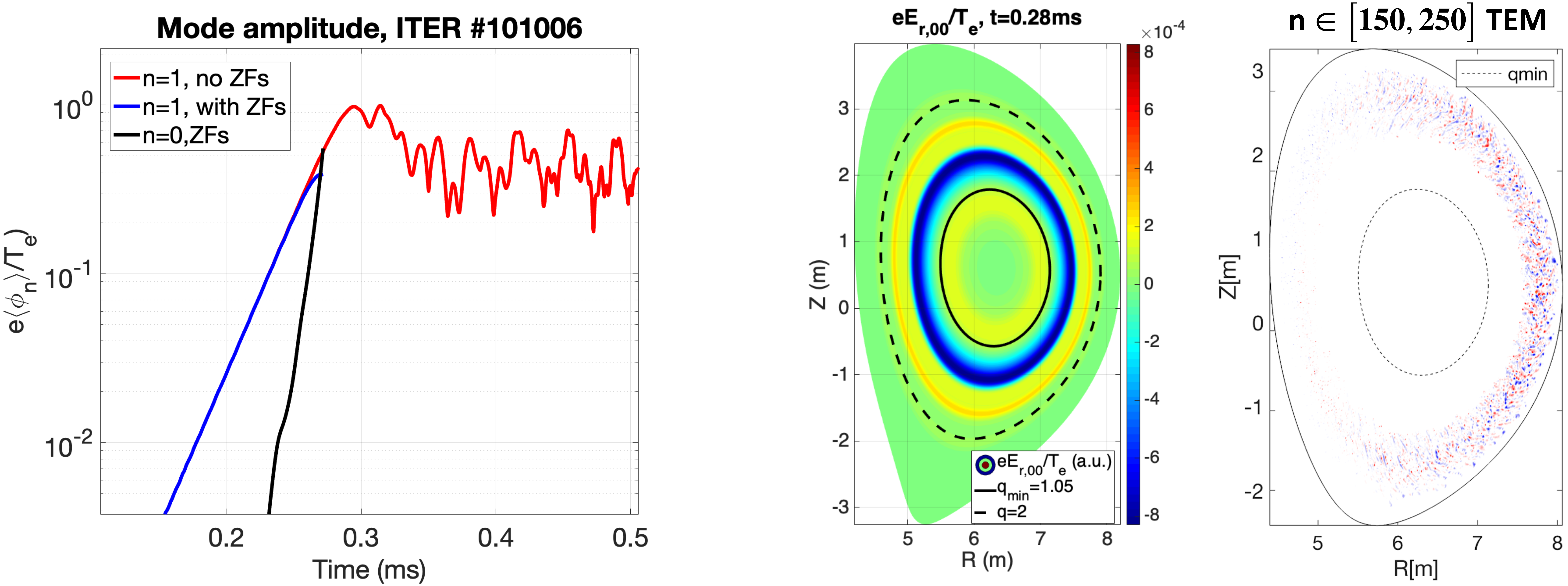

- ➢ **Nonlinear** GTC simulations performed again keeping **only n=1 mode, with and without zonal flows**
- ➢ **ZFs inclusion** again **lowers saturation amplitude,** from $|\delta B/B_0|\sim 4\times10^{-4}$ to 1×10^{-4} **at** q_{min}
- ➢ Fishbone-induced $\omega_{E\times B}/\gamma_{TEM} \sim 3$ **at saturation,** could lead to **ITB formation** in this **ITER scenario**
- ➢ **Long time** simulation **with zonal flows and fishbone** to be performed with **GTC**

Marginal EP transport in ITER scenario

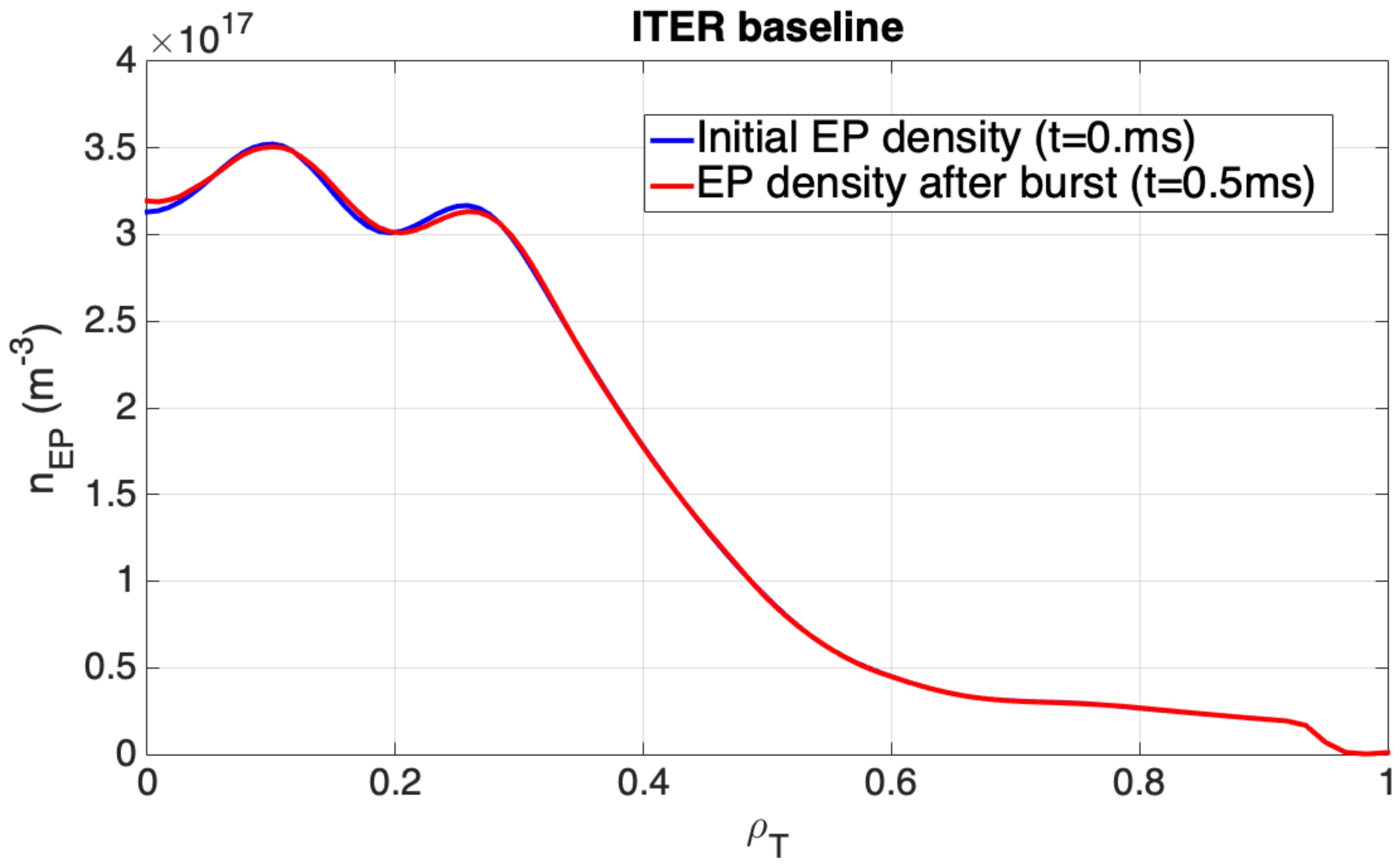

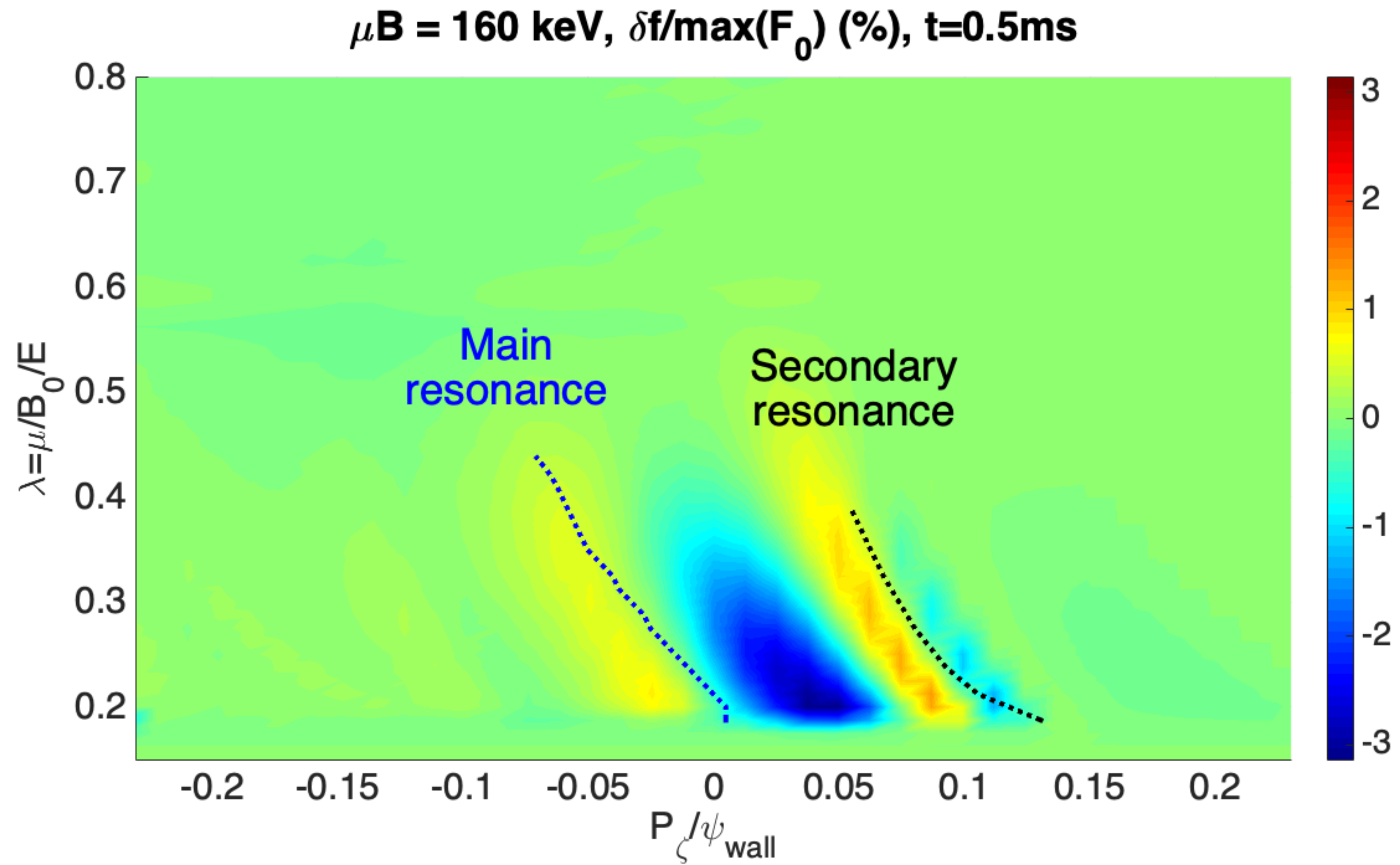

- **Inward** and **outward EP fluxes** exist due to **positive and negative pressure gradients**

- **EP redistribution** is **marginal**, up to **2%** of **initial density profile** [1] without zonal flows. **Similar levels** were found for the **alpha-fishbone** in **ITER 15 MA DT** scenarios [2]

- **NBI pressure drive too low** to cause **large redistribution**

- **Hole and clump** structures **form** in **phase space, but saturate at low amplitude**

[1] G. Brochard et al. 2022, to be submitted to *Phys. Rev. Lett.*
[2] G. Brochard et al. 2020b, *Nucl. Fusion*

Conclusions and perspectives

- ➢ **Zonal flows** can be force-driven by **fishbone modes** and **dominate their saturation**

- ➢ Simulated **fishbone saturation levels** in **quantitative agreement** with **ECE** and **neutron drop** measurements on **DIII-D with zonal flows**

- ➢ **Zonal flows reduce** available **resonant EPs,** providing the **mechanism** for **fishbone saturation**

- ➢ **Fishbone-induced zonal flows** may lead to **microturbulence suppression,** supported by **ion-ITB formation** after fishbone bursts **in DIII-D**

- ➢ **Cross-scales** simulations on DIII-D and ITER **required** to confirm **fishbone-induced ITBs causality**

- ➢ **High performance scenarios** could be developed in **ITER** by **triggering benign fishbones**

Outline

I) Interplay fishbone/zonal flows in gyrokinetic simulations

A) Experimental fishbone validation on a DIII-D discharge

B) Predicted fishbone dynamics in ITER PFPO-2 scenario

II) Computation of CoMs EP distribution in IMAS

A) Versatile method for coordinate transformation

B) Application for NBI and alpha distributions in a JET-DT pulse

Versatile method for CoM distribution construction

I) Construction of **CoM Jacobian** on a **cartesian** $(E, \lambda = \mu B_0/E, P_\varphi)$ **grid**

II) Inputs from **Fokker-Planck codes** or **experimental measurements**

III) 3D C^2 spline function of the CoM distribution F($(E, \lambda, P_\varphi, \sigma$=-1,1)

Full-F codes

3D **Monte-Carlo sampling** based on spline CoM distribution

Backward transformation in 5D/6D cartesian/Boozer coordinates

δF codes

IV) C^1 first order derivatives along CoM ∂_i F($(E, \lambda, P_\varphi, \sigma)$)

IV) Chain rule operations to obtain C^1 $\nabla F|_{\mu,v_{||}}$ and $\partial_{v_{||}} F|_{\mu,X}$

- A **cartesian CoM grid** is first built to determine **orbits' nature** and J_{CoM}
- **Distributions/markers** in « regular » **(E,p,R,Z)** coordinates are loaded from **FK codes** or **experimental measurements**
- A C^2 **spline** of the **3D CoM distribution** is defined to ensure **good numerical properties** for both **full-F** and δf **codes**
- A **backward** $(E, \lambda, P_\varphi, \sigma)$ **->** (E, p, R, Z) **transformation** is used to **load markers uniformly along orbits for full-F codes**
- For δf **codes**, the **weigh equation** can be fully defined by using C^1 **first-order CoM derivatives (**using a **chain rule)**

Construction of a smooth CoM jacobian

Generalised midplane

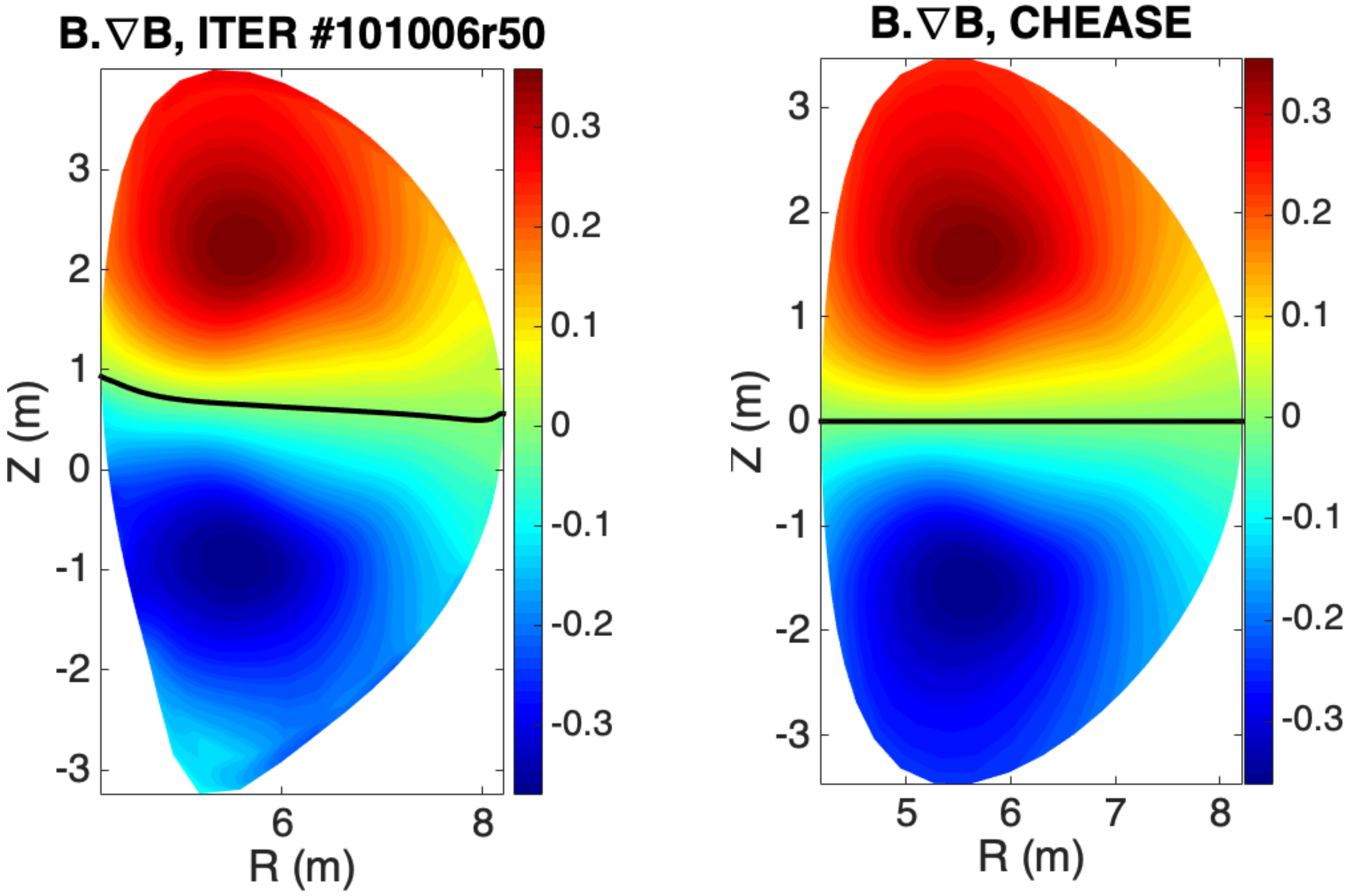

- A method based on a **cartesian CoM grid** (E, λ, P_φ) avoid some **singularities** on $\boldsymbol{J_{CoM}}$ and $\boldsymbol{\Delta V_{CoM}}$ observed in [1]
- $J_{CoM} \propto \sum_\sigma \tau_b(E, \lambda, P_\varphi)$, **orbit tracing necessary** to obtain τ_b in 3D, requiring a **backward transformation** to initialise markers in **5D/6D space** on each (E, λ, P_φ) vertice
- **Transformation is performed** on **midplane** $\boldsymbol{R_{mid} \equiv B \cdot \nabla B = 0}$, intersected by all EPs orbits [1]

(E, λ, P_φ) -> (E,$\frac{v_\parallel}{v}$,R_{mid}) transformation

$$v_\parallel(R_{mid}) = \frac{P_\varphi + Ze\psi(R_{mid})}{mB(R_{mid})/B^\varphi(R_{mid})}$$

$$\lambda(R_{mid}) = \left(1 - \frac{v^2_{\parallel(R_{mid})}}{v^2}\right)\frac{B_0}{B(R_{mid})}$$

exactly correct in 6D for the gyroangle such as $v_\theta = 0$

- For a **given vertice** on cartesian CoM grid $(\boldsymbol{E_i, \lambda_j, P_{\varphi,k}})$, the **coupled set of equations** on $(\boldsymbol{v_\parallel, \lambda})$ implicit in R_{mid} is solved to obtain **($\frac{v_\parallel}{v}$,R_{mid})**
- This **backward transformation** on the generalized midplane **does not require orbit tracing**

[1] A. Bierwage et al. *2022, Comput. Phys. Commun.*

Backward transformation and orbit classification

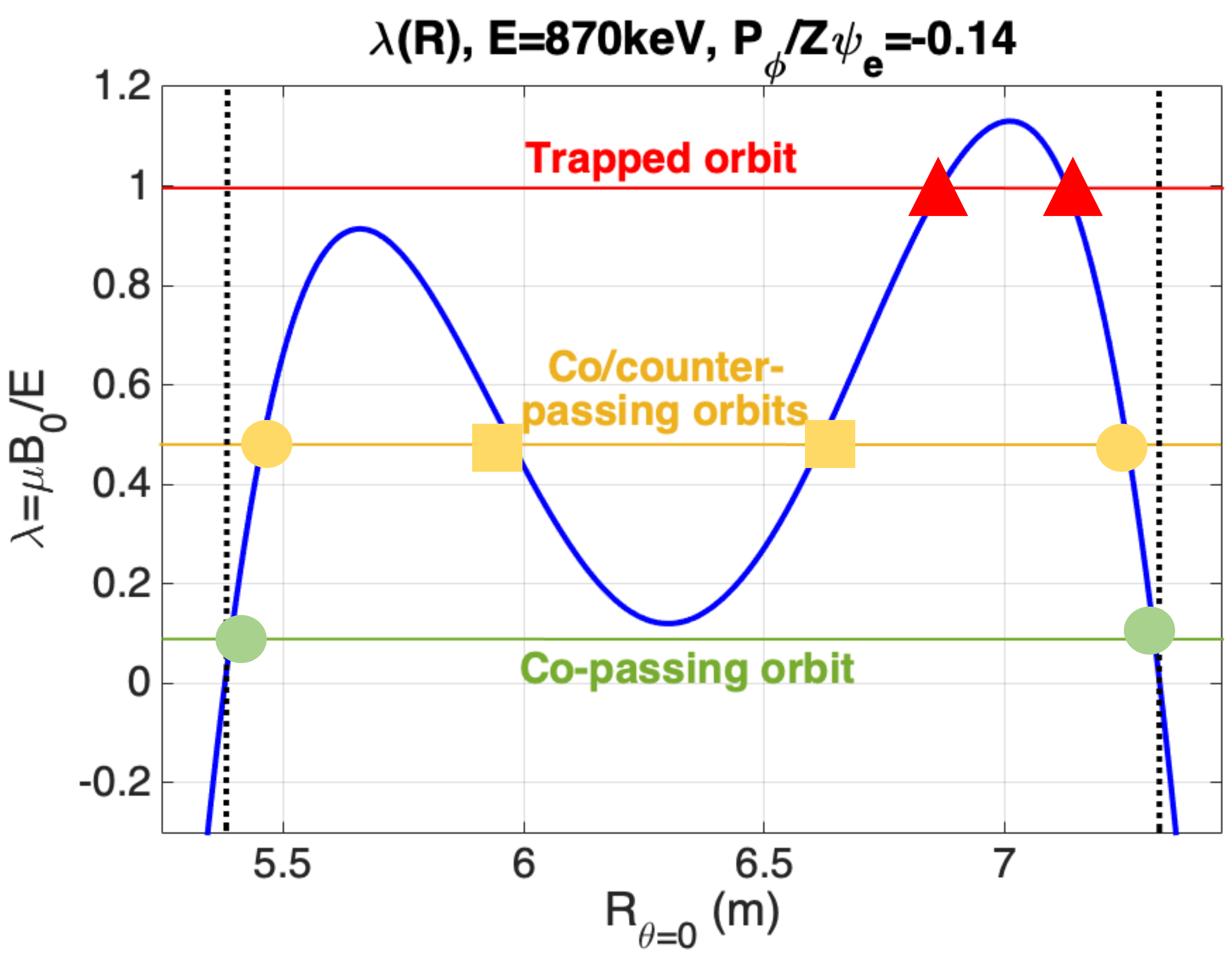

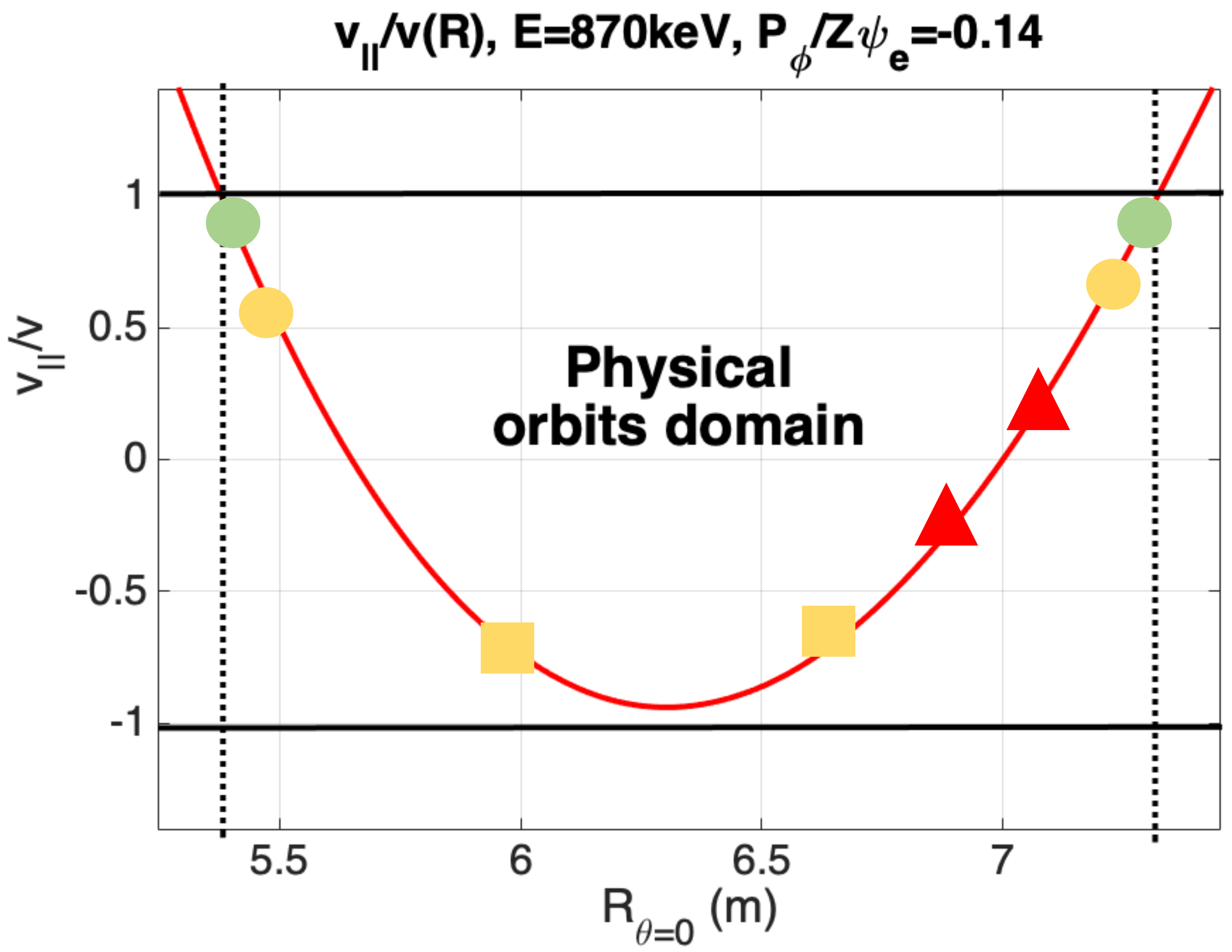

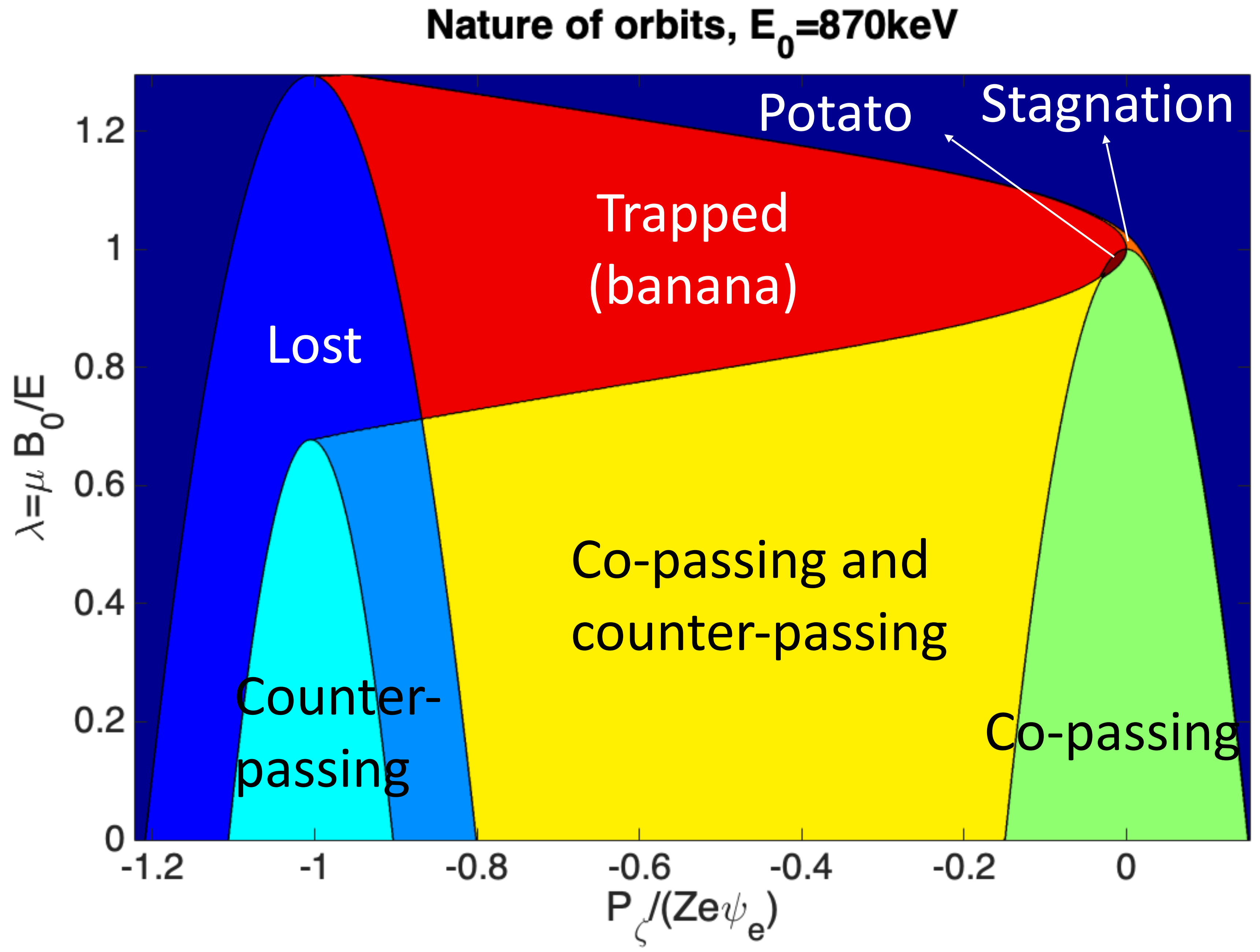

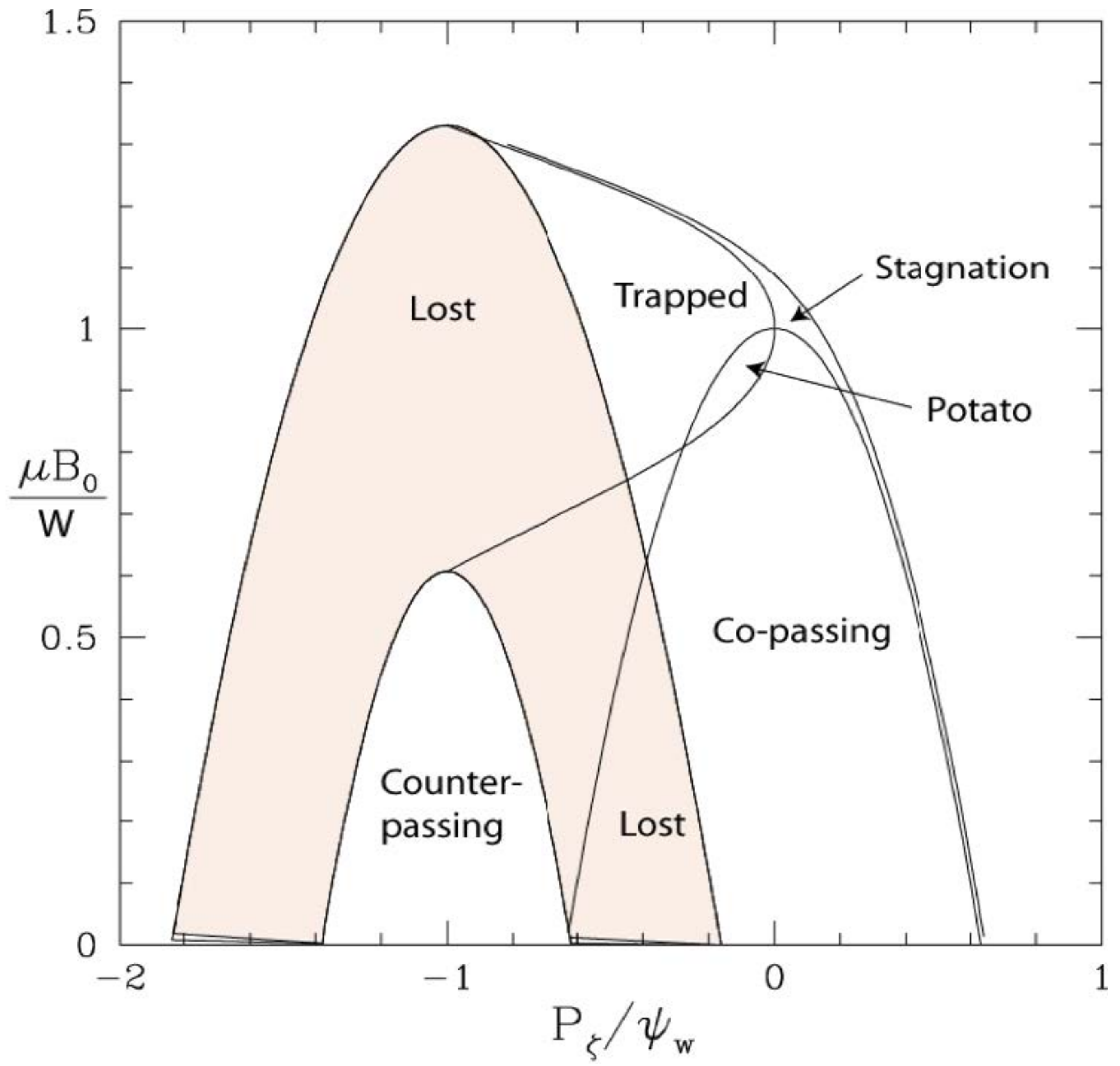

- The **solutions** of $\lambda[R_{mid}, v_{\parallel}\left(R_{mid}, P_{\varphi,k}\right)] = \lambda_j$ are **obtained numerically** by scanning $\boldsymbol{R_{mid}}$, for $v_{\parallel} \in [-v_i, v_i]$
- For **each orbit**, the algorithm finds **two solutions**, on the LFS and HFS of the $B \cdot \nabla B = 0$ midplane
- **8 types of orbits** are identified based on the **values for** $\boldsymbol{(R_{mid}, v_{\parallel})}$ on the **OLFS** and **OHFS**
- In the $\left(P_{\varphi}, \lambda\right)$ **phase space** at fixed energy, the **topology** is **identical to** White's . A **2000x2000** grid was used

Accuracy of the backward transformation

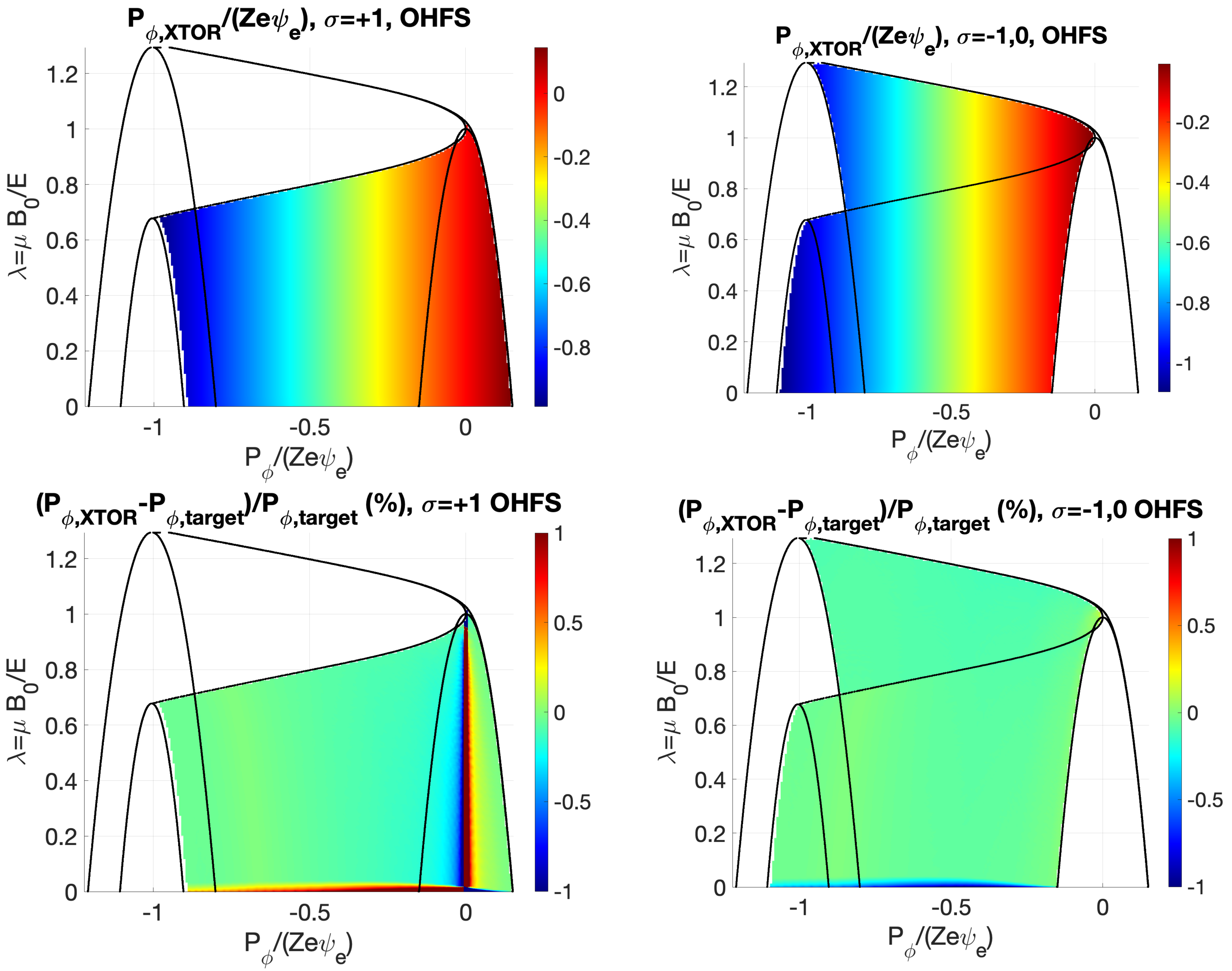

- ➢ The backward transformation is tested with the **XTOR-K 6D pusher** on a **200x200 (P_φ, λ) grid** at fixed energy
- ➢ For **each target ($P_{\varphi,i}$, λ_j),** the corresponding **(R_{mid}, $v_\parallel$)** are identified on the **OHFS**
- ➢ **P_φ is re-computed** from the markers **6D position**
- ➢ The error on P_φ is under 1%, showing **good numerical accuracy** of the backward transformation
- ➢ **Similar results** are obtained for λ

« Analytic » construction of CoM jacobian

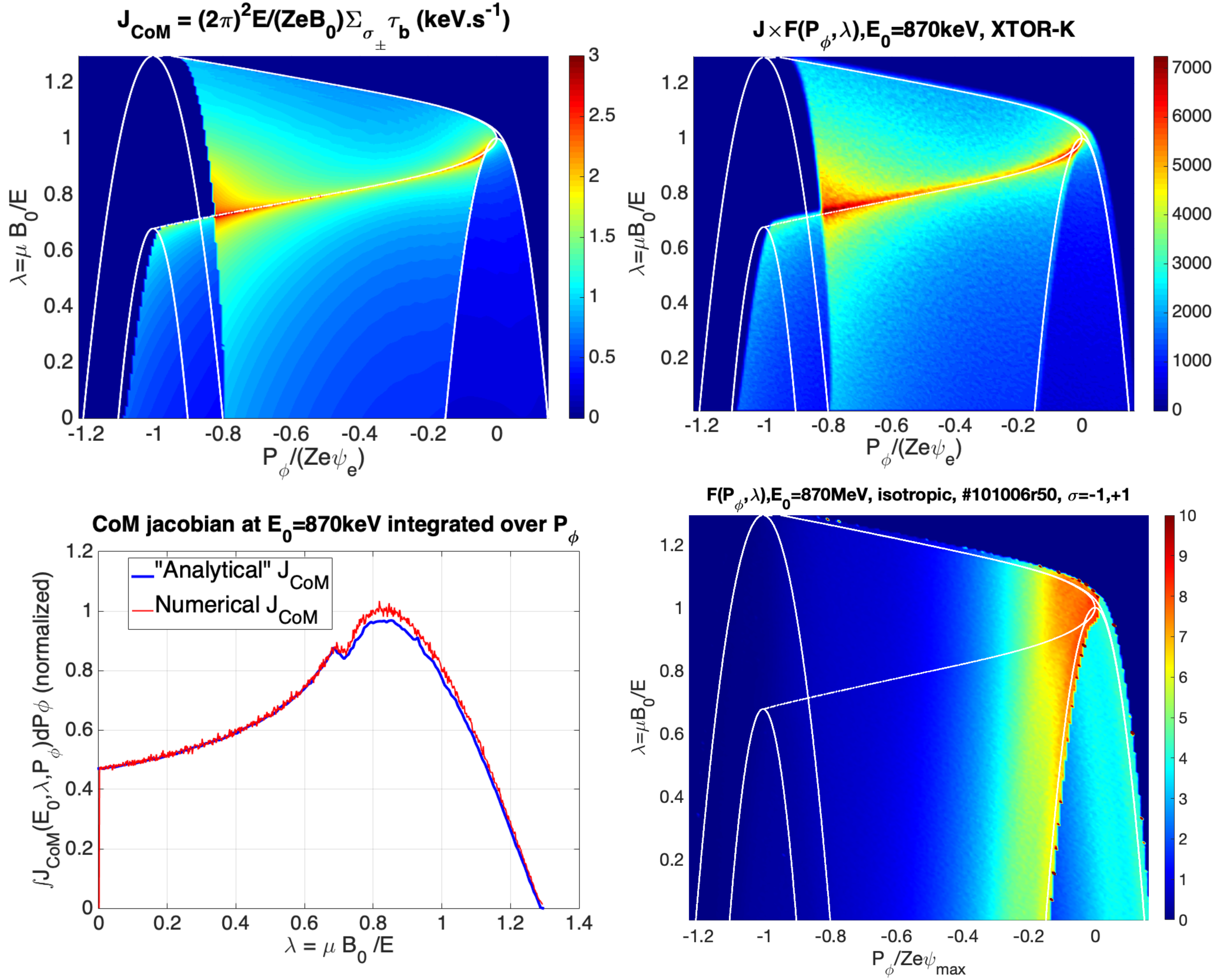

- J_{CoM} is **theorically defined** as

$$J_{CoM} = \frac{(2\pi)^2 E}{ZemB_0}\sum_{\sigma=\pm 1}\tau_B(E,\lambda,P_\varphi)$$

- $\boldsymbol{J_{CoM}}$ can be obtained **on the** $(\boldsymbol{E},\boldsymbol{\lambda},\boldsymbol{P_\varphi})$ grid from the **bounce time** for **each orbit**
- J_{CoM} **is succesfully compared** with the **histogram** of a flat, isotropic and monoenergetic distribution as $\boldsymbol{H_{CoM} = F_{CoM}\times J_{CoM}}$
- **Small inaccuracies** remain near the **trapped-passing boundary**
- With a **realistic density profile**, most particles are **located near topological boundaries** of the (P_φ,λ) grid

Outline

I) Interplay fishbone/zonal flows in gyrokinetic simulations

A) Experimental fishbone validation on a DIII-D discharge

B) Predicted fishbone dynamics in ITER PFPO-2 scenario

II) Computation of CoMs EP distribution in IMAS

A) Versatile method for coordinate transformation

B) Application for NBI and alpha distributions in a JET-DT pulse

Fishbone-induced ion ITBs in JET-DT

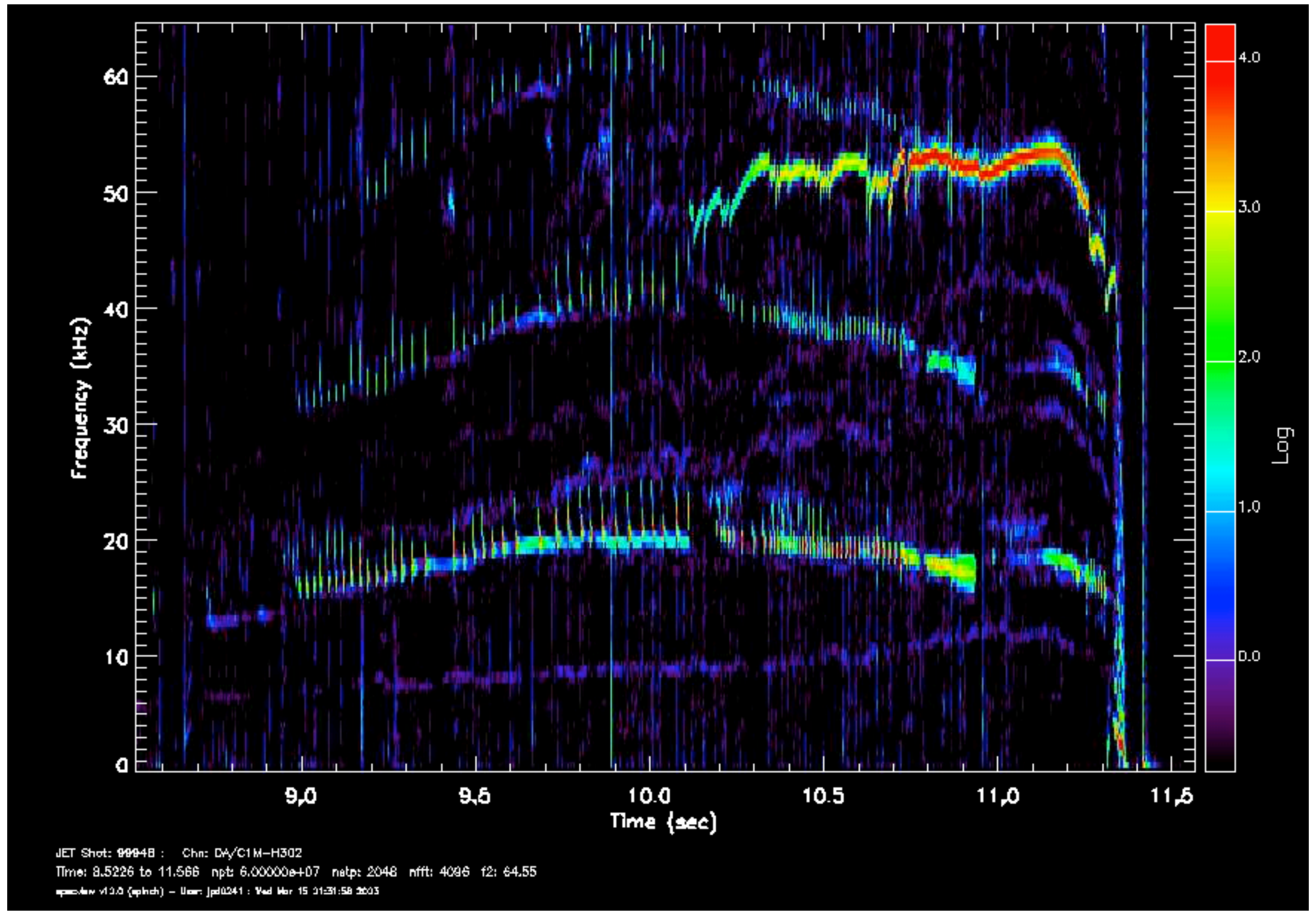

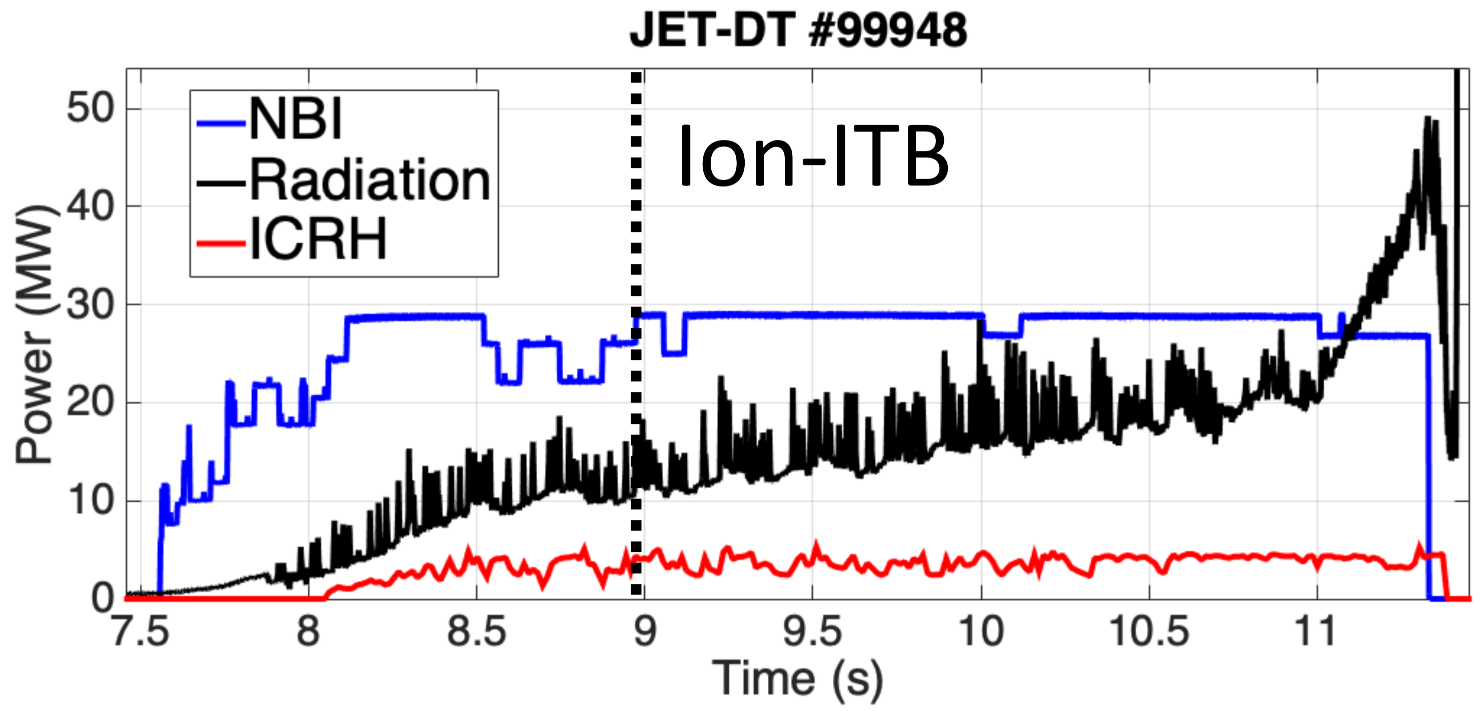

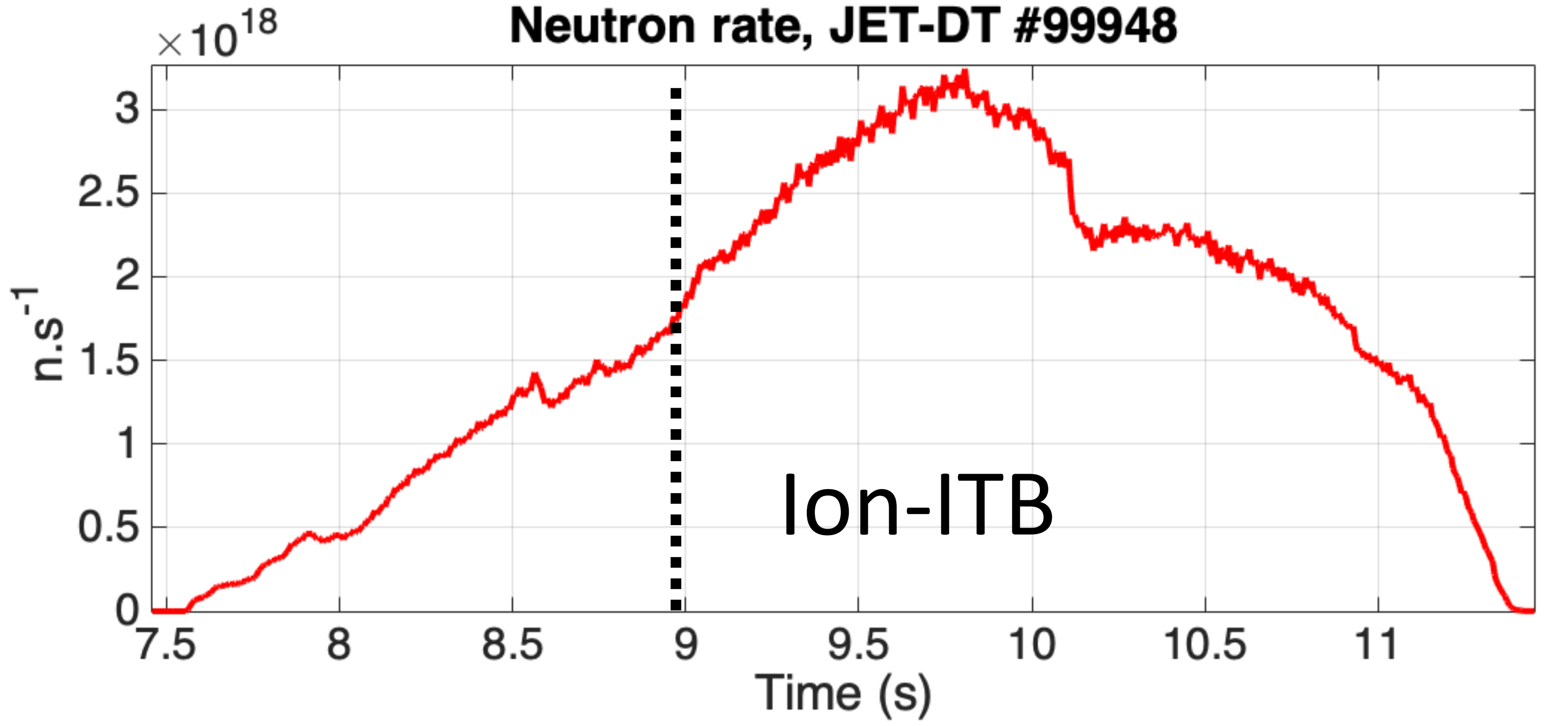

- **JET DT pulse** #99948 experienced a **2x increased fusion gain with Q=0.32** after onset of **fishbone bursts**
- **Ion-ITB formation** is visible after t=9s at q=2, **no electron ITB identified**
- There is a **possible causality** between **fishbone** starting at **t=9s** and the **ion-ITB**, similar to [1] on **DIII-D**
- **Nonlinear gyrokinetic** and **kinetic-MHD** need to be performed with **realistic CoM pds** to **verify** this **causality**

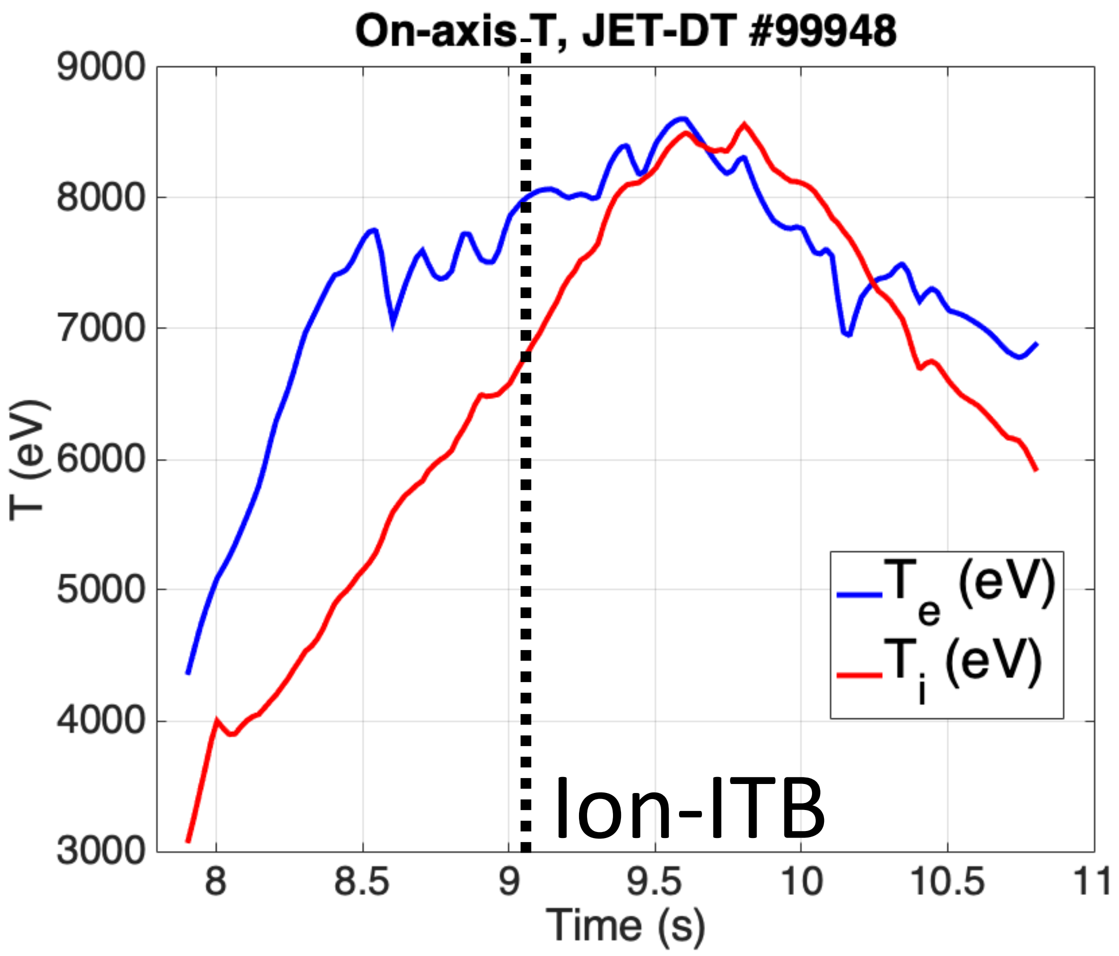

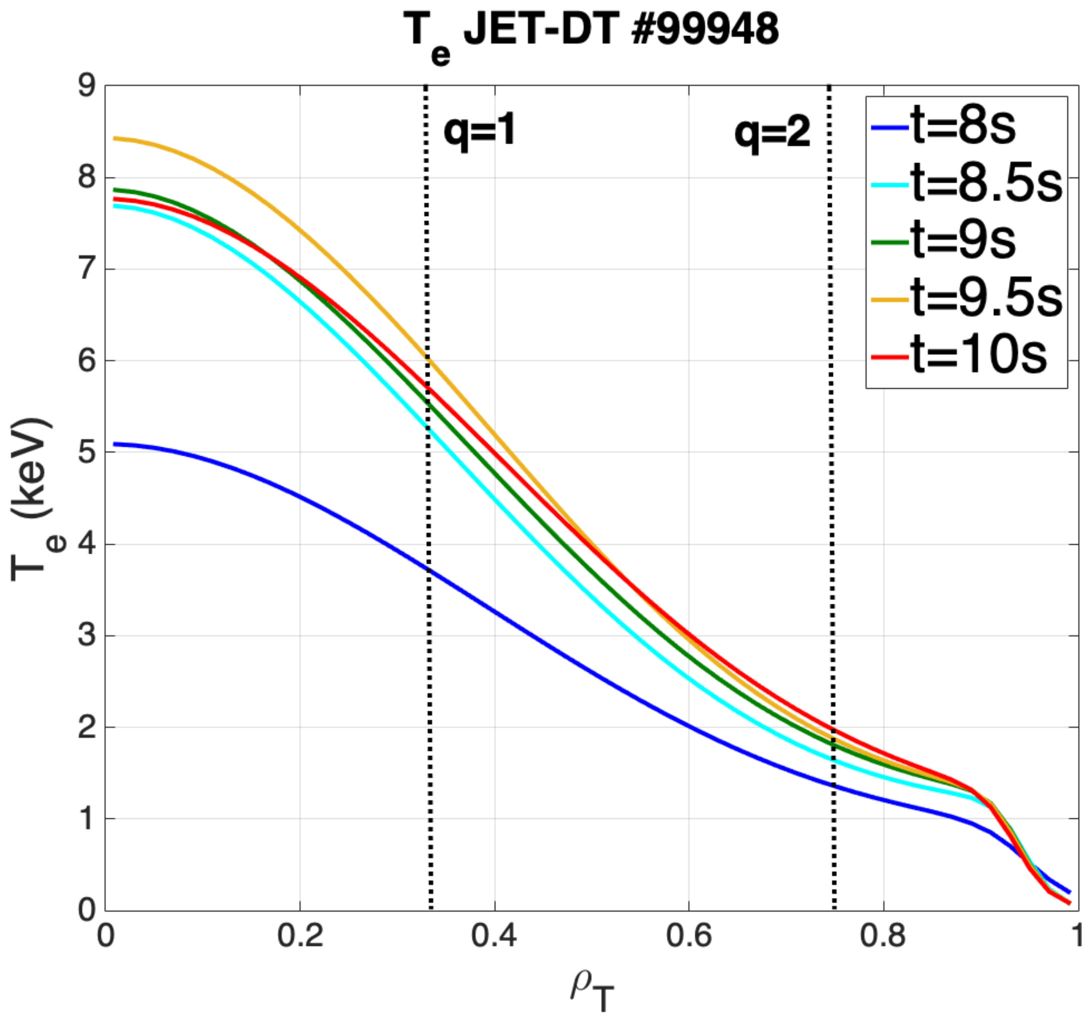

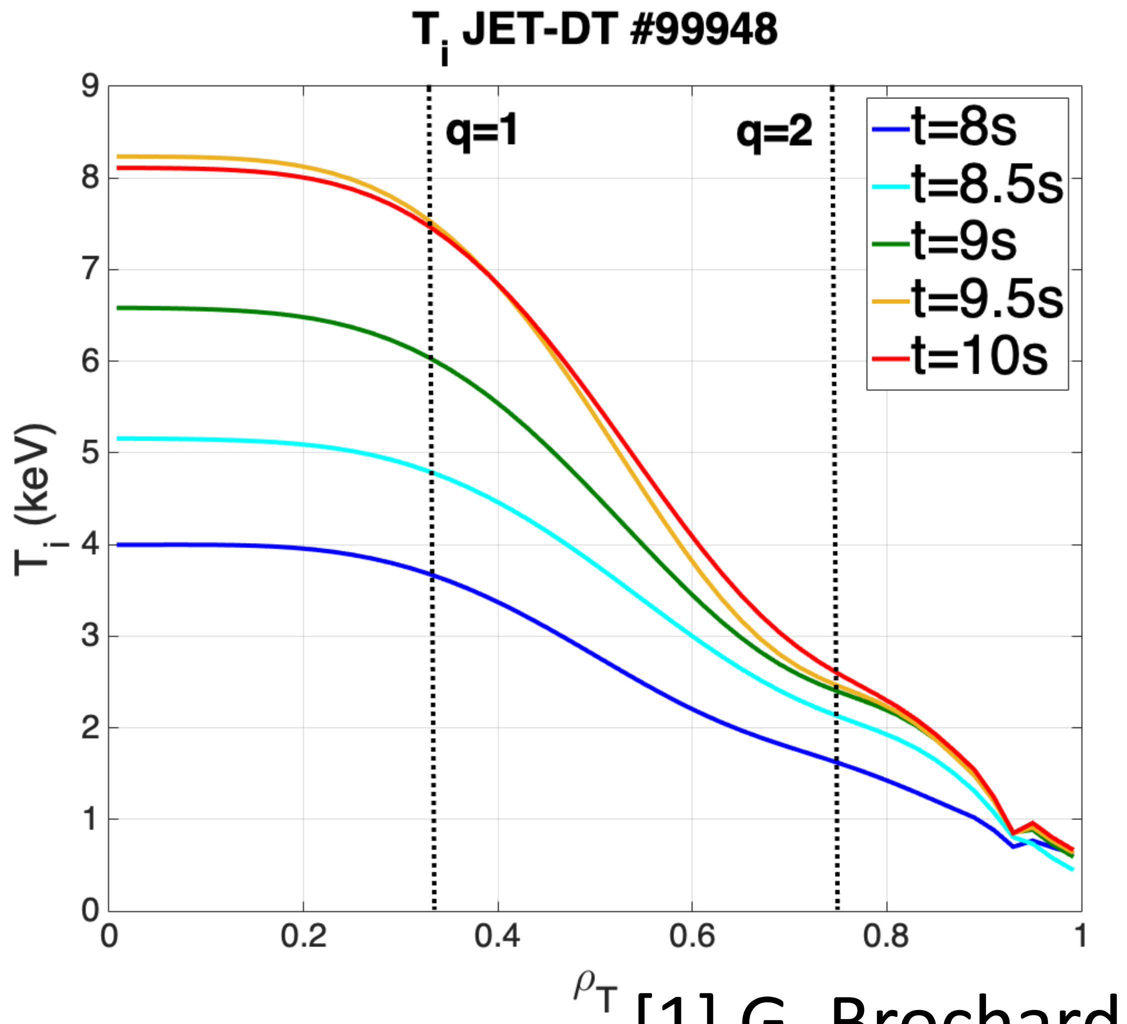

[1] G. Brochard et al. 2023, submitted to *Phys. Rev. Lett.*

JET-DT #99948 : Fast-ion distributions

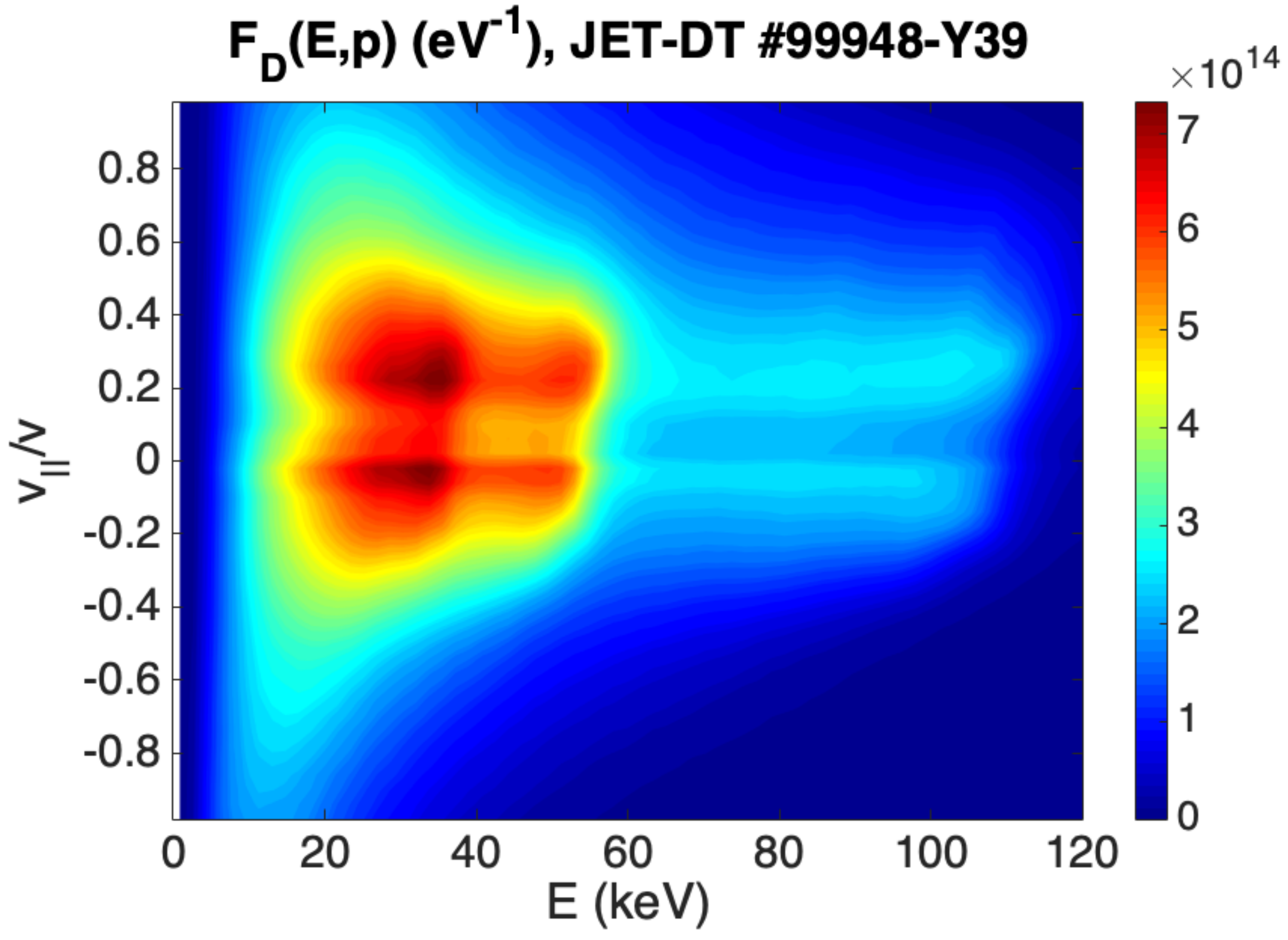

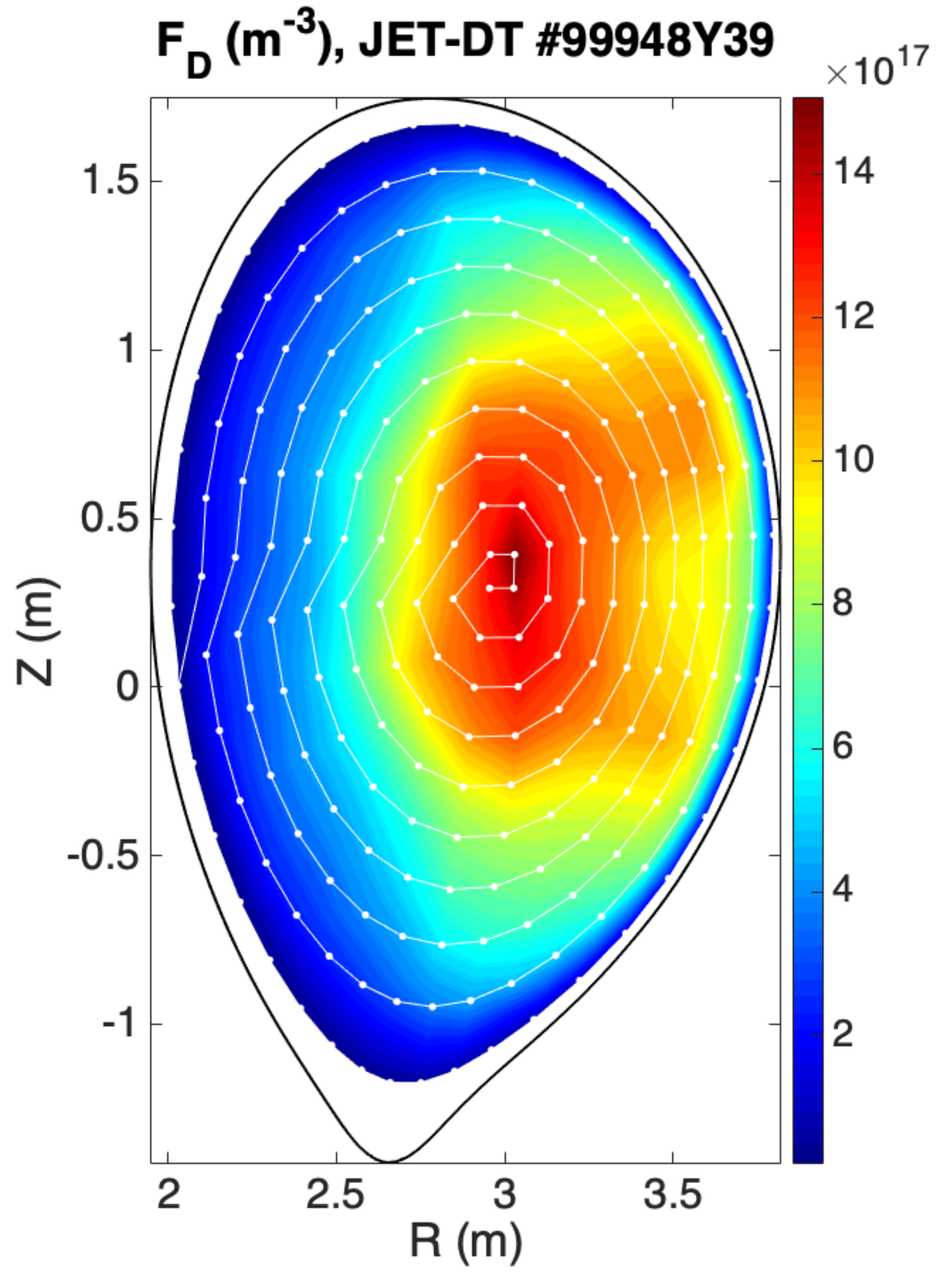

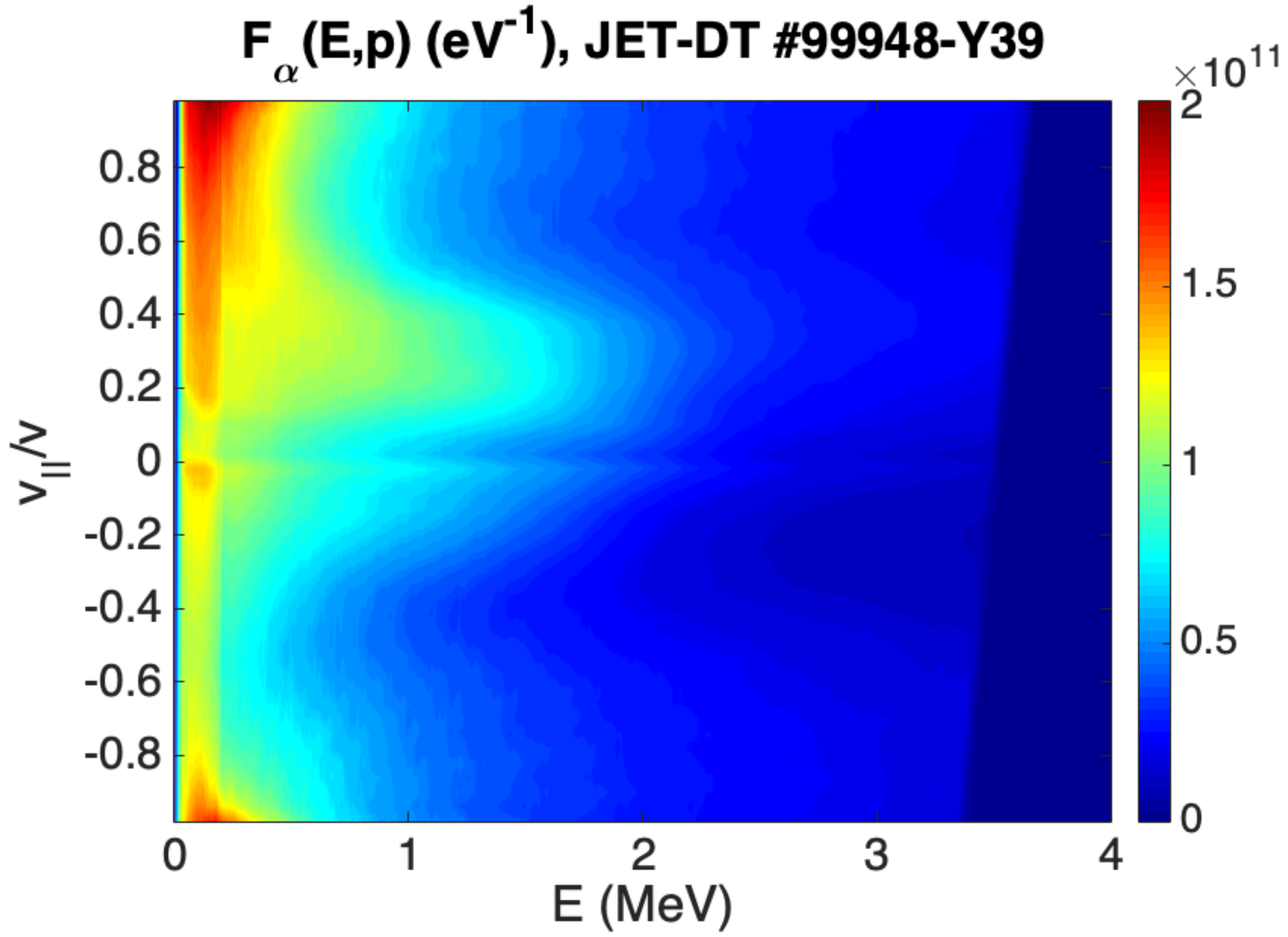

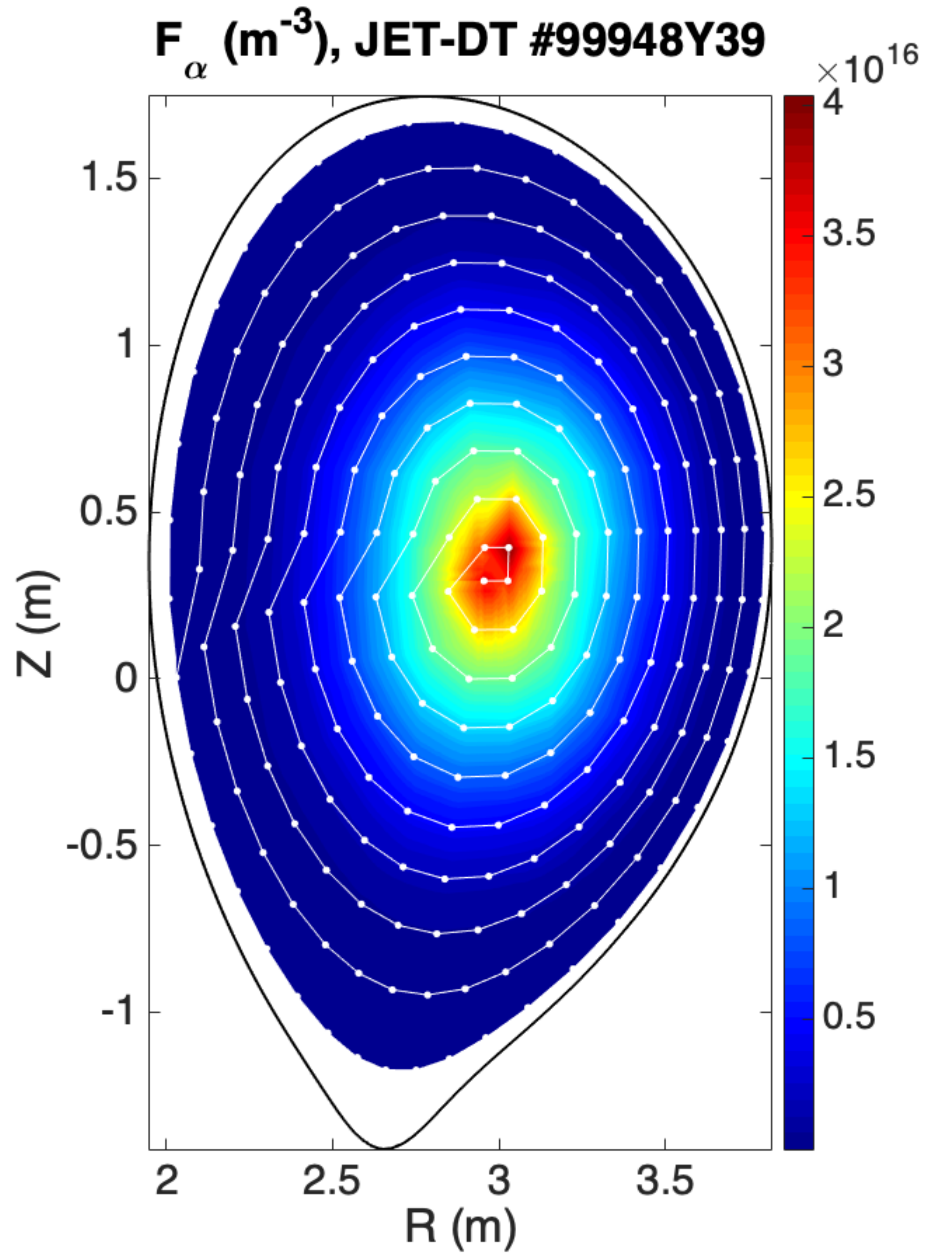

- **Distributions** in the **(E, $\frac{v_\parallel}{v}$,R,Z) phase space** are provided from **TRANSP-NUBEAM** for **alphas** and **NBI**
- **256k markers** are used for both **alphas** and **NBI** to reproduced distributions
- **Resolution** in the $(E, \frac{v_\parallel}{v})$ space is **relatively ok** : N_E = 70 (NBI) – 340(α), $N_{v_\parallel}$ = 50.
- A **low spatial resolution** is used : **220 grid points on ~10 flux surfaces**. It **restricts** heavily P_φ **resolution** in **CoM space**. A 2D **cartesian re-mapping** with a **18x18 grid** is performed
- A **H-minority** heated by **ICRH** is also present, but **not modelled by NUBEAM**

Jacobian construction on CoM grid

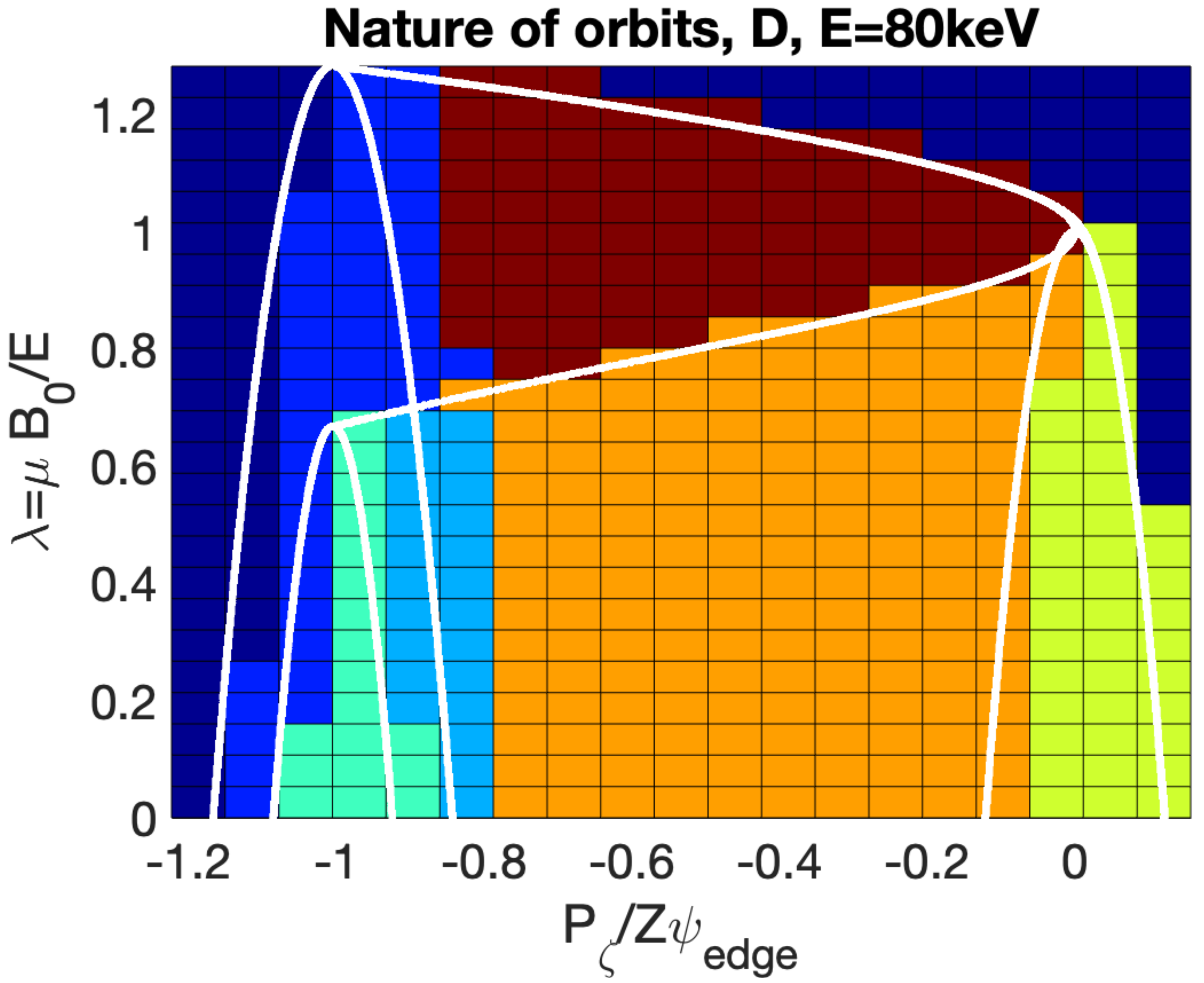

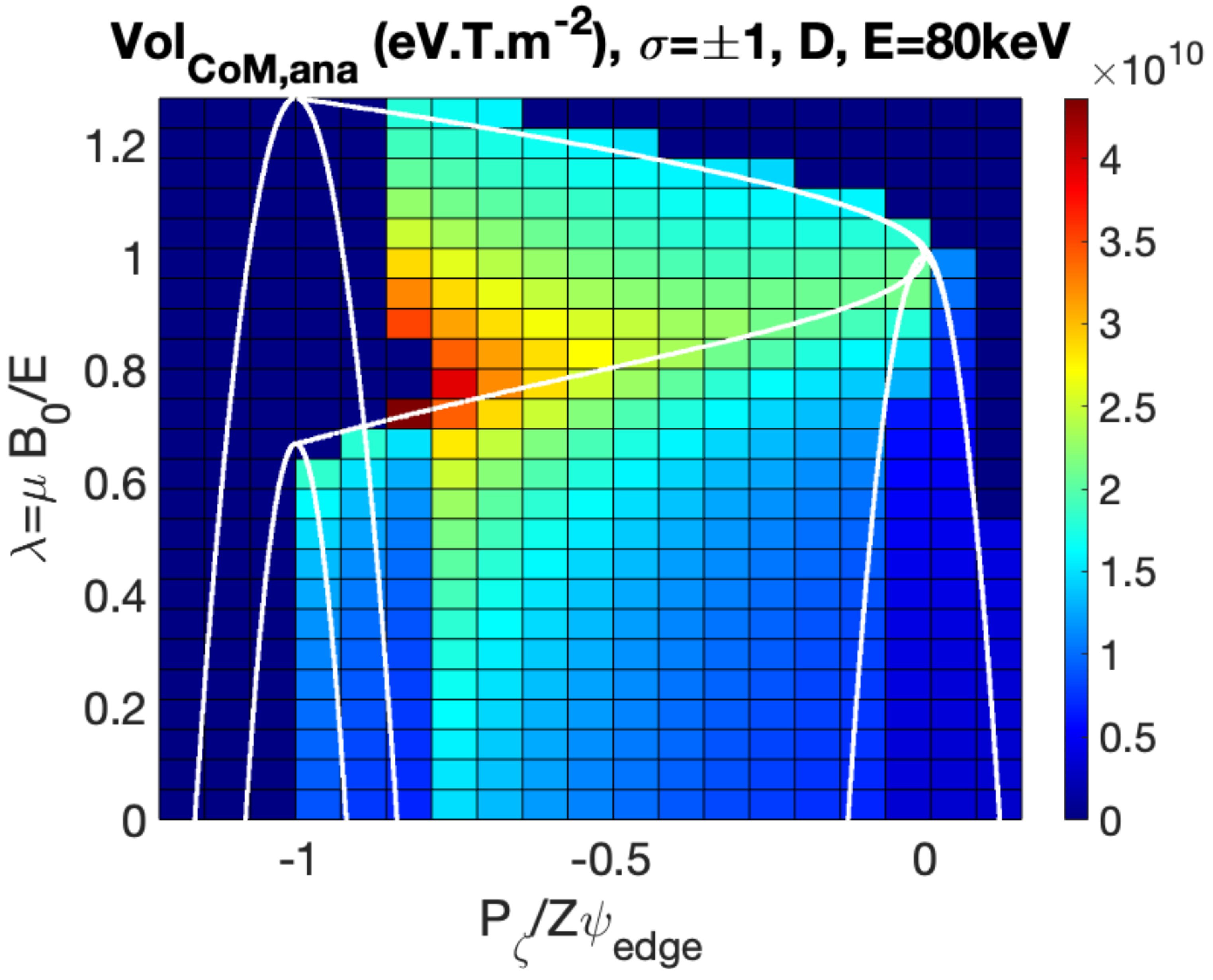

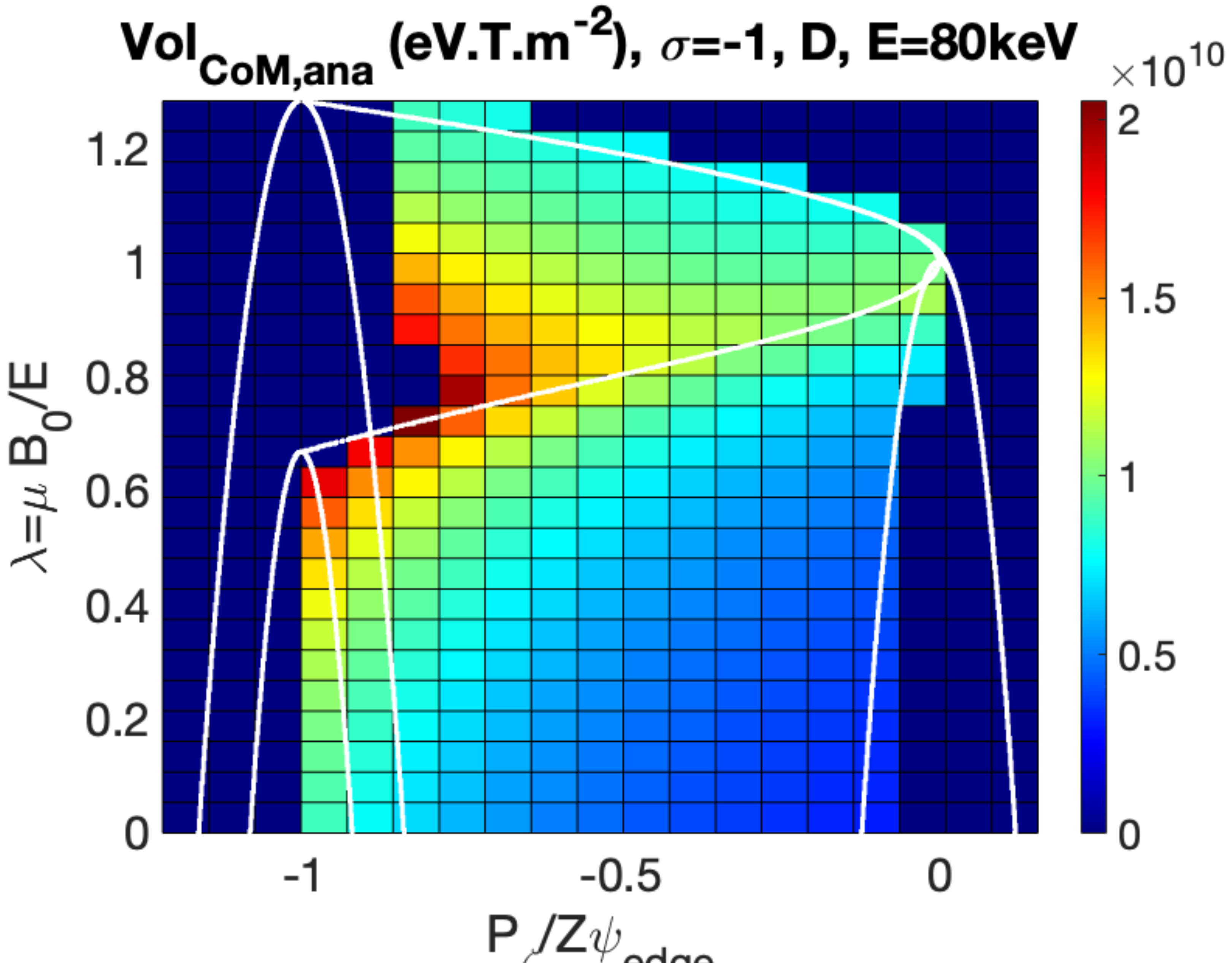

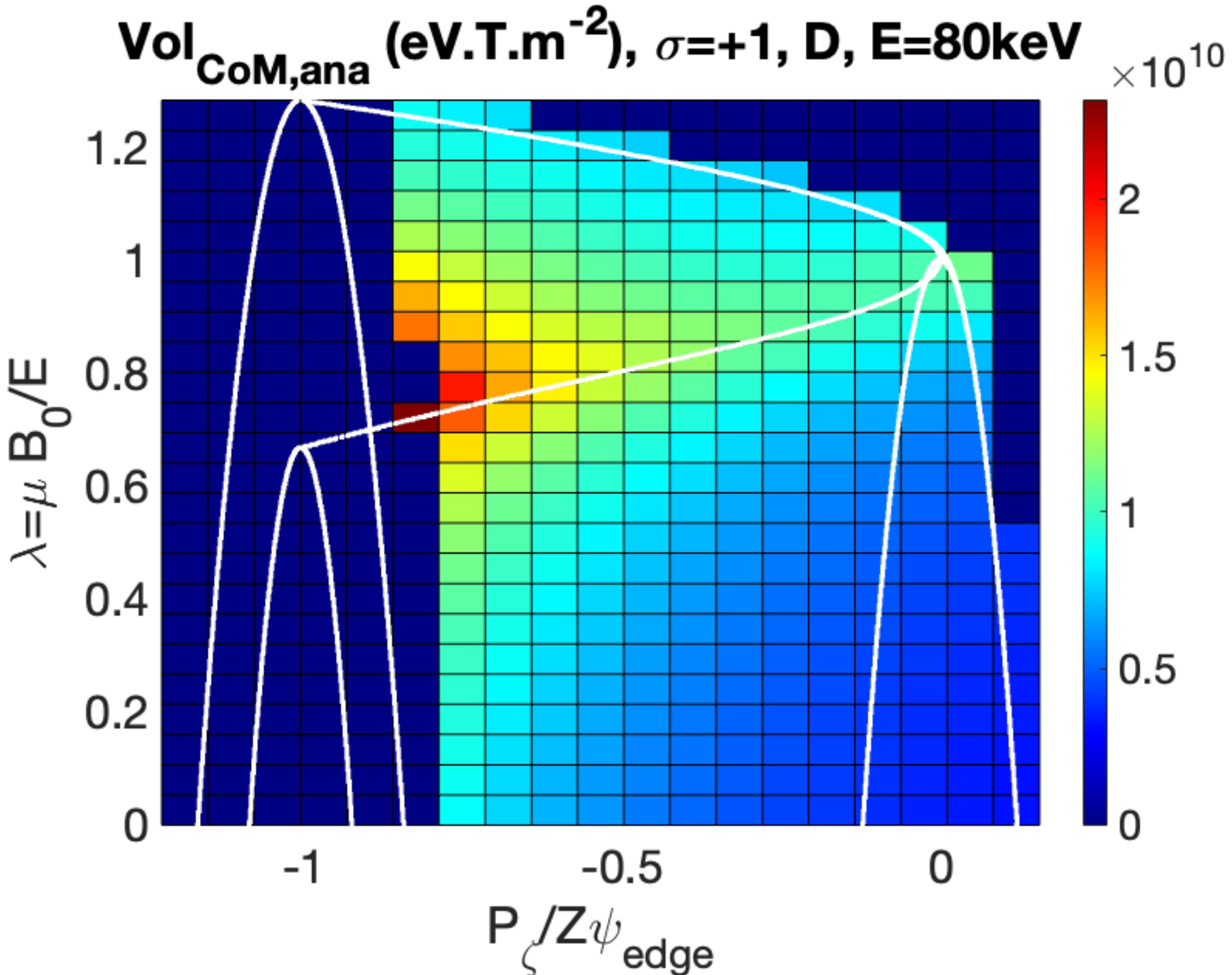

- The **CoM grid** used has the **resolution : (N_E=50, N_λ=25, N_{P_φ}=20)**
- $\Delta V_{CoM} = \mathbf{J}_{CoM}\Delta\mathbf{E}\Delta\lambda\Delta\mathbf{P}_\varphi$ is **rather smooth** on the **CoM grid**
- **Co-passing** and **counter-passing** orbits treated **separately** when they both exist on CoM grid (**degeneracy**)
- **Trapped orbits** contribution **split in two** to ensure J_{CoM} **continuity** over **trapped-passing boundary**

Alternative Jacobian construction

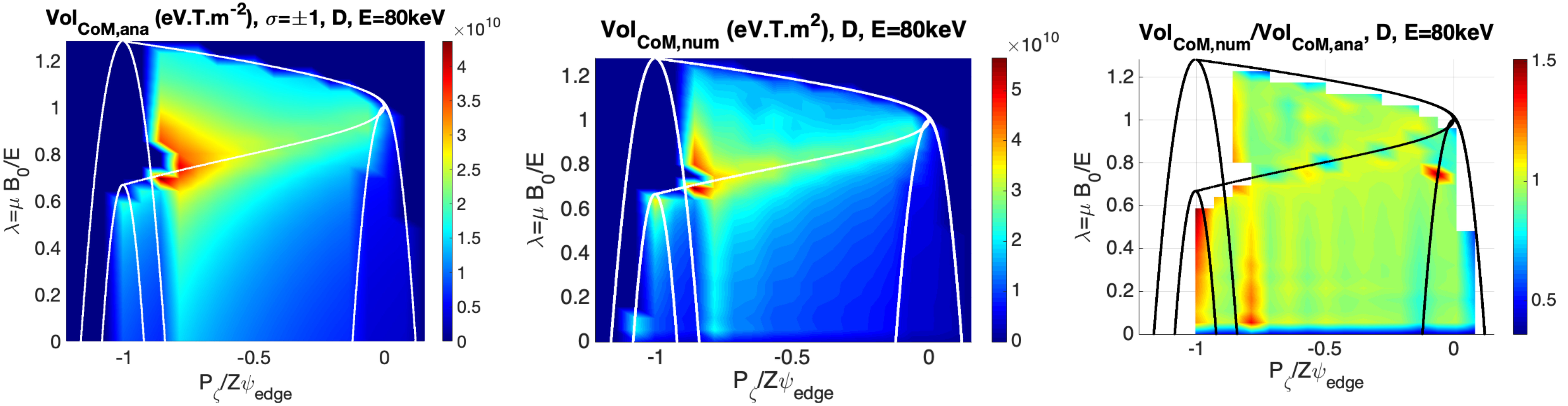

➢ ΔV_{CoM} can also be computed numerically using the (E,p,R,Z)->CoM coordinate transform as

$$\Delta V_{CoM}(E,\lambda,P_\varphi,\sigma) = \sum_{i}^{N_{EpRZ}} \delta_3(\mathrm{X}_{EpRZ,i} - \mathrm{X}_{CoM})\Delta E \Delta\lambda \Delta P_\varphi$$

➢ The **two methods compare well**, **except** at the **domain edge** due to the 3rd **order interpolation**

➢ **Both Jacobian methods** can be used to compute **CoM distributions**

Interpolation between (E,p,R,Z)-> CoM distribution

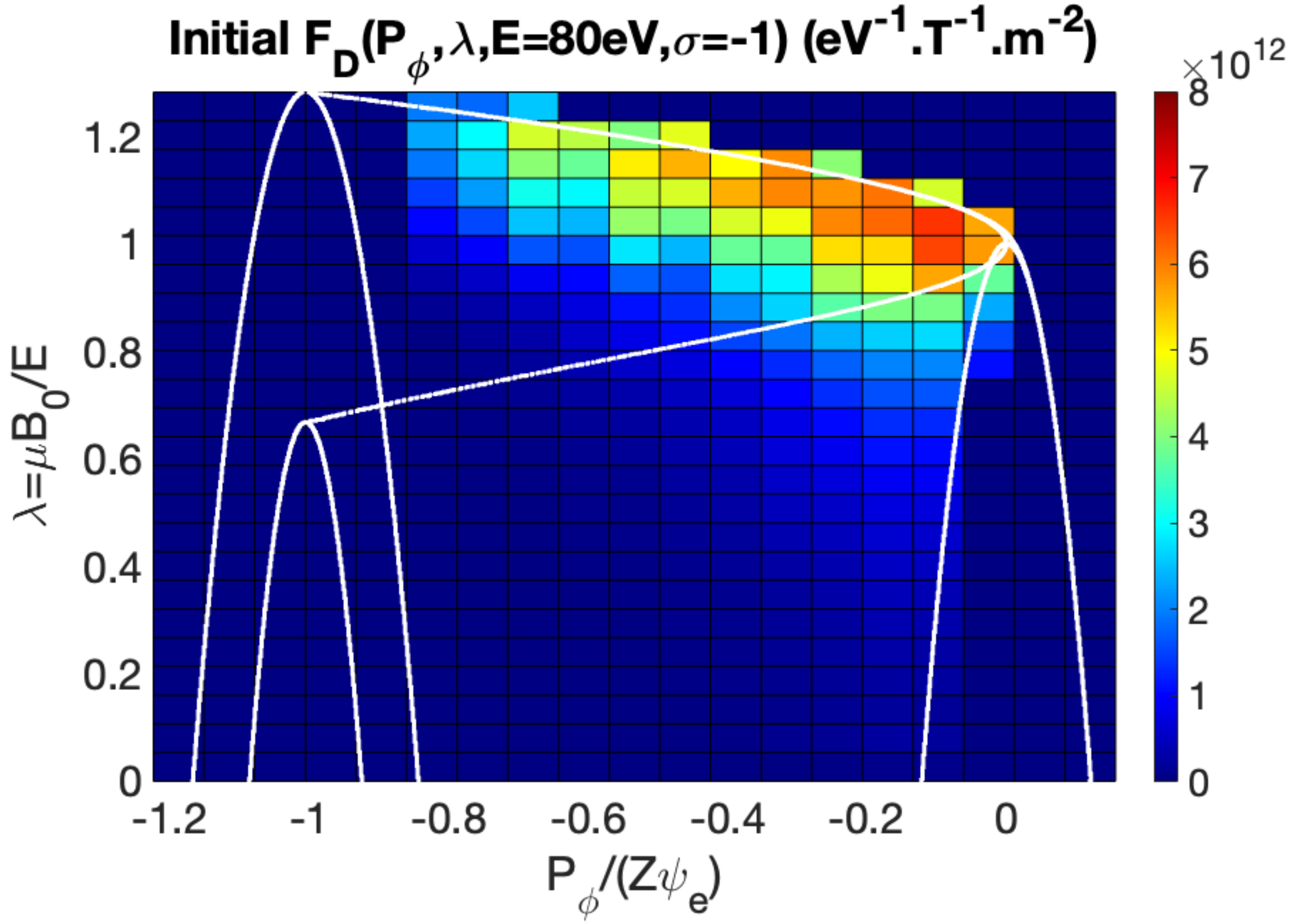

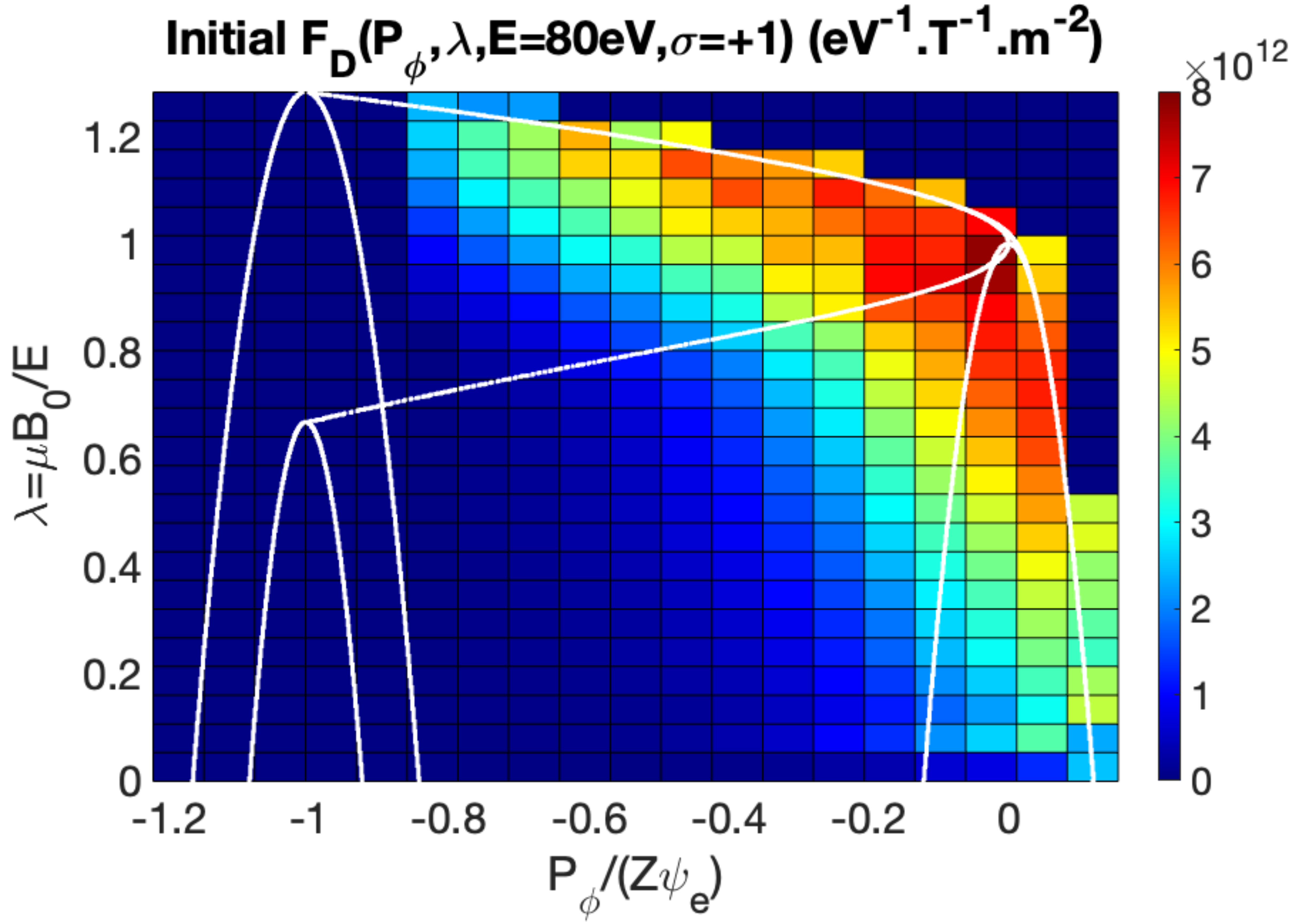

- The **CoM D beam distribution** is computed as $F_D(E,\lambda,P_\varphi,\sigma) = \sum_i^{N_{EpRZ}} \delta_3(\mathrm{X}_{EpRZ,i} - \mathrm{X}_{CoM}) F_D(E,p,R,Z)\frac{\Delta V_{EpRZ}}{\Delta V_{CoM}}$
- $F_{D,CoM}$ needs also to be **separated** in two between **co-going** and **counter-going orbits** ($\sigma = \pm 1$)

Spline construction, D beam

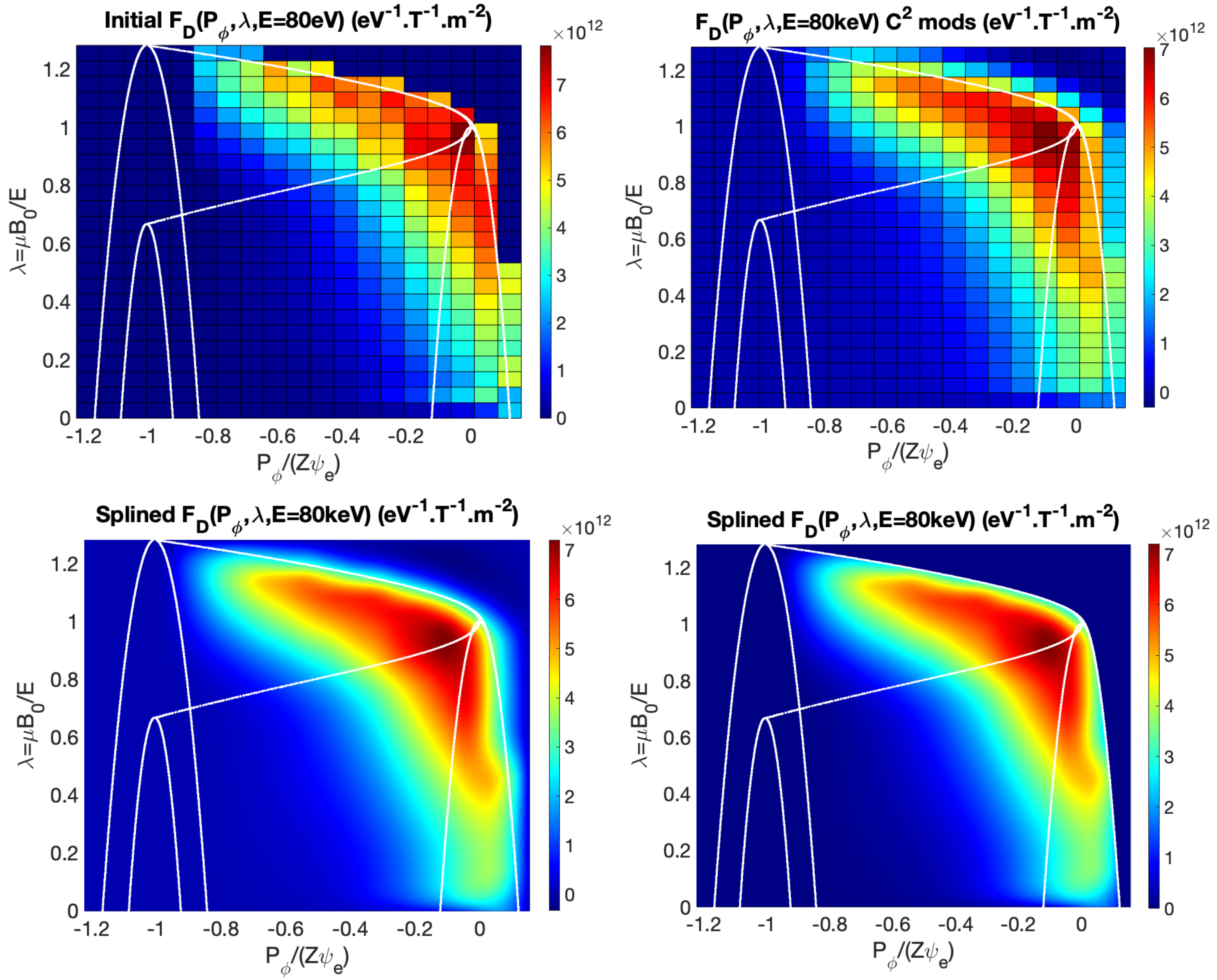

- C^2 **CoM distribution** defined with **2nd order 3D B-spline** :

$$F_{D,s}(E,\lambda,P_\varphi) = \sum_{i=0}^{2}\sum_{j=0}^{2}\sum_{k=0}^{2} a_{ijk} x_E^i x_\lambda^j x_{P_\phi}^k, \;\; x \in [0,1]$$

- **Distribution** on **CoM grid** slightly **adjusted** to satisfy C^2 **condition**

$$F(x_{i+1}) = \frac{3}{4}F(x_i) + \frac{1}{2}F'(x_i) + \frac{1}{4}F(x_{i+2})$$

- Samples out of **topological boundaries** removed via **backward** CoM -> (E,p,R,Z) **transformation**

- **Markers** in **5D/6D full-F codes** (cylindrical/Boozer coordinates) initialised via **backward transformation**

1st order derivatives in CoM space

- **First order C^1 derivatives** of the **CoM distribution** directly obtained from the **3D spline**

- In δF **codes**, the derivatives used in the **weight equation** can be computed through the **chain rule**

$$\nabla F|_{\mu,v_{||}} = \nabla E|_{\mu,v_{||}} \frac{\partial F}{\partial E} + \nabla \lambda|_{\mu,v_{||}} \frac{\partial F}{\partial \lambda} + \nabla P_\varphi|_{\mu,v_{||}} \frac{\partial F}{\partial P_\varphi}$$

$$\frac{\partial F}{\partial v_{||}}|_{\mu,X} = \frac{\partial E}{\partial v_{||}}|_{\mu,X} \frac{\partial F}{\partial E} + \frac{\partial \lambda}{\partial v_{||}}|_{\mu,X} \frac{\partial F}{\partial \lambda} + \frac{\partial P_\varphi}{\partial v_{||}}|_{\mu,X} \frac{\partial F}{\partial P_\varphi}$$

- The **forward transformation (E,p,R,Z) -> CoM** can be used for each marker to determine **which of the splined CoM distributions** to use (**co-going or counter-going**)

EP frequencies in CoM space

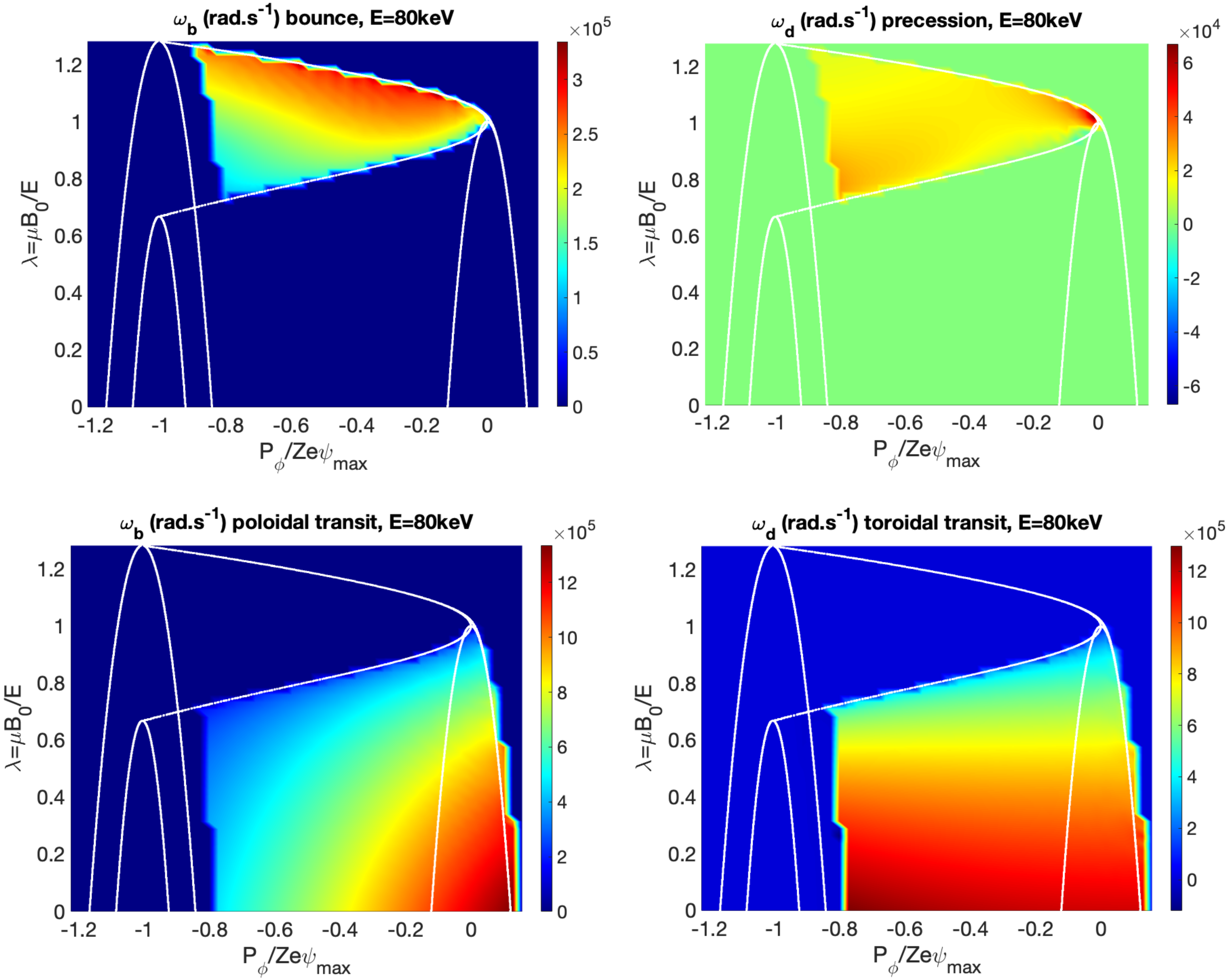

- **EP frequencies** (ω_b, ω_d) can be obtained in the **CoM spaces** through **orbit analysis** ($\theta(t), \varphi(t)$ traces)
- These mappings enable **identification of resonant plans** for a given mode frequency
- **IDS** will be created to store these informations **for a given scenario**

Conclusions

- A **versatile** method to initialise **CoM distributions** in **full-F** and δF codes from **experimental** and **Fokker-Planck inputs** was presented

- An **analytical backward CoM -> (E,p,R,Z) transformation** was successfully created, allowing **precise orbit characterisation** in CoM space

- Using XTOR-K's particle pusher, the **CoM Jacobian** is **accurately computed** on a **cartesian CoM grid**

- A **JET-DT pulse** with **potential fishbone-induced microturbulence stabilisation** is used to test the CoM distribution transformation method

- The **NUBEAM (E,p,R,Z) distribution** is transformed into a **CoM distribution**, separating CoM space between **co-going** and **counter-going topological regions**

- **3D B-spline** are used to define C^2 **CoM distributions** and their C^1 **first-order derivatives**. The **backward transformation** is used to **enforce the CoM space topological boundaries**

Perspectives

- ➢ **Re-process** the D-T beam and alpha distributions with **NUBEAM input using finer resolution**
- ➢ Perform loop **forward** $(E, p, R, Z) \to (E, \lambda, P_{\varphi}, \sigma)$ and **backward** $(E, \lambda, P_{\varphi}, \sigma) \to (E, p, R, Z)$ **transformations** to **quantity errors made** during distribution conversion
- ➢ **Test** the **CoM initialisation** in **first principles codes** such as **XTOR-K** (full-F) and **GTC** (δF)
- ➢ **Implement** the method in **IMAS** as to be compatible with the **EP stability workflow**
- ➢ **Accommodate IMAS** outputs for all EP codes across the **EP community**
- ➢ Perform **nonlinear kinetic-MHD** and **gyrokinetic** simulations to study **fishbone-microturbulence** interaction for the **JET-DT pulse #99948**

Nonlinear validation against ECE measurements

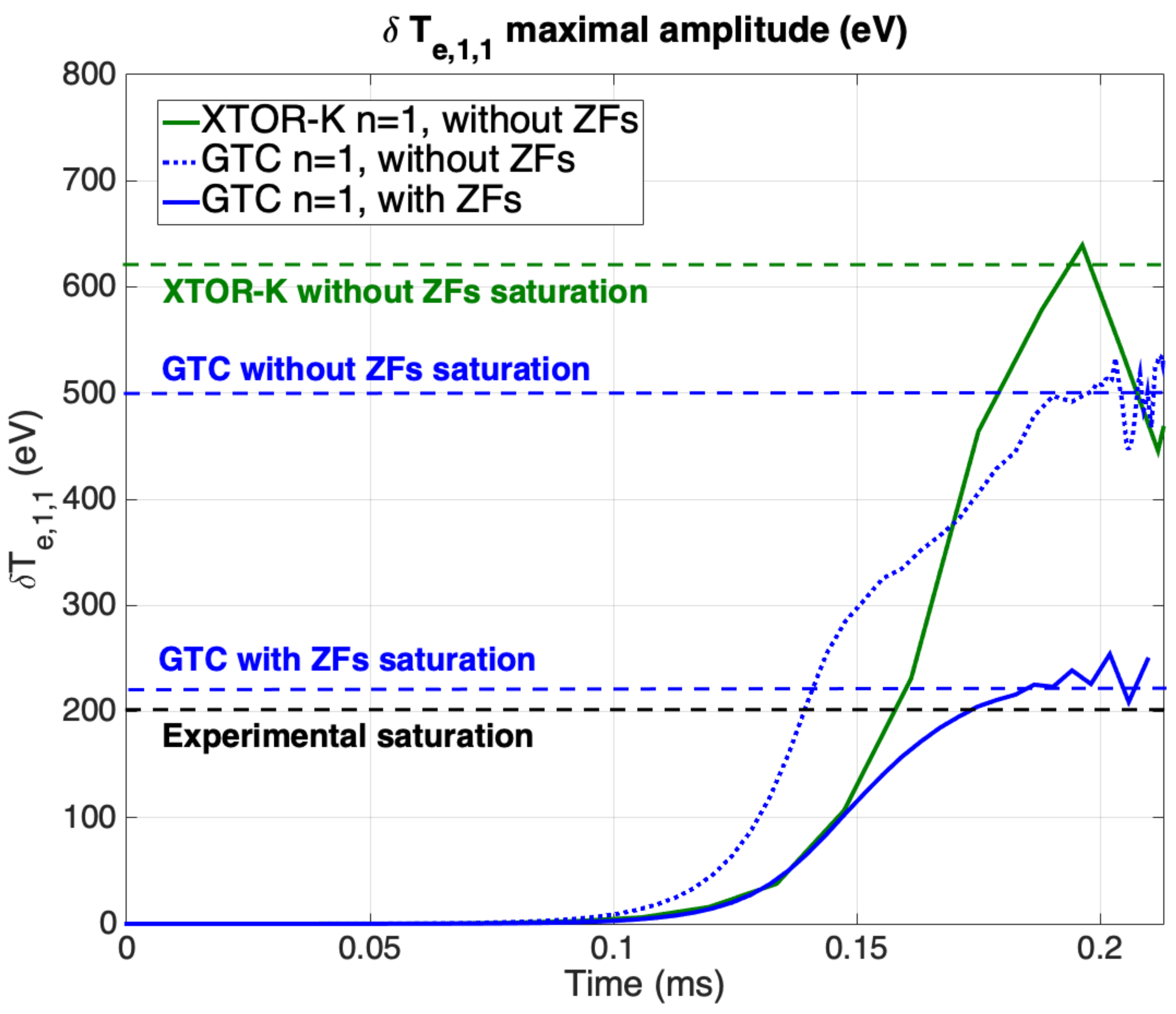

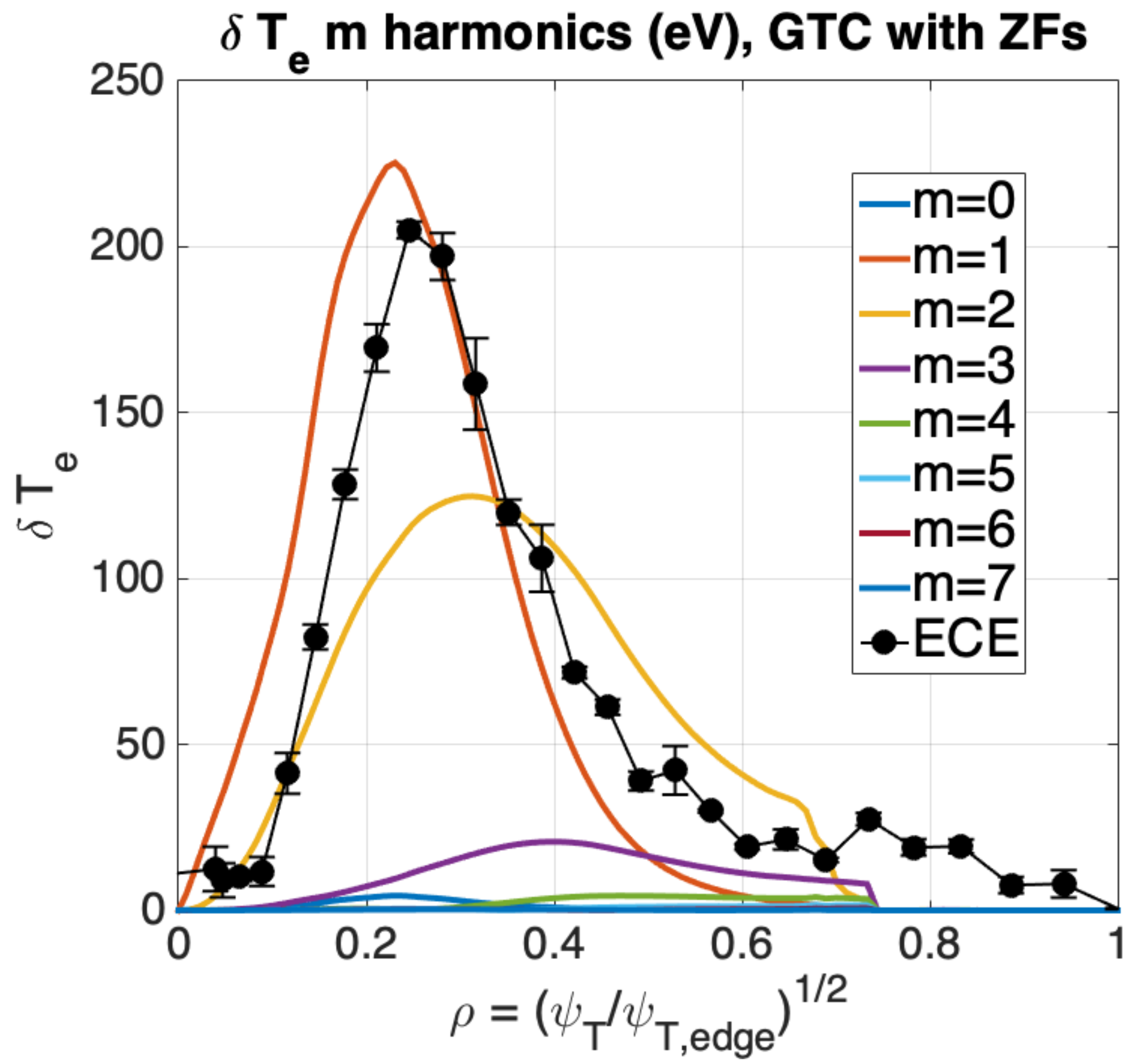

Sensitivity of fishbone amplitude on q_{min}

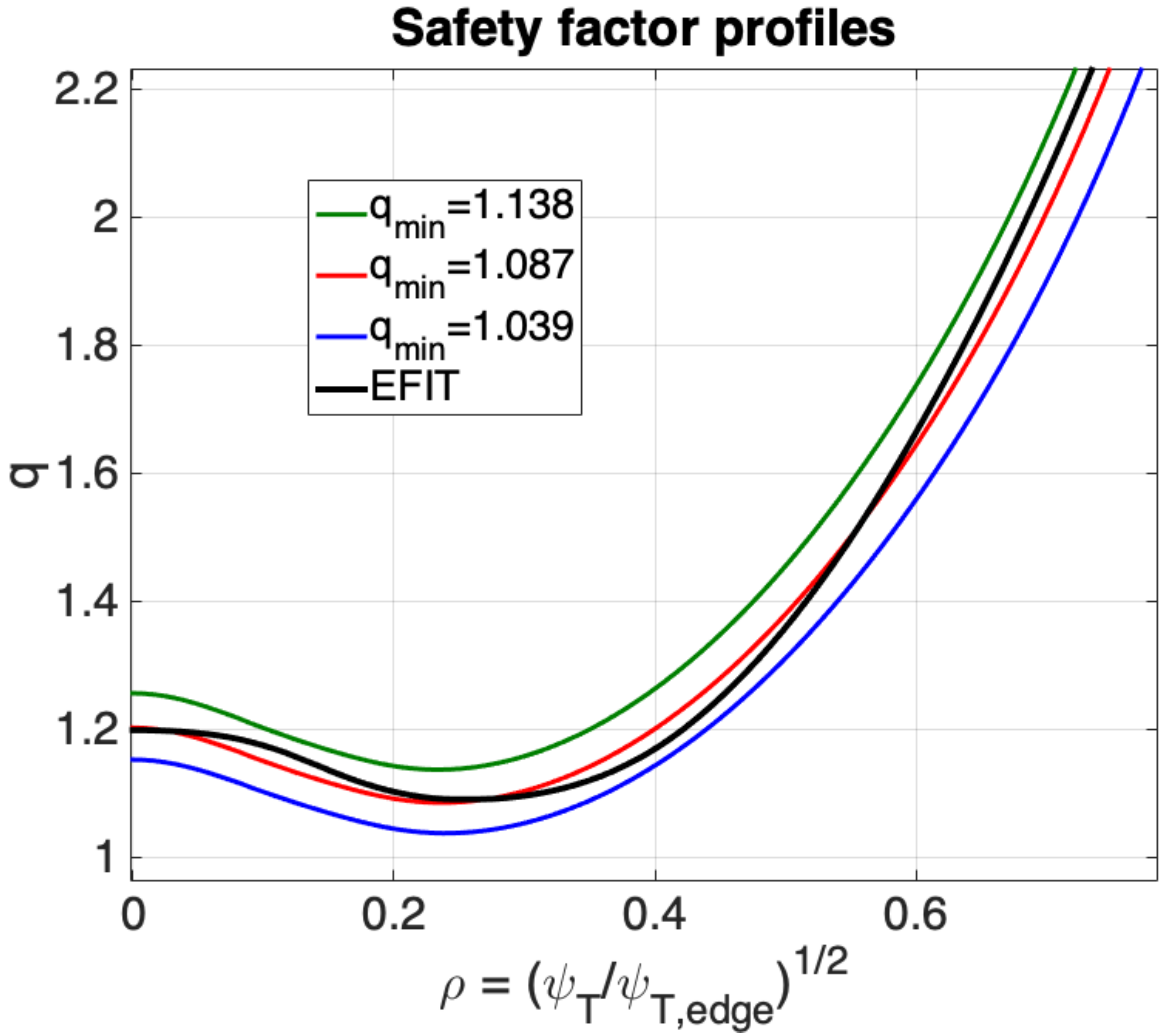

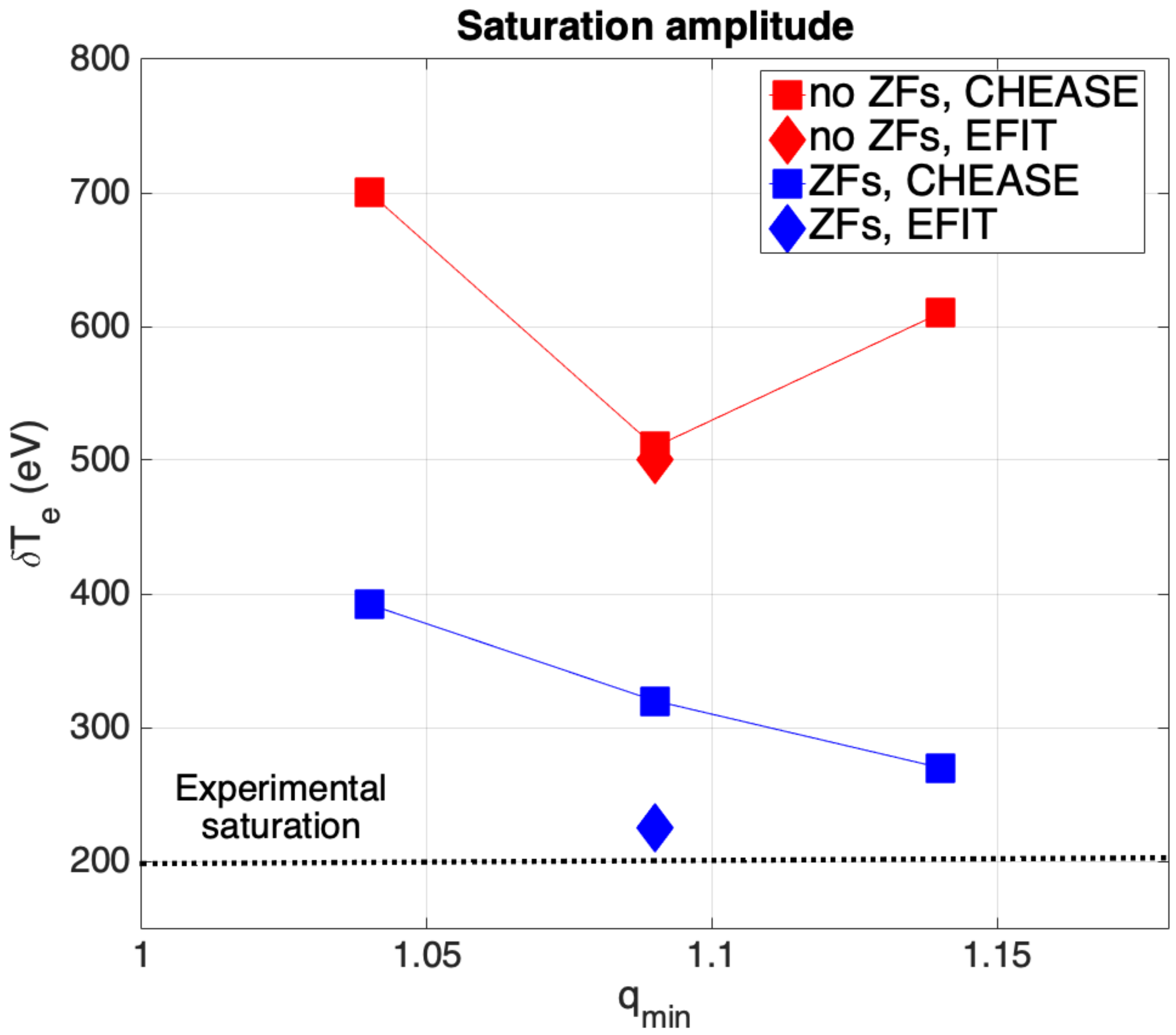

- **CHEASE** used to produced a **set of q profiles** with **different** q_{min} **values**
- **Saturation amplitudes sensitive to** q_{min} values and **magnetic shear**
- **Zonal flows** inclusion **decreases significantly saturation amplitude** for all cases

Zonal flows prevent large EP radial excursion

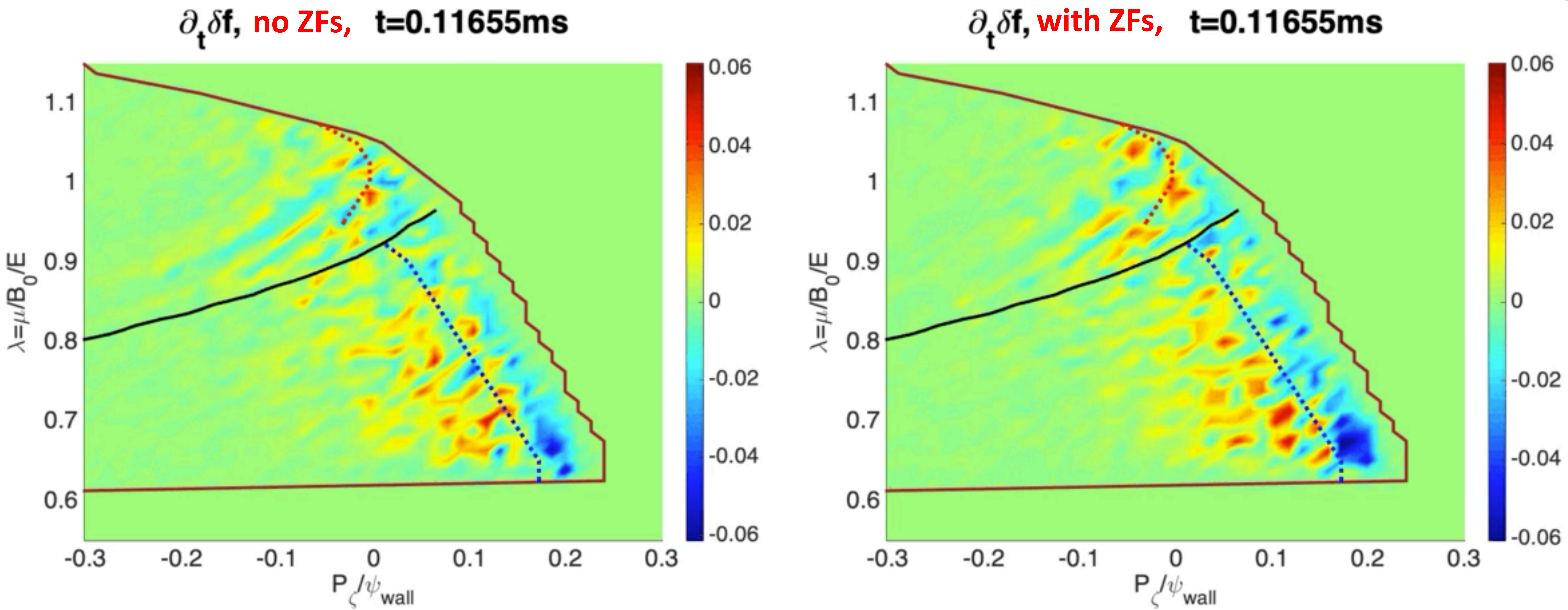

- ➢ **Hole and clump** structures **appear** around both **trapped** and **passing resonances**
- ➢ **EP transport** from **passing resonance stops earlier** with **zonal flows**
- ➢ **Zonal flows prevent hole** and **clump** in **trapped** region to **move** as **mode chirps down**

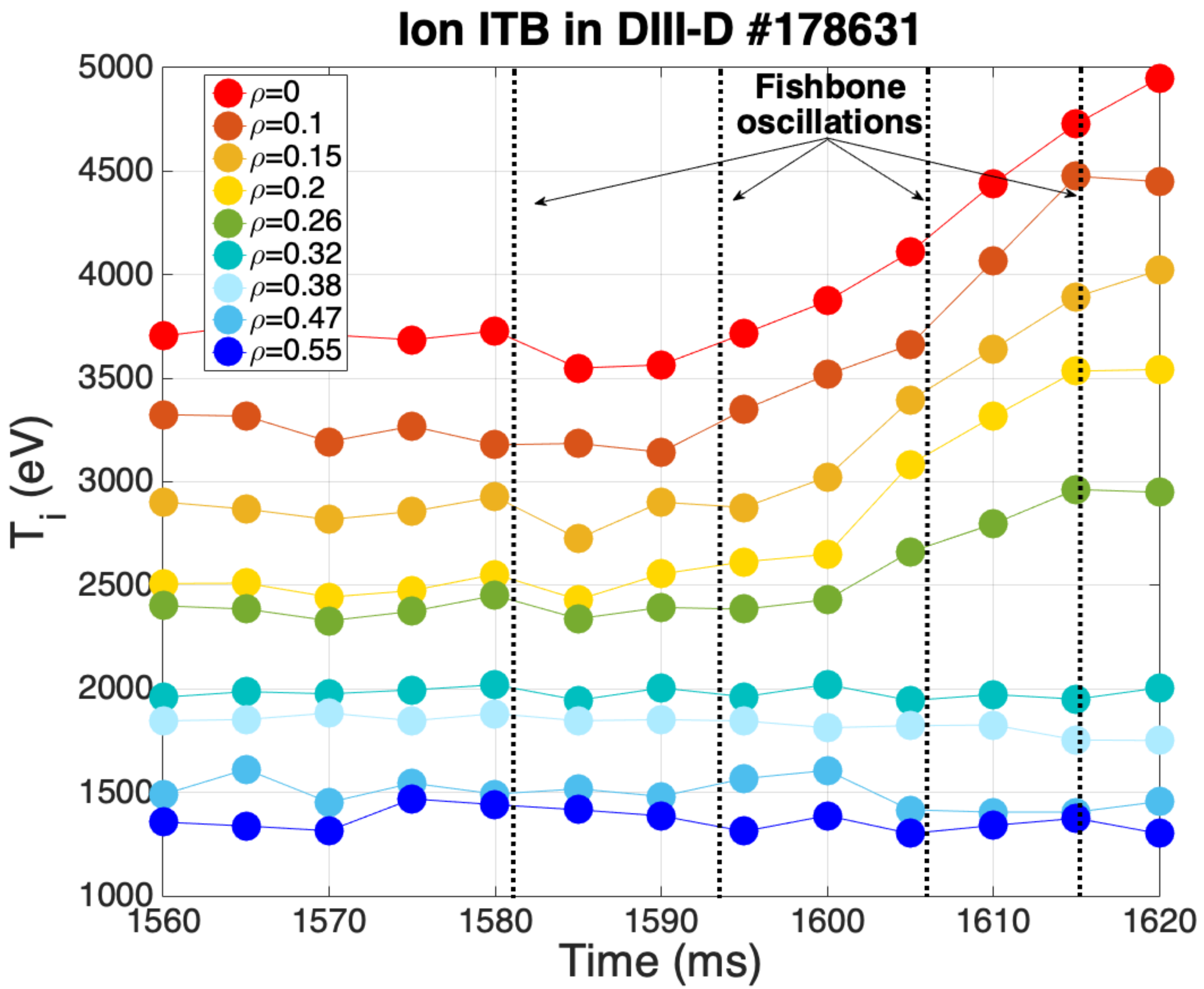

Ion ITB in DIII-D #178631
Fishbone oscillations
ρ=0
ρ=0.1
ρ=0.15
ρ=0.2
ρ=0.26
ρ=0.32
ρ=0.38
ρ=0.47
ρ=0.55
T_i (eV)
Time (ms)

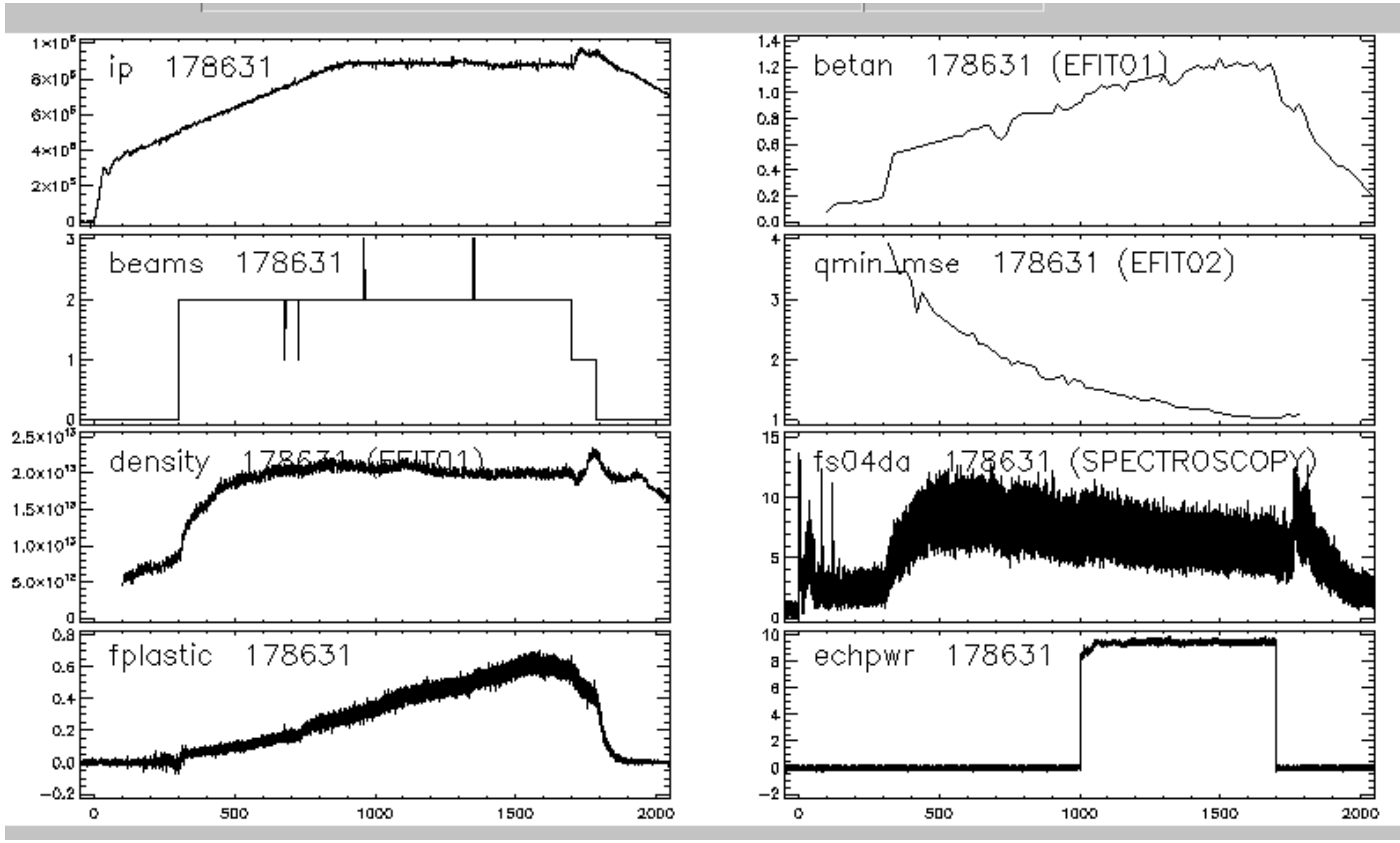

ip 178631
betan 178631 (EFIT01)
beams 178631
qmin_mse 178631 (EFIT02)
density 178631 (EFIT01)
fs04da 178631 (SPECTROSCOPY)
fplastic 178631
echpwr 178631

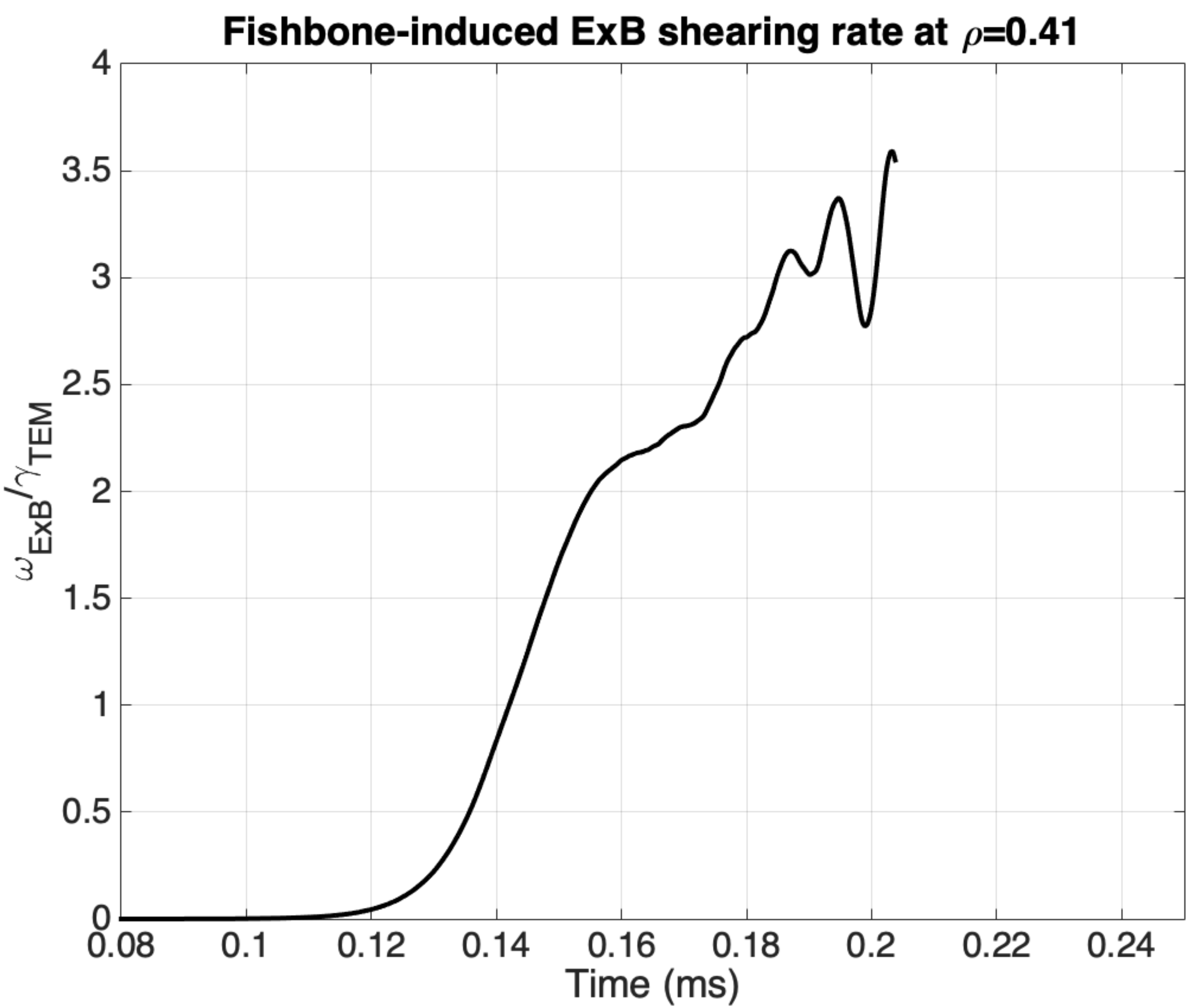
Fishbone-induced ExB shearing rate at ρ=0.41
$\omega_{ExB}/\gamma_{TEM}$
Time (ms)
0
0.5
1
1.5
2
2.5
3
3.5
4
0.08
0.1
0.12
0.14
0.16
0.18
0.2
0.22
0.24

DIII-D

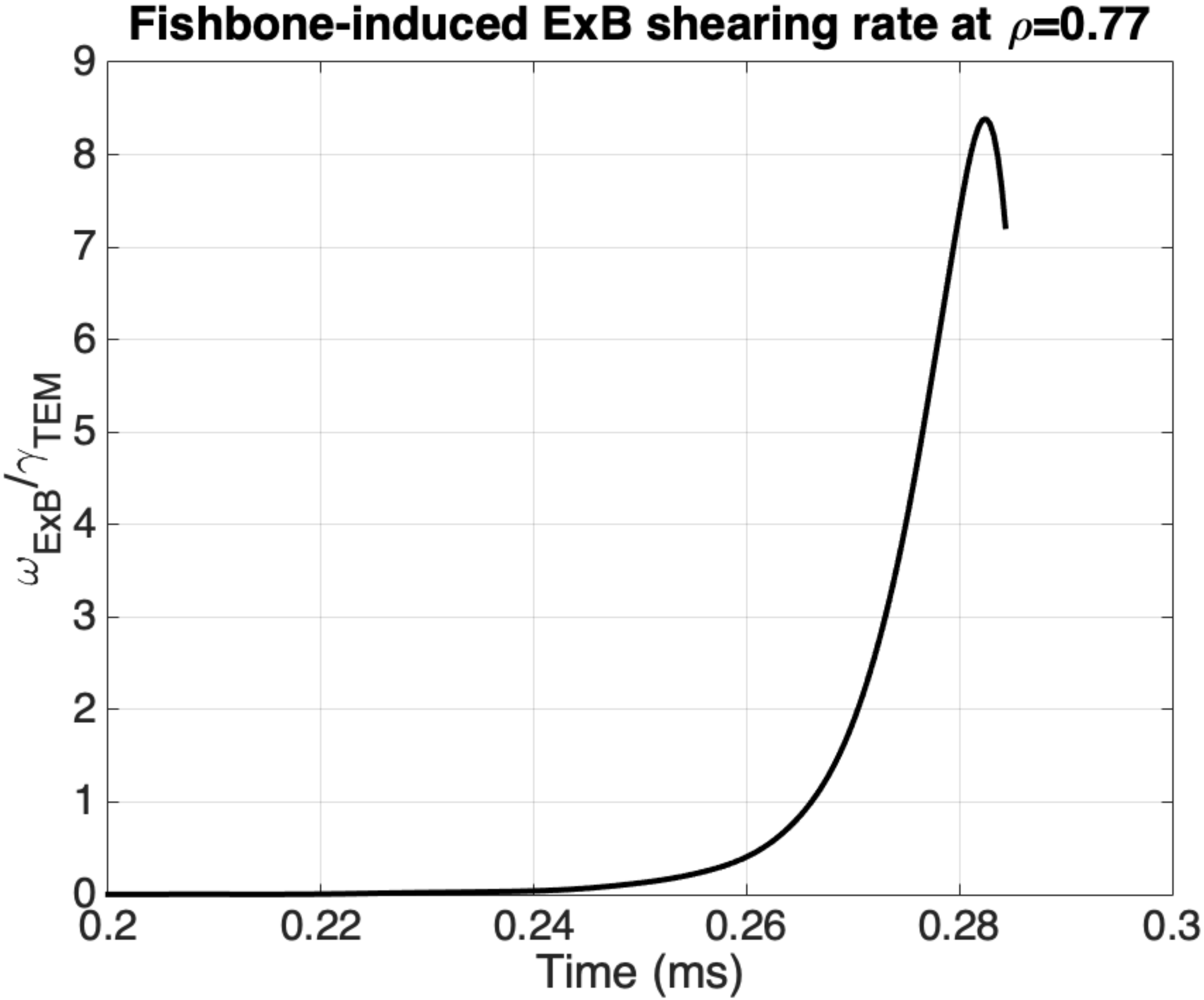
Fishbone-induced ExB shearing rate at ρ=0.77
$\omega_{ExB}/\gamma_{TEM}$
Time (ms)
0
1
2
3
4
5
6
7
8
9
0.2
0.22
0.24
0.26
0.28
0.3

ITER

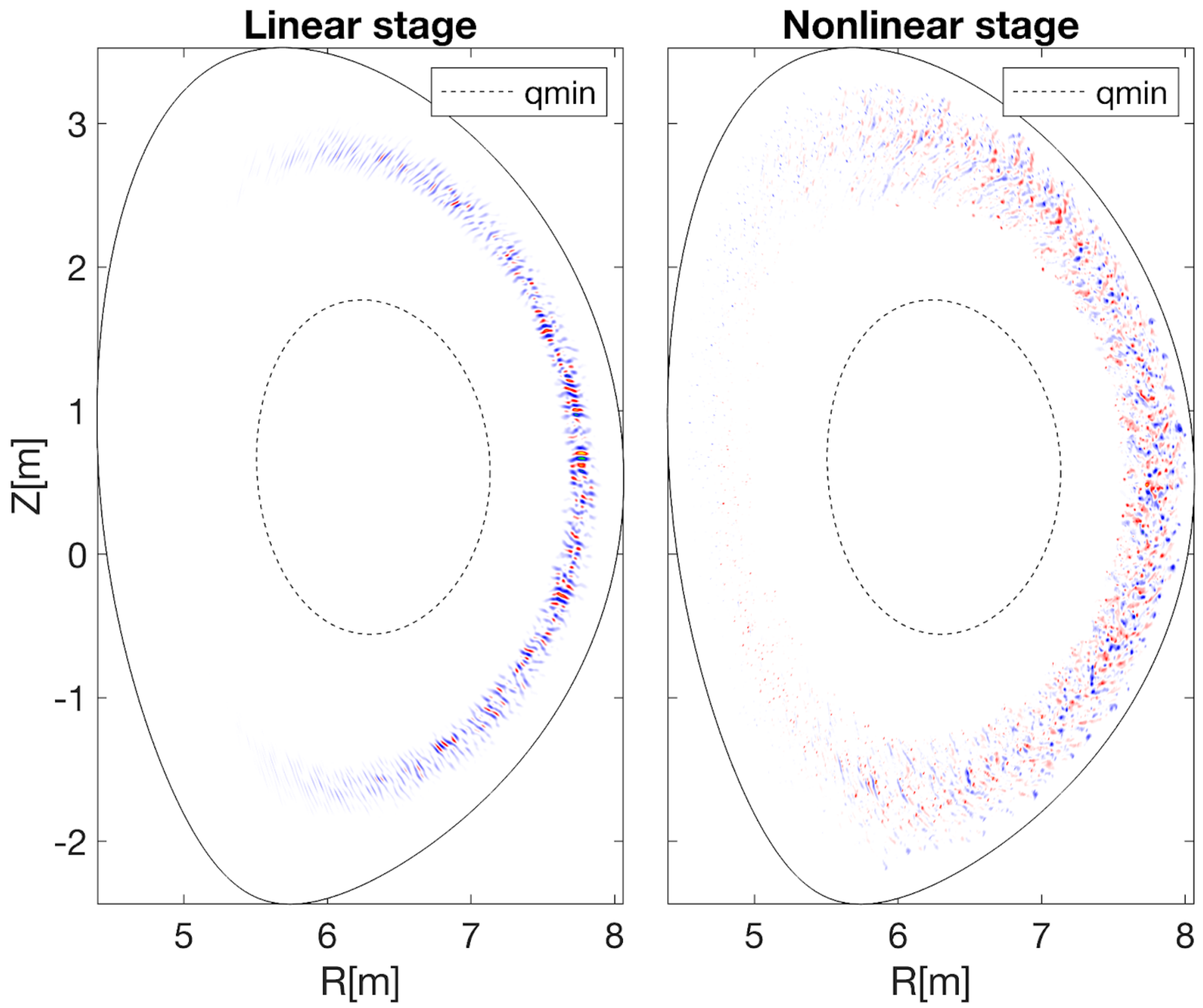
Linear stage
Nonlinear stage
qmin
qmin
Z[m]
3
2
1
0
-1
-2
5
6
7
8
R[m]
5
6
7
8
R[m]

GTC gyrokinetic model

Nonlinear gyrokinetic equation

$$(\partial_t + \dot{\mathbf{X}} \cdot \nabla + \dot{v}_\parallel \cdot \nabla_{v_\parallel})F = 0$$

Poisson equation

$$\frac{Z_i^2 n_i}{T_i}(\phi - \tilde{\phi}) = \sum_s q_s n_s \delta n_s$$

Ampère equations

$$en_e \delta u_{\parallel,e} = \nabla_\perp^2 \delta A_\parallel + e \sum_{s \neq e} Z_s n_s \delta u_{\parallel,s}$$

$$\delta B_\parallel B_0 (1 + \sum_s \beta_s) = -4\pi \sum_s \delta P_{\perp,s}$$

Electron continuity equation

$$\frac{\partial \delta n_e}{\partial t} = -\nabla \cdot \left[n_{e,0} u_{e,\parallel} \frac{\mathbf{B}_0 + \delta \mathbf{B}_\perp}{B_0} + n_e \mathbf{v}_E - \frac{P_{e,\parallel} \mathbf{b}_0 \times \boldsymbol{\kappa}}{eB_0} - \frac{P_{e,\perp} \mathbf{b}_0 \times \nabla B_0}{eB_0^2} - \frac{P_{e,\perp} \mathbf{b}_0 \times \nabla \delta B_\parallel}{eB_0^2} \right]$$

Adiabatic perturbed electron pressure

$$\delta P_{e,\perp} = en_{e,0} \phi_{eff} + \frac{\partial (n_{e,0} T_{e,0})}{\partial \psi_0} \delta \psi - 2 \frac{\delta B_\parallel}{B_0} n_{e,0} T_{e,0}$$

$$\delta P_{e,\parallel} = en_{e,0} \phi_{eff} + \frac{\partial (n_{e,0} T_{e,0})}{\partial \psi_0} \delta \psi - \frac{\delta B_\parallel}{B_0}$$

[1] W.Deng et al., *Nucl. Fusion*, **52**, 023005 (2012)

[2] G.Dong et al., *Phys. Plasmas,* 24, 081205 (2017)

Reduction to linear ideal MHD

Poisson equation

$$\delta n = -\frac{Z_i^2 n_i}{eT_i}(\phi - \tilde{\phi})$$

Perpendicular Ampère law

$$\delta B_\parallel = -4\pi \frac{\delta P_\perp}{B_0}$$

Parallel Ampère law

$$en_e \delta u_\parallel = \nabla_\perp^2 A_|$$

Continuity equation

$$\frac{\partial \delta n}{\partial t} + \mathbf{B}_0 \cdot \nabla\left(\frac{n_0 \delta u_\parallel}{B_0}\right) + \delta \mathbf{B}_\perp \cdot \nabla\left(\frac{n_0 u_{\parallel,0}}{B_0}\right) + \frac{\boldsymbol{\kappa} \times \mathbf{B}_0}{eB_0^2} \cdot \nabla\left(2P_0 \frac{\delta B_\parallel}{B_0} - \delta P_\parallel - \delta P_\perp\right)$$
$$-\frac{P_0}{eB_0^2}\mathbf{b}_0 \times \nabla B_0 \cdot \frac{\nabla \delta B_\parallel}{B_0} - \frac{\mathbf{b}_0 \times \nabla \delta B_\parallel}{eB_0} \cdot \nabla P_0 = 0$$

➢ This physical model leads to the following dispersion relation

$$\frac{\omega^2}{v_A^2}\nabla_\perp^2 \phi + \mathbf{B}_0 \cdot \nabla\left[\frac{\nabla_\perp^2 (k_\parallel \phi)}{B_0}\right] - (\nabla(k_\parallel \phi) \times \mathbf{b}_0) \cdot \nabla\left(\frac{J_{\parallel,0}}{\mu_0 e B_0}\right) + \frac{\boldsymbol{\kappa} \times \mathbf{B}_0}{eB_0^2} \cdot \nabla\left(2P_0 \frac{\delta B_\parallel}{B_0} - \delta P_\parallel - \delta P_\perp\right)$$
$$-\frac{P_0}{eB_0^2}\mathbf{b}_0 \times \nabla B_0 \cdot \frac{\nabla \delta B_\parallel}{B_0} - \frac{\mathbf{b}_0 \times \nabla \delta B_\parallel}{eB_0} \cdot \nabla P_0 = 0$$

[1] W.Deng et al., *Nucl. Fusion*, **52**, 023005 (2012)
[2] G.Dong et al., *Phys. Plasmas,* 24, 081205 (2017)

Identical mode structure for electrostatic potential

Experimental linear validation requires inward q=1 surface

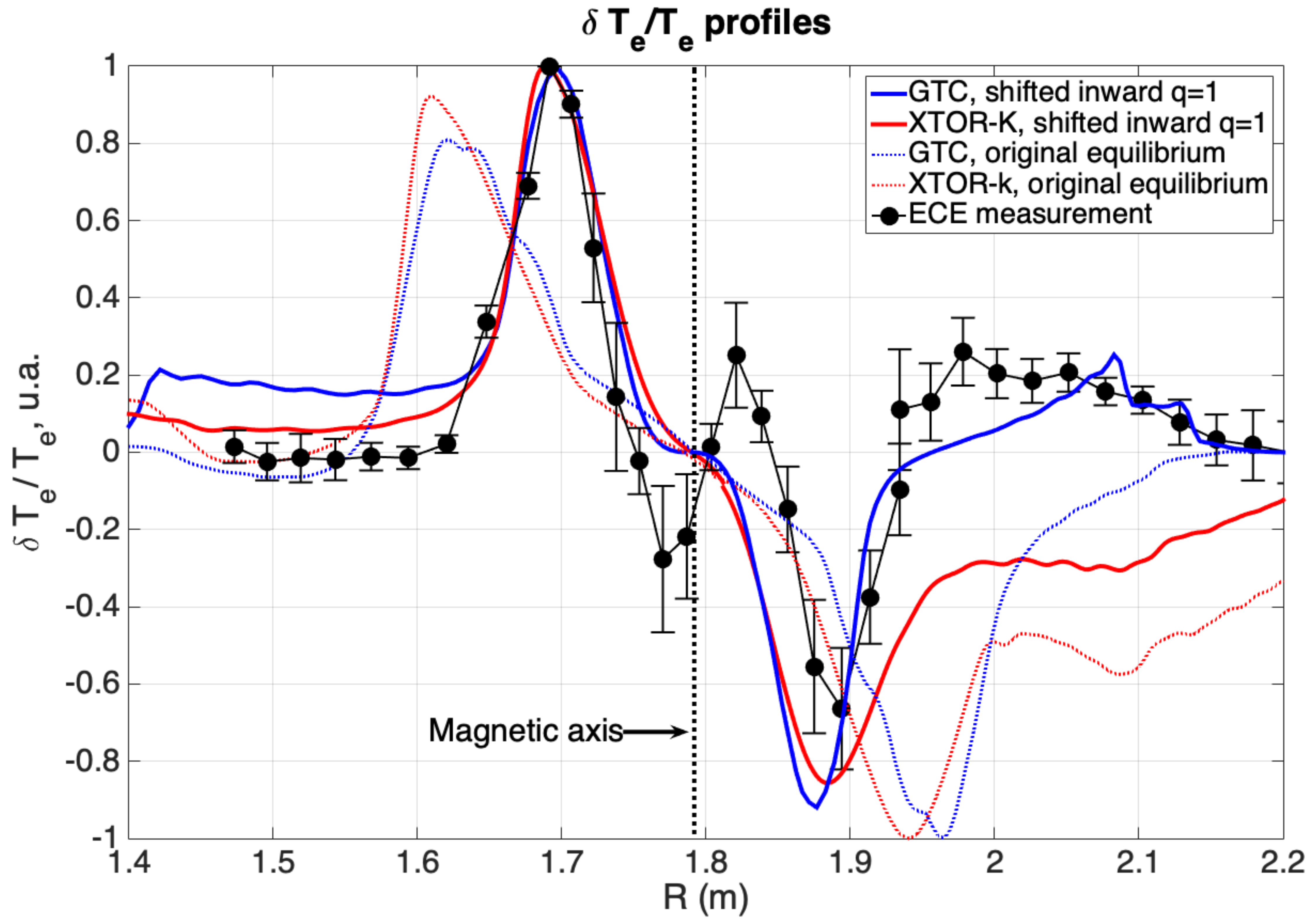

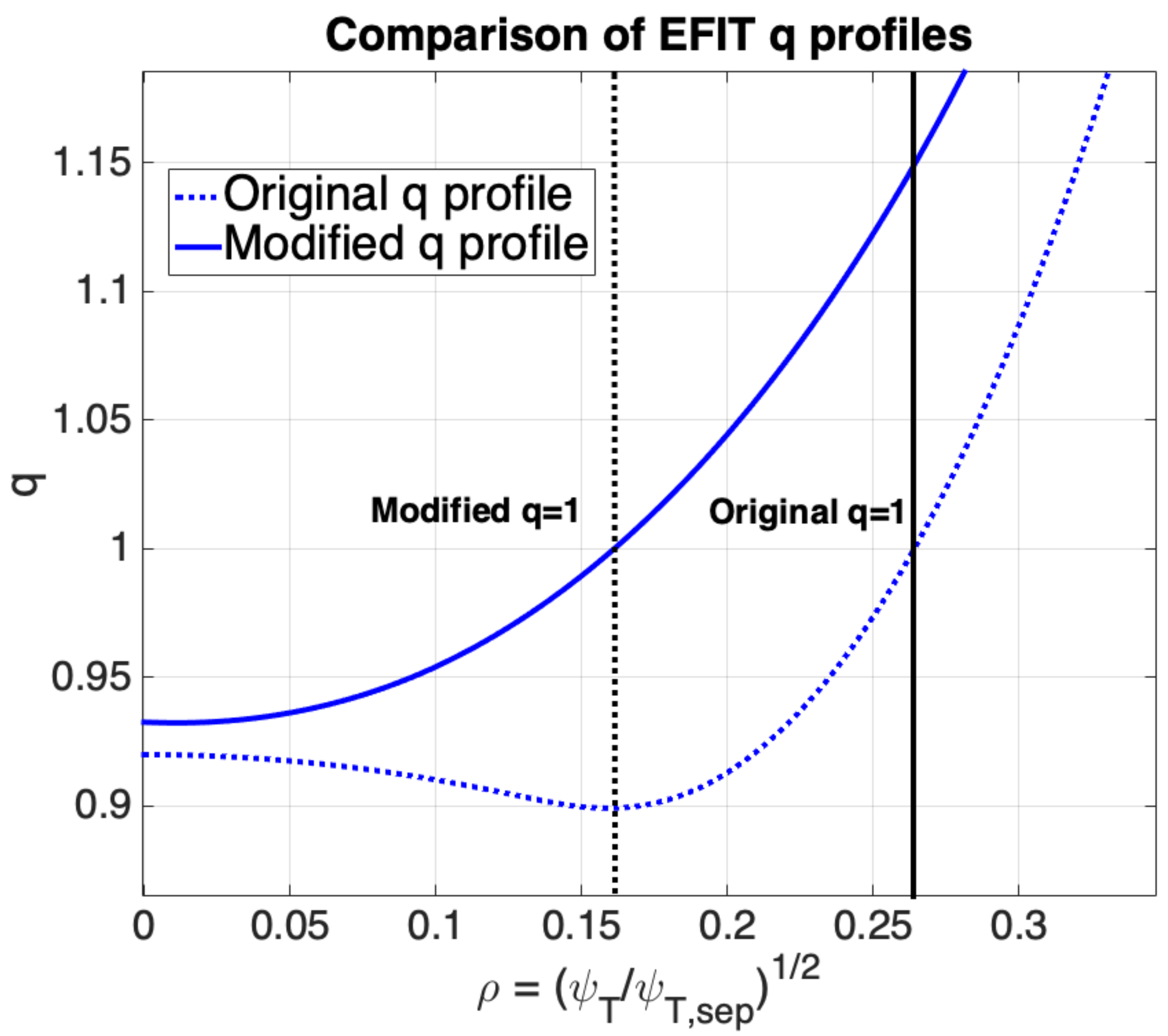

➢ The **EFIT reconstruction** needs to be adjusted to recover a **correct position** for **q=1**

➢ **Both MHD equilibria** are **equally plausible** due to the **experimental uncertainties**

➢ **A fair agreement** is obtained for the internal kink **linear mode structure** between the **ECE measurement** for **fluid** simulations with **GTC** and **XTOR-K**

Necessary inputs for eigenvalue codes/ reduced models

HALO	1st order CoM derivatives on a $(E, \mu, P_\varphi, \sigma)$ grid
NOVA	1st order CoM derivatives on a $(E, \lambda, P_\varphi, \sigma)$ grid
LIGKA	1st order CoM derivatives on a $(E, \lambda, P_\varphi, \sigma)$ grid
RBQ	Same as NOVA

Necessary inputs for initial value codes

XTOR-K / JOREK	• **Full orbit 6D** markers in **phase space cylindrical coordinates** for full-F PIC simulations
GTC	• **Gyrokinetic 5D** markers in **Boozer coordinates** for full-F PIC simulations • $\nabla F\|_{\mu,v_\parallel}$ and $\partial_{v_\parallel} F\|_{\mu,X}$ derivatives evaluated at **Boozer +** $(v_\parallel,\mu)$ **coordinates** for δF PIC simulations (distributions at **gyrocenters**)
MEGA	• **Gyrokinetic 5D** markers in **cylindrical +** (v,λ) **coordinates** for full-F PIC simulations • First order **CoM derivatives** on a $(E,\lambda,P_\varphi,\sigma)$ grid for δF PIC simulations (distributions at **guiding centers**)
M3D-C1	• $\nabla F\|_{\mu,v_\parallel}$ and $\partial_{v_\parallel} F\|_{\mu,X}$ derivatives evaluated at **cylindrical +** $(v_\parallel,\mu)$ **coordinates** for δF PIC simulations (distributions at **guiding centers**) (similar to GTC)
GYSELA	• **Distributions of gyrocenters** on a (R,phi,Z , $v_\parallel,\mu$) grid for **full-F semi-lagrangian** simulations
ORB-5	• $\nabla F\|_{\mu,v_\parallel}$ and $\partial_{v_\parallel} F\|_{\mu,X}$ derivatives evaluated at **field aligned +** $(v_\parallel,\mu)$ **coordinates** for δF PIC simulations (distributions at **gyrocenters**) (to confirm)
FAR-3D	• Specific fluid closure to obtain kinetic effects in gyro-fluid simulations, kinetic module currently being implemented

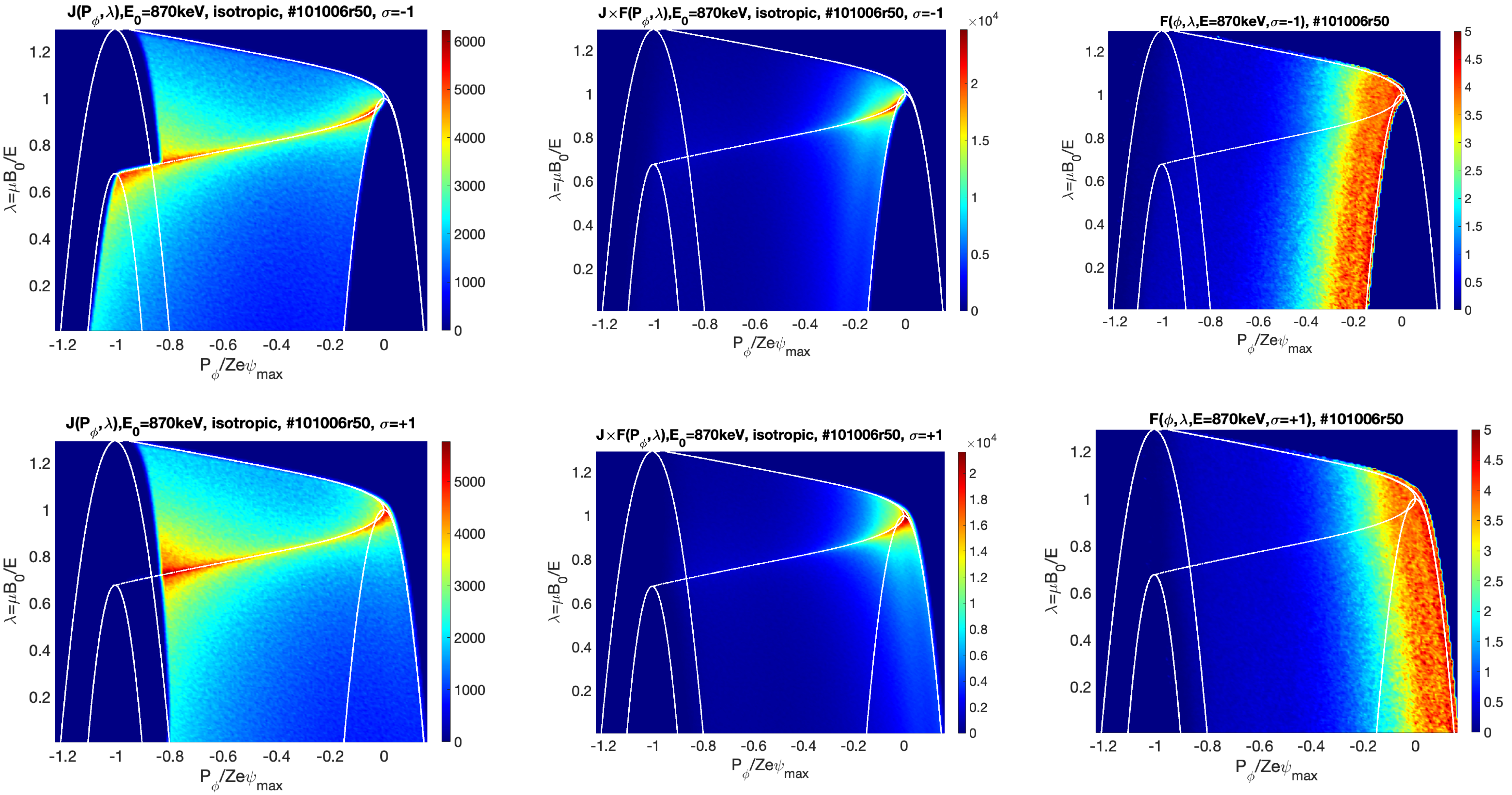
J(Pφ,λ),E0=870keV, isotropic, #101006r50, σ=-1
J×F(Pφ,λ),E0=870keV, isotropic, #101006r50, σ=-1
F(φ,λ,E=870keV,σ=-1), #101006r50
J(Pφ,λ),E0=870keV, isotropic, #101006r50, σ=+1
J×F(Pφ,λ),E0=870keV, isotropic, #101006r50, σ=+1
F(φ,λ,E=870keV,σ=+1), #101006r50
λ=μB0/E
Pφ/Zeψmax
×10^4

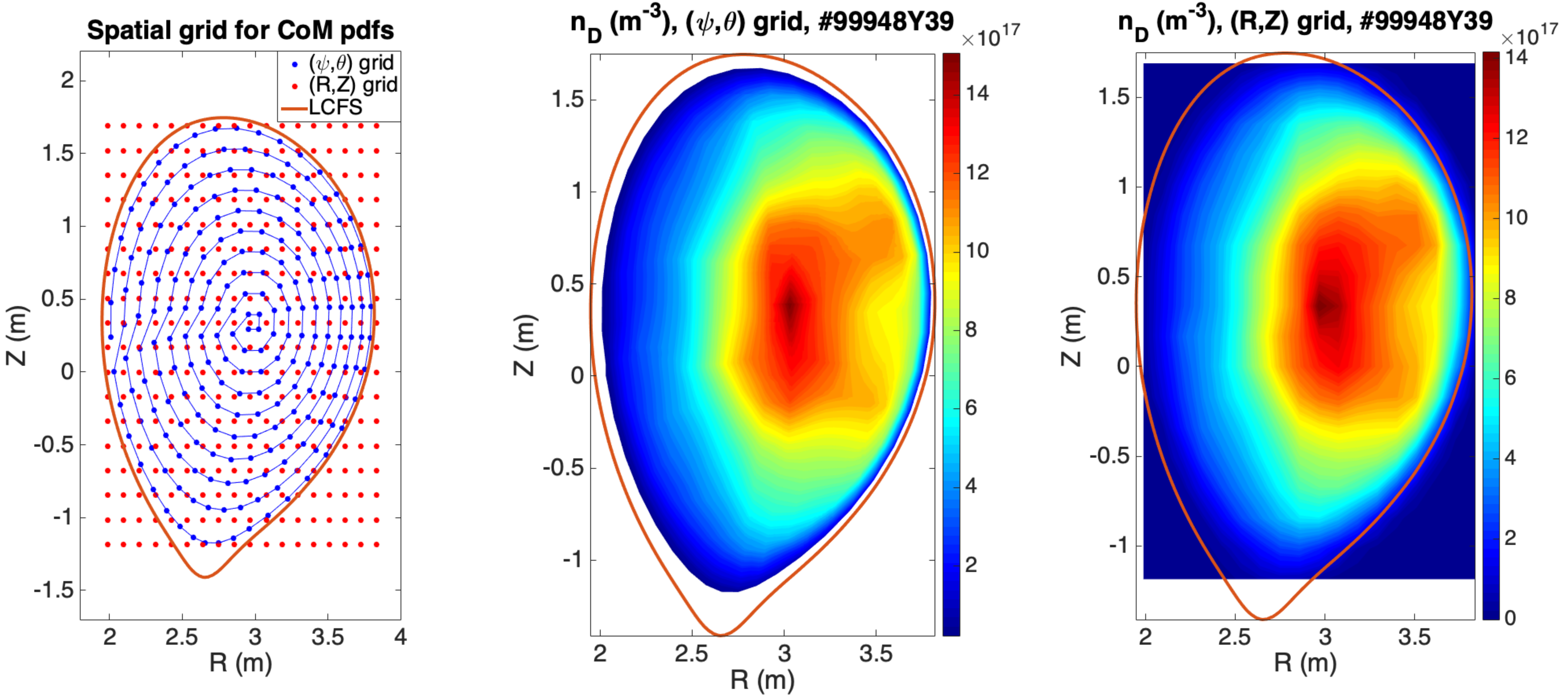

Spatial grid for CoM pdfs
(ψ,θ) grid
(R,Z) grid
LCFS
Z (m)
R (m)
n_D (m^-3), (ψ,θ) grid, #99948Y39
×10^17
n_D (m^-3), (R,Z) grid, #99948Y39

Spline pdf and derivatives (trapped orbits)

Spline pdf and derivatives (co-passing orbits)

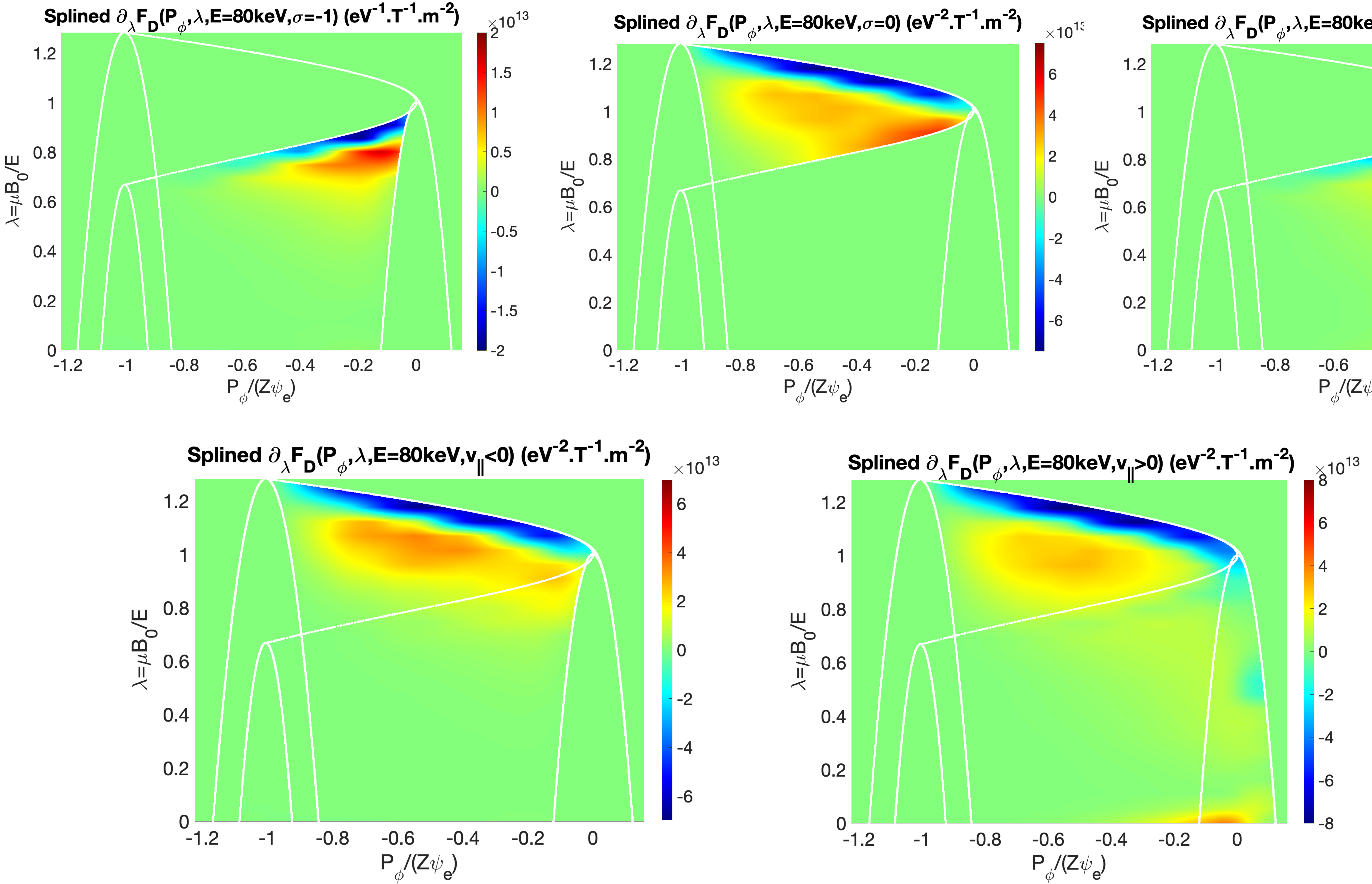

Splined $\partial_\lambda F_D(P_\phi,\lambda,E=80\text{keV},\sigma=-1)$ $(eV^{-1}.T^{-1}.m^{-2})$
Splined $\partial_\lambda F_D(P_\phi,\lambda,E=80\text{keV},\sigma=0)$ $(eV^{-2}.T^{-1}.m^{-2})$
Splined $\partial_\lambda F_D(P_\phi,\lambda,E=80\text{keV},\sigma=+1)$ $(eV^{-2}.T^{-1}.m^{-2})$
Splined $\partial_\lambda F_D(P_\phi,\lambda,E=80\text{keV},v_{\|}<0)$ $(eV^{-2}.T^{-1}.m^{-2})$
Splined $\partial_\lambda F_D(P_\phi,\lambda,E=80\text{keV},v_{\|}>0)$ $(eV^{-2}.T^{-1}.m^{-2})$
$\lambda=\mu B_0/E$
$P_\phi/(Z\psi_e)$
$\times 10^{13}$

Precision of λ initialisation in XTOR-K

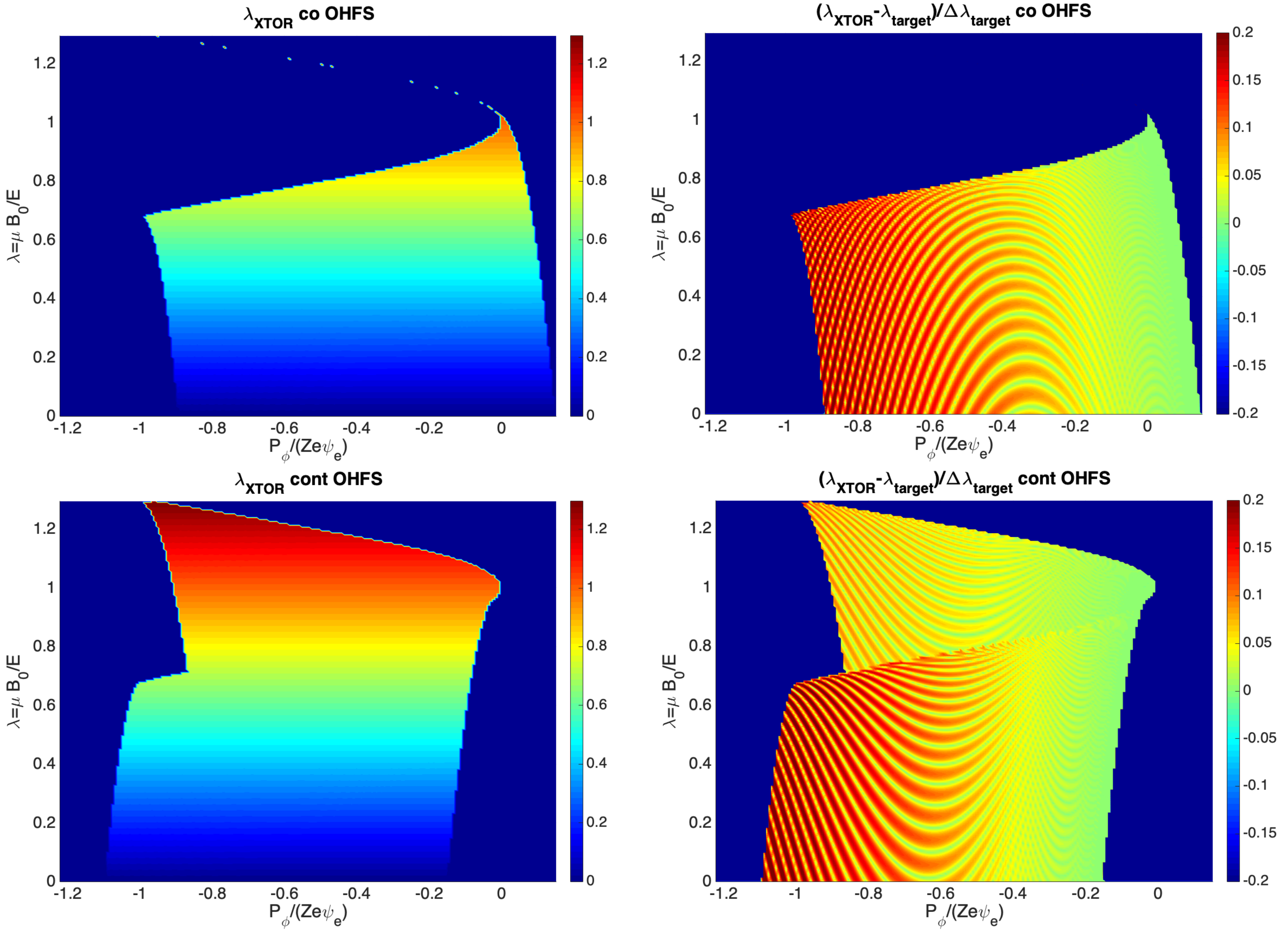

- ➢ Particles initialized on a 200x200 (P_φ, λ) grid
- ➢ Initialisation precision satisfying
- ➢ Finite errors due to interpolation over the poloidal plane

Alpha CoM distributions